Chem Soc Rev

REVIEW ARTICLE

View Article Online
View Journal | View Issue

Cite this: *Chem. Soc. Rev.*, 2014, **43**, 5561

Tuning the structure and function of metal–organic frameworks *via* linker design

Weigang Lu,[a] Zhangwen Wei,[a] Zhi-Yuan Gu,[a] Tian-Fu Liu,[a] Jinhee Park,[b] Jihye Park,[a] Jian Tian,[a] Muwei Zhang,[a] Qiang Zhang,[a] Thomas Gentle III,[a] Mathieu Bosch[a] and Hong-Cai Zhou*[a]

Metal–organic frameworks (MOFs) are constructed from metal ions/clusters coordinated by organic linkers (or bridging-ligands). The hallmark of MOFs is their permanent porosity, which is frequently found in MOFs constructed from metal-clusters. These clusters are often formed *in situ*, whereas the linkers are generally pre-formed. The geometry and connectivity of a linker dictate the structure of the resulting MOF. Adjustments of linker geometry, length, ratio, and functional-group can tune the size, shape, and internal surface property of a MOF for a targeted application. In this critical review, we highlight advances in MOF synthesis focusing on linker design. Examples of building MOFs to reach unique properties, such as unprecedented surface area, pore aperture, molecular recognition, stability, and catalysis, through linker design are described. Further search for application-oriented MOFs through judicious selection of metal clusters and organic linkers is desirable. In this review, linkers are categorized as ditopic (Section 1), tritopic (Section 2), tetratopic (Section 3), hexatopic (Section 4), octatopic (Section 5), mixed (Section 6), desymmetrized (Section 7), metallo (Section 8), and N-heterocyclic linkers (Section 9).

Received 2nd January 2014

DOI: 10.1039/c4cs00003j

www.rsc.org/csr

Introduction

Metal–organic frameworks (MOFs), also known as porous coordination polymers, are crystalline coordination networks consisting of metal ions/clusters and organic linkers.[1–3] Although coordination polymers were reported in the literature sporadically before 1990, the systematic design and construction of coordination polymers by using organic molecular building blocks and metal ions appeared in the early half of the 1990s.[4] Representative work includes porous coordination polymers with pyridyl ligands[5] and metal–organic frameworks with permanent porosity.[6] More than 20 000 MOF structures have been reported and studied since then.[7]

MOFs are made by linking inorganic and organic building units through coordination bonds. The inorganic units can be

[a] *Department of Chemistry, Texas A&M University, College Station, TX 77842-3012, USA. E-mail: zhou@chem.tamu.edu; Fax: +1 979 845 1595; Tel: +1 979 845 4034*
[b] *Korea Electrotechnology Research Institute 12, Bulmosan-ro 10 beon-gil, Seongsan-gu, Changwon-si, Gyeongsangnam-do, 642-120, Republic of Korea*

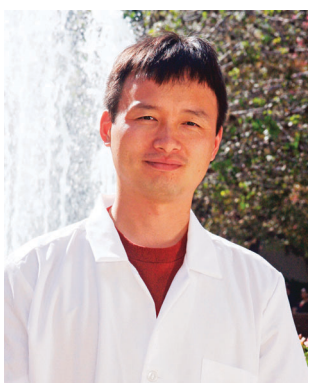

Weigang Lu

Weigang Lu obtained his PhD in Organic Chemistry (2002) from Sun Yat-Sen University. After independent research at Sun Yat-Sen University (2002–2005) and a visiting scholar stint at the Hong Kong University of Science & Technology (2005–2008), he joined Prof. Hong-Cai Zhou's group at Texas A&M University. Now he is an assistant research scientist. His research interest focuses on rational design and synthesis of porous polymers and their energy-related applications.

Hong-Cai Zhou

Hong-Cai "Joe" Zhou obtained his PhD in 2000 from Texas A&M University under the supervision of F. A. Cotton. After a post-doctoral stint at Harvard University with R. H. Holm, he joined the faculty of Miami University, Oxford, in 2002. Since the fall of 2008, he has been a professor of chemistry at Texas A&M University. His research interest focuses on gas storage and separations that are relevant to clean energy technologies.

metal ions or clusters; the latter is widely designated as secondary building units (SBUs),[8] although linkers can also be viewed as SBUs geometrically as well. The organic units (linkers/bridging-ligands) are carboxylates, or other organic anions, such as phosphonate, sulfonate, and heterocyclic compounds. In 1999, two archetypical MOFs, MOF-5 (Zn_4O(**bdc**)$_3$, **bdc** = terephthalate)[9] and HKUST-1 (Cu_3(**btc**)$_2$, **btc** = 1,3,5-benzenetricarboxylate),[10] were synthesized and characterized, symbolizing a benchmark in MOF chemistry with their high porosity indicated by crystal structures and confirmed by low-pressure gas sorption studies. In 2005, another representative MOF, chromium(III) terephthalate (MIL-101), with high chemical stability was reported. The Brunauer–Emmer–Teller (BET) and Langmuir surface areas of MIL-101 are over 4100 and 5900 $m^2\ g^{-1}$, respectively.[11] In the same year, MOF-74 (Zn_2(**dhbdc**), **dhbdc** = 2,5-dihydroxy-1,4-benzenedicarboxylate), was reported.[12] Since then, significant work has been performed on this **dhbdc** linker (later on **dobdc** and **dot** were used as linker abbreviation) with different metals. Arguably the most famous member of the MOF-74 family is Mg-MOF-74, which was found to significantly outperform all other physisorptive materials in low pressure adsorption of CO_2.[13] By expanding the original phenylene unit of **dot** to 2, 3, 4, 5, 6, 7, 9, and 11 phenylene units, a series of Mg-MOF-74 isostructural analogues (termed IRMOF-74-I to IRMOF-74-XI) with pore apertures ranging from 14 to 98 Å were reported. The large pore apertures were demonstrated to accommodate green fluorescent protein without unfolding.[14] In 2012, NU-110E was reported with a progressively acetylene-expanded hexatopic linker. It has the highest experimental BET surface area of any porous materials reported to date (7140 $m^2\ g^{-1}$).[15] Overall, MOF research is still a burgeoning field as evidenced by not only the escalating number of research papers published each year but also the ever-expanding scope of applications.[16,17] With the help of computational simulation and validation, novel structures and practical applications are continuously increasing.

MOFs are attractive to scientists in academia and industry alike because of their diverse and tunable porosities. Ideally, by judiciously selecting SBUs and linkers, MOFs can be tailor made as matrixes with controlled pore size, shape, and functionality for specific applications. To achieve framework design, a high degree of predictability must be integrated prior to synthesis. In reality, however, it is hard to realize even a well-educated design, especially when extending it to more complicated cases (for example, polytopic linkers), not to mention that other factors (temperature, solvent, and substrate composition/concentration) would also affect the product crystallinity and morphology. The term 'MOF' was originally used in a relatively narrow sense, with SBUs as polyatomic clusters built entirely with strong covalent bonds.[18] Once the synthesis of the SBU is established, it could be used to direct the assembly of ordered frameworks with rigid organic linkers; thus, it is highly possible to predict the chemistry of the yielded crystalline materials. This approach, proposed by Yaghi and co-workers as "reticular synthesis", has triggered systematic investigation of diverse properties of MOFs with pore metrics varied and functionalized.[19] In other words, on the premise of forming SBUs with fixed linking geometries, the MOF structures in the assembly procedures can be anticipated with predesigned linkers (primarily regarding those with rigid and robust geometries). The orientation of organic linkers will result in the construction of MOFs with predetermined structural topologies. Overall, it is the combination of both SBUs (as connectors) and organic ligands (as linkers) that determines the final framework-topology. For example, a diamondoid net can be constructed from 4-connected tetrahedral clusters and ditopic linear linkers,[4] and a cubic net can be formed from 6-connected octahedral clusters and ditopic linear linkers[9] (Scheme 1).

This review highlights the synthesis of MOFs through linker design with specific focus on tuning the topology and functionality for different applications. It is not intended to be an exhaustive literature survey of either the structural features or properties of MOFs due to the overwhelming amount of related literature. The use of phosphonate and sulfonate linkers for the construction of MOFs is not included; for this the reader is directed to detailed recent reviews.[21,22] Flexible linkers for MOF

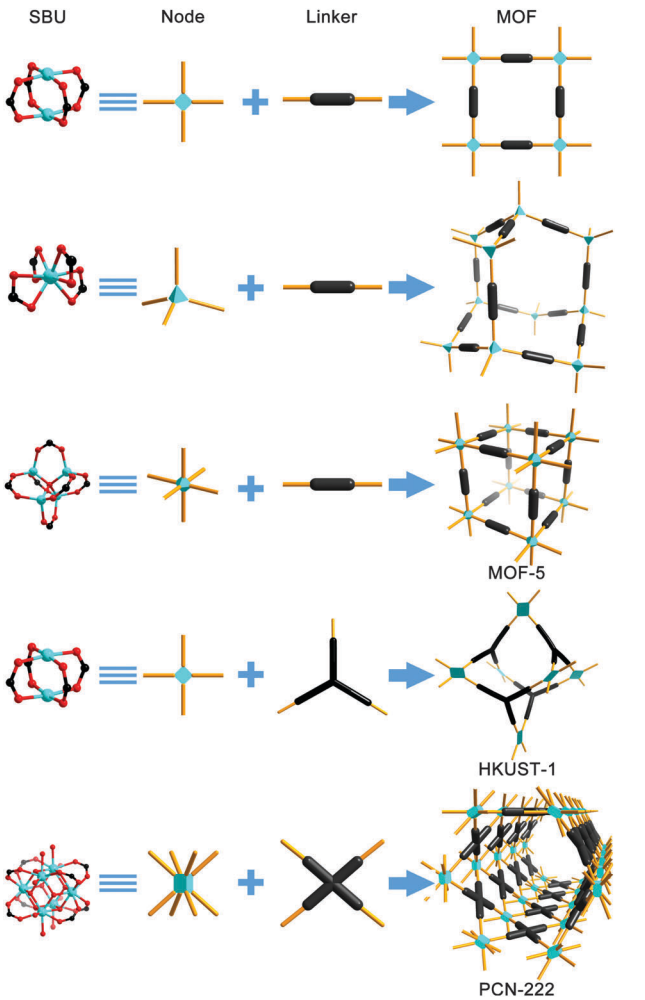

Scheme 1 Graphical illustration of the construction of some representative coordination polymers/MOFs from SBUs and rigid linkers. MOF-5,[9] HKUST-1,[10] PCN-222.[20]

synthesis are covered by another review in the same issue. Our goal is to review recent development in the carboxylate and N-heterocyclic linkers, and to demonstrate the connectivity between SBUs and organic linkers in the synthesis of MOFs.

1 Ditopic carboxylate linkers

Ditopic carboxylate linkers have been well studied since the beginning of the MOF field due partly to their ready accessibility and perhaps partly to their easily perceivable structures in combination with different SBUs.

1.1 Ditopic carboxylate linkers with 4-connected paddle-wheel clusters

The *in situ* aggregation of metal ions into M–O–C metal clusters/SBUs is dependent on the reaction conditions; the same starting materials (metal salts and organic linkers) could lead to different crystal structures. For example, the reaction between zinc nitrate [$Zn(NO_3)_2$] and terephthalate (**bdc**) gives crystalline MOF-5 [Zn_4O(**bdc**)$_3$] under solvothermal conditions;[9] however, slow vapour diffusion at room temperature of triethylamine–toluene into a *N,N′*-dimethylformamide (DMF)–toluene solution containing a mixture of $Zn(NO_3)_2$–H_2**bdc** yields colourless prism-shaped crystals of Zn(**bdc**)(DMF)(H_2O).[23] In this structure, the SBU is a square planar dizinc paddle-wheel unit instead of an octahedral $Zn_4O(CO_2)_6$ cluster in MOF-5. By linking square planar building units and linear ditopic linkers, it is evident that the Zn(**bdc**)(DMF)(H_2O) structure is a two dimensional (2D) sheet as opposed to the three dimensional (3D) network in MOF-5 structure.

Similar to zinc acetate, copper acetate can also adopt the paddle-wheel structure with two solvent molecules completing the coordination sphere. The dinuclear paddle-wheel unit $Cu_2(CO_2)_4$ has been particularly reticulated with organic linkers into extended frameworks. We note that there is a great deal of flexibility a linker may provide. Take 4,4′-biphenyldicarboxylate (**bpdc**) as an example; although the two phenyl rings are tilted with respect to each other, the two carboxylate-group planes are close to coplanar, and the SBU squares linked by **bpdc** are coplanar. Continuation of this simple translation produces a 2D sheet with **sql** topology (MOF-118, Fig. 1).[24] In the case of 2,2′-dicyano-4,4′-biphenyldicarboxylate (cn**bpdc**), however, the two carboxylate-group planes are perpendicular to each other forced by the two cyano groups at 2 and 2′ positions. As a result, an $\sim 90^\circ$ twist leads to a 3D network with **nbo** topology (MOF-601, Fig. 1).[24] Generally speaking, the twisted angle of linear dicarboxylates plays a crucial role in determining both the dimensionality and topology of the final network structure. Substituents with varied bulkiness could be introduced to adjust the dihedral angle, while linker length might not necessarily a prerequisite for topological control.

It should be pointed out that 90° dihedral angle does not guarantee that the two carboxylates are perpendicular to each other. For example, 2,2′-dihydroxy-1,1′-binaphthalene-5,5′-dicarboxylate (5,5′-**bda**) was used to synthesize a chiral MOF

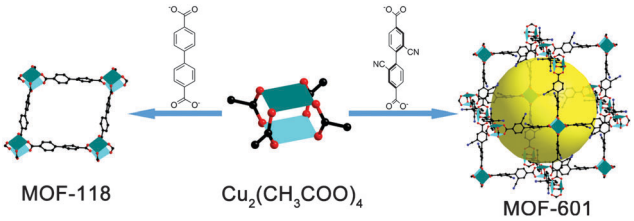

Fig. 1 Examples of the dimensionality and topology of MOF products dictated by the twisted angle of dicarboxylates. Close-to-coplanar dicarboxylates and square paddle-wheels lead to a 2D sheet structure (MOF-118[24]), while close-to-perpendicular dicarboxylates and square paddle-wheels lead to a 3D network (MOF-601[24]). The large yellow sphere represents the largest van der Waals sphere that would fit in the cavity without touching the framework. All hydrogen atoms have been omitted, and only one orientation of disordered atoms is shown for clarity. Color scheme: Cu (turquoise); O (red); C (black).

with $Cu(NO_3)_2$ under solvothermal conditions. Although the two phenyl rings bearing carboxylates are almost perpendicular to each other, hydrogens at 4 and 4′ positions force the two carboxylates to twist and adopt a nearly coplanar conformation. As a result, a 2D sheet [Cu_2(5,5′-**bda**)$_2$] containing dicopper paddle-wheel SBUs was formed.[25]

It could be concluded that a linear linker with two carboxylates predisposed at right angle would reticulate the squares as desired to produce a MOF with **nbo**-type structure. Since the angle between the two carboxylates within 1,4-benzenedicarboxylates is known to be directly related to the size and nature of substituents at the *ortho* position, 2-bromo-1,4-benzenedicarboxylate (*o*-Br-**bdc**) is expected to provide the ideal right angle for **nbo** type structure. Indeed, reaction of equimolar amounts of *o*-Br-**bdc** acid and $Cu(NO_3)_2$ in DMF in a capped vial at room temperature afforded blue cubic crystals named MOF-101.[26] The crystal structure confirmed that the linker caused the reticulation of the neighbouring square SBUs perpendicular to each other and ultimately into an extended network with **nbo** topology. We can only speculate that it might not form the **nbo** type structure at raised temperature because the right-angle conformation would not be overly predominating; thermodynamic factors have to be taken into consideration when predicting the possible structures of the final product.[26–28]

1.2 Ditopic carboxylate linkers with 6-connected octahedral clusters

Tetranuclear octahedral $Zn_4O(CO_2)_6$ SBU can be hydrothermally obtained and has been known in basic zinc acetate for some 40 years. By replacing the acetate with ditopic carboxylate **bdc**, the rigid and divergent character of the replacing linker allows the articulation of the clusters into a 3D framework with an elegantly beautiful cubic structure. This new iconic MOF-5 had truly unprecedented surface area, porosity, and stability. Nitrogen gas sorption measurements at cryogenic temperature show reversible isotherms with no hysteresis. The Langmuir surface area was estimated at 2900 $m^2\ g^{-1}$ assuming a monolayer coverage of N_2. Using the Dubinin–Raduskhvich equation, pore volumes of 0.61–0.54 $cm^3\ cm^{-3}$ were calculated;

the values are higher than those of zeolites, which generally have pore volumes in the range of 0.18–0.47 cm^3 cm^{-3}.[9] With the isolation and desolvation performed in anhydrous solvents and in an inert atmosphere, the BET and Langmuir surface areas of this MOF can reach 3800 and 4400 m^2 g^{-1}, respectively.[29]

As Prof. O'Keeffe once commented, MOF-5 changed the way we thought about such materials.[18] The same SBU could be connected by ditopic carboxylate linkers with different lengths to produce a variety of materials with the same network topology, a strategy for reticulating metal clusters and organic linkers into extended networks.[30] An *N,N′*-diethylformamide (DEF) solution of $Zn(NO_3)_2$ and H_2**bdc** is heated (85° to 105 °C) in a closed vessel to give crystalline MOF-5 (IRMOF-1) in 90% yield. Replacing **bdc** with other ditopic carboxylate linkers, such as functionalized **bdc**, **ndc**, **bpdc**, **hpdc**, **pdc**, and **tpdc**, yields IRMOF-2 through -16 (Fig. 2), including the non-interpenetrating structures from **bpdc**, **hpdc**, **pdc**, and **tpdc**. As a result, a new class of porous materials isoreticular to MOF-5 were constructed from the octahedral $Zn_4O(CO_2)_6$ clusters and the rigid ditopic linkers, demonstrating not only that a 3D porous system can be functionalized with organic groups such as –Br, $–NH_2$, $–OC_3H_7$, OC_5H_{11}, $–C_2H_4$, and $–C_4H_4$ but also that its pore size can be expanded with the long molecular struts such as biphenyl, tetrahydropyrene, pyrene, and terphenyl. The homogeneous periodic pores can be incrementally varied from 3.8 to 28.8 angstroms.[31,32] Interestingly, the slightly longer linker, diacetylene-1,4-bis-(4-benzoate), led to a quadruply interpenetrated IRMOF-62 probably due to its slenderness.[33] The intrinsic value of this design approach lies in the ability to control and direct the reticulation of building blocks into extended networks in which specific properties can be targeted. This is probably the first example to show that crystalline

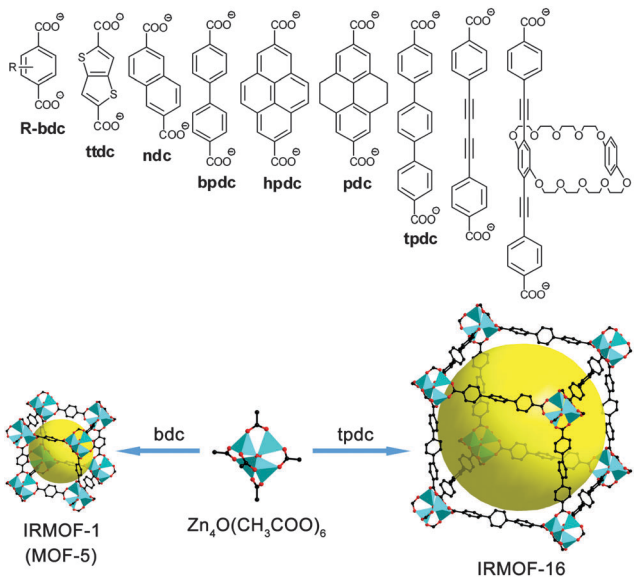

Fig. 2 Some representative ditopic carboxylate linkers and illustration of formation of extended IRMOF networks by replacing acetate with rigid dicarboxylates. Color scheme: Zn (turquoise polyhedra); O (red); C (black).

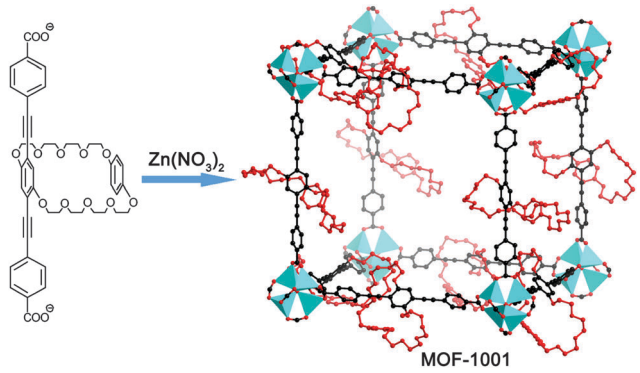

Fig. 3 Synthesis of MOF-1001, a non-interpenetrating cubic structure isoreticular to MOF-5; crown ethers are placed throughout the whole framework.[35] Color scheme: Zn (turquoise polyhedra); O (red); C (black); macrocyclic polyethers (red).

materials could be made by design, at least in a narrow sense. The successful utilization of SBUs in the formation of certain predicted structures and their impact on identifying networks with optimal porosity are evident.

An interesting application of reticular chemistry has been demonstrated in molecular recognition. MOFs have been largely relying on nonspecific binding interactions to host small molecular guests. Two-nanometer ditopic carboxylate linkers with pre-incorporated 34- and 36-membered macrocyclic polyethers as recognition modules were used to assemble crystalline primitive cubic frameworks isoreticular to MOF-5 (Fig. 3). The pre-incorporated macrocyclic polyethers function effectively in preventing interpenetration and engaging in specific binding. MOF-1001 is capable of docking paraquat dication (PQT^{2+}) guests within the macrocycles in a stereoelectronically controlled fashion. This act of specific complexation yields quantitatively the corresponding MOF-1001 pseudorotaxanes, as confirmed by X-ray diffraction and by solid- and solution-state nuclear magnetic resonance spectroscopic studies performed on MOF-1001, its pseudorotaxanes, and their molecular strut precursors. A control experiment involving the attempted inclusion of PQT^{2+} inside a highly porous framework (MOF-177[34]) devoid of polyether struts showed negligible uptake of PQT^{2+}, indicating the importance of the macrocyclic polyether in PQT^{2+} docking.[35]

1.3 Ditopic carboxylate linkers with 6-connected trigonal-prismatic clusters

The isoreticular MOF series (IRMOFs) have established that MOFs can be tailored for targeting specific applications by adjusting the length of linkers and varying the functional groups attached to the linker. One of the major deterrents for MOFs being used in industrial or commercial applications is the instability of many carboxylate-based MOFs in the presence of liquid water or even high humidity. In particular, IRMOFs degrade in the presence of small amounts of water at room temperature.[29,36] Studies on metal analogues have unravelled the ability of metals different from zinc to stand higher water concentrations at high temperatures.[37] To overcome the lability

of the Zn–carboxylate bond, different metal ions have been explored in an effort to identify more stable MOF materials.

For a given linker, increasing the charge of the metal usually leads to an enhancement of the hydrothermal stability of the resulting MOF.[40] Since the first report on chromium(III) dicarboxlate MOF,[41,42] a great deal of efforts have been expended on constructing MOFs with trivalent metal ions due partly to their much improved stability and partly to their interesting properties such as swelling and breathing effects. The hydrothermal reaction of **bdc** with chromium nitrate [$Cr(NO_3)_3$], fluorhydric acid, and H_2O at 220 °C for 8 hours can produce a highly crystallized green powder of chromium terephthalate with the formula $Cr_3F(H_2O)_2O(\mathbf{bdc})_3{\cdot}nH_2O$ (where n is ~25), based on chemical analysis. It is made from the linkage of **bdc**s and inorganic trimers that consist of three chromium atoms in an octahedral environment with four oxygen atoms of the bidendate dicarboxylates, one μ_3O atom, and one oxygen atom from the terminal water or fluorine group. Octahedra are related through the μ_3O atom to form the trimeric building unit. The four vertices of the building unit are occupied by the trimers, and the organic linkers are located at the six edges of the building unit. Crystal structure of this mesoporous material, MIL-101 (MIL stands for Materials Institute Lavoisier), shows a hexagonal window of 16 Å opening and an inner free cage diameter of 34 Å (Fig. 4). The as-synthesized MIL-101 is an unusually porous material whose unit cell has an unprecedented volume of about 702 000 Å^3, meaning that it has about 90% empty space once the solvent molecules normally filling its pores are removed. It exhibits BET and Langmuir surface areas larger than 4100 and 5900 m^2 g^{-1}, respectively.[11] MIL-101 is acknowledged for being stable under an air atmosphere and is not altered when treated with various organic solvents at ambient temperature or in solvothermal conditions. These properties, together with high adsorption capacities, make MIL-101 an attractive candidate for the adsorption of gas or incorporation of large molecules.[43] Tinkering reaction conditions can lead to a new MOF, MIL-88, with the same trimeric SBU but a different connection mode; the follow-up study on a series of functionalized dicarboxylate (**bdc**, **ndc**, and **bpdc**) MOFs with MIL-88 topology suggests that the swelling behaviour is largely related to the incorporated functionalities.[38,39] Interestingly, if the hydrothermal reaction is held for 3 days instead of 8 hours, another new MOF, MIL-53, with infinite SBU will be obtained.[41,42] This suggests that MIL-101 is a kinetic product, while MIL-53 is a thermodynamic product. Cr^{3+}, as hard Lewis acid, bonds strongly to carboxylate; therefore the ligand dissociation process is slow and takes long time to reach thermodynamic equilibrium. Other trivalent cations, such as V^{3+}, Fe^{3+}, and Al^{3+}, have also been extensively studied in combination with either elongated or functionalized ditopic carboxylate linkers.[44–50]

1.4 Ditopic carboxylate linkers with 12-connected clusters

Zirconium is one of the common transition metals on earth, and is obtained mainly from the mineral zircon. Like other group 4 elements, zirconium is highly resistant to corrosion and has a high affinity for hard oxygen donor ligands.[51] $Zr_6O_4(OH)_4(CO_2)_{12}$, as a new 12 connected inorganic brick, was first reported in 2008 and has been the highest coordination cluster reported for a MOF to date.[52]

UiO-66 (UiO = University of Oslo) was prepared under standard solvothermal conditions using $ZrCl_4$ as a metal precursor, **bdc** as the organic linker, and DMF as the solvent. The connectivity of UiO-66 was determined by powder X-ray diffraction (PXRD) to be a cubic structure close packed with octahedral cage (Fig. 5). It was demonstrated that this unique regular octahedral cage can be easily expanded with increasing length of the linkers. For example, UiO-67 is a Zr-MOF with

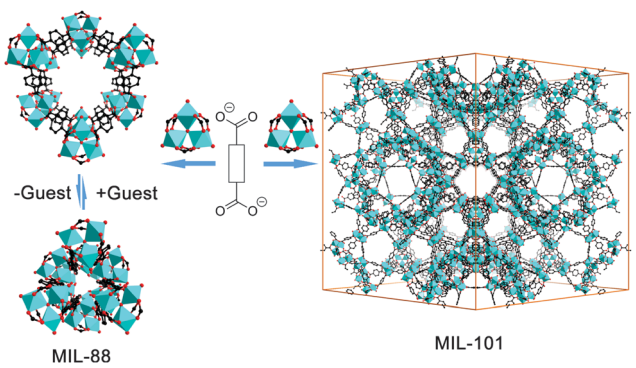

Fig. 4 Illustration of the assembly of MIL-101[11] and MIL-88[38,39] from ditopic carboxylate linkers and trigonal-prismatic clusters; metal ions can be Cr^{3+}, V^{3+}, Fe^{3+}, and Al^{3+}. For MIL-88, the swelling effect is illustrated; ditopic linkers could be **bdc**, **ndc**, and **bpdc** with/without functionalities. Color scheme: Cr (turquoise polyhedra); O (red); C (black).

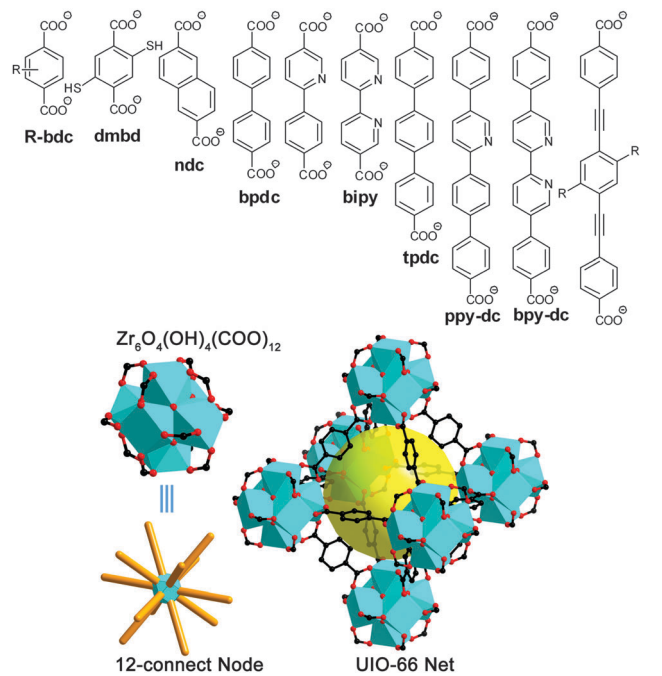

Fig. 5 Some representative ditopic carboxylate linkers used in the synthesis of UiO-MOFs. $Zr_6O_4(OH)_4(CO_2)_{12}$ SBU cluster, UiO-66[52] octahedral cage. Color scheme: Zr (turquoise polyhedra); O (red); C (black).

bpdc as linker and UiO-68 **tpdc** as linker, and both of them are isoreticular structures to UiO-66.[52] Structural resistance toward solvents and mechanical pressure is critical for the application of MOFs. The resistance of UiO-66 MOF toward solvents like water, DMF, benzene, and acetone was investigated by stirring the desolvated sample in the solvents for 24 h. The UiO-66 material has further been exposed to high pressure up to 10.000 kg cm^{-2}. Evidently, the powder XRD pattern remains virtually unaltered by the applied treatment. The Langmuir surface area of UiO-66 is 1187 m^2 g^{-1}; extending the linkers to two and three benzene rings increases the surface areas of the materials to 3000 and 4170 m^2 g^{-1}, respectively.[52]

A thiol-functionalized MOF isostructural to UiO-66, Zr-**dmbd**, was designed and synthesized by reacting $ZrCl_4$ and dimercapto-1,4-benzenedicarboxylate (**dmbd**). Zr-**dmbd** crystals can lower the Hg^{2+} concentration in water below 0.01 ppm and effectively take up Hg from the vapor phase. They also feature a nearly white photoluminescence that is distinctly quenched after Hg uptake.[53]

Reactions of $ZrCl_4$ with azide-functionalized **tpdc** led to highly stable Zr-MOFs isostructural to UiO-68 with tunable loadings of azide groups inside the pores. The system offers an ideal platform for facile pore surface engineering through the introduction of various functional groups with controlled loadings *via* the click reaction. Remarkably, the resultant click products have been demonstrated to possess well-retained frameworks and accessible functionalized pores.[54]

Two porous and stable Zr-MOFs with elongated bpy- or ppy-containing dicarboxylate linkers [dibenzoate-substituted 2,2′-bipyridine (**bpy-dc**), dibenzoate-substituted 2-phenylpyridine (**ppy-dc**)] provide large channels for accommodating Cp*Ir complexes (Cp* is the pentamethylcyclopentadienyl ligand). These two MOFs were demonstrated to be an interesting platform to study water oxidation pathways owing to the elimination of multimolecular degradation pathways. Oxidative modification of the Cp* rings of the immobilized Ir complexes was observed with Ce^{4+} as an oxidant.[55]

The use of even longer ditopic carboxylate linkers (three phenylenes plus two acetylenes) led to porous interpenetrated zirconium–organic frameworks (PIZOFs) constructed with SBU same as in previous UiO structures. This new family of Zr-MOFs also shows stability towards atmospheric moisture, high heat resistance, large voids, and a broad variability of substituents at the linkers, including functional groups ready for postsynthetic modification.[56]

Functionalization of UiO-66 can be realized through a postsynthetic linker exchange.[57–59] The ability of UiO analogues to exchange readily in aqueous environments indicates that the structure might not be as chemically inert as first suggested.[52] Stability and degradation mechanisms of MOF materials containing $Zr_6O_4(OH)_4(CO_2)_{12}$ SBU have been studied and it has been shown that the chemical and thermal stability of these Zr-MOFs can be significantly altered by the attached functional group as well as the length of the organic linker.[60]

It is worth noting that a bent dicarboxylate linker, dithieno-[3,2-*b*;2′,3′-*d*]-thiophene-2,6-dicarboxylate (**dttdc**), facilitated formation of an 8-connected cluster and led to a new framework with **reo** topology. Two moisture stable materials, $Zr_6O_6(OH)_2$(**dttdc**)$_4$ [DUT-51(Zr)] (DUT = Dresden University of Technology) and isotopic $Hf_6O_6(OH)_2$(**dttdc**)$_4$ [DUT-51(Hf)], with extra-wide and accessible pores were obtained.[61] No interpenetration was observed in these structures; therefore the extra-wide pores are evidently the consequence of reduced linker/cluster ratio (6/1 in UiOs, 4/1 in DUT-51).

MOFs with 12-connected SBUs are still scarce. Besides UiOs, MIL-125 is another known highly porous MOF constructed from 12-connected metal–oxo–hydroxo clusters and carboxylate linkers. When a solution of DMF–methanol containing titanium tetraisopropoxide and H_2**bdc** was heated at 150 °C, a well crystallized white hybrid solid denoted MIL-125 or $Ti_8O_8(OH)_4$(**bdc**)$_6$ was isolated and was studied using PXRD techniques.[62] A closer look at the structure showed that one $Ti_8O_8(OH)_4(CO_2)_{12}$ SBU is connected to 12 other neighbouring SBUs in a similar fashion to UiOs with four linkers in the plane of the octameric wheel, four above and four below. However, $Ti_8O_8(OH)_4(CO_2)_{12}$ is not a regular octahedral building unit, and the four linkers in the plane of the octameric wheel extend further than the four above and the four below. Therefore, MIL-125 is a quasi-cubic tetragonal structure and crystallizes in the *I*4/*mmm* space group, while UiOs are cubic structures and crystallize in the higher symmetry space group $Fm\bar{3}m$.[52] Apart from its structure, titanium is a very attractive candidate due to its low toxicity, redox activity, and photocatalytic properties. MIL-125 and its amine-functionalized analogue[63] open new perspectives for the development of photocatalysis within MOF-based materials.

1.5 Ditopic carboxylate linkers with infinite chain clusters

Tetraanionic 2,5-dioxido-1,4-benzene-dicarboxylate (**dobdc**/**dhbdc**/**dot**) is known to be the organic strut for MOF-74, in which both the aryloxide and carboxylate moieties are bonded to the metal sites. If aryloxide was blocked by an alkyl chain and zinc salt was used, most likely isoreticular MOF-5 structure would be the product under solvothermal conditions (Fig. 6).[31] Clearly, the adjacent aryloxide is essential for forming MOF-74 structure. In Zn-MOF-74,[12] helical Zn–O–C rods of composition $[O_2Zn_2](CO_2)_2$ are constructed from 6-coordinated Zn^{2+} centres, where each Zn has three carboxyl groups, and two hydroxyl groups are bound as doubly bridging. The infinite inorganic rod-type SBUs are linked by the benzene units of the **dobdc** to produce **bnn** parallel rod packing and one-dimensional

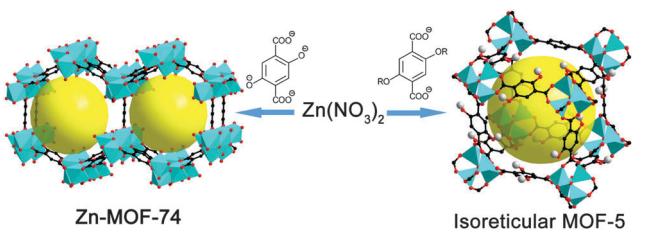

Fig. 6 Synthesis of Zn-MOF-74[12] (**dobdc** as linker) and isoreticular MOF-5[31] (aryloxide blocked **dobdc** as linker).

channels of dimension 10.3 × 5.5 Å^2. Although **dobdc** is tetraanionic, we consider it to be a ditopic linker because the aryloxide and adjacent carboxylate coordinate to the same SBU. Since the discovery of Zn-MOF-74, significant work has been performed on this **dobdc** linker. Mg-MOF-74 (Mg/**dobdc**) was found to significantly outperform all other physisorptive materials in low pressure physisorption of CO_2.[13] CO_2 sorption isotherms of Mg/**dobdc** measured at 296 K showed an uptake of 23.6 wt% at 0.1 atm and 35.2 wt% at 1 atm. The value for Mg/**dobdc** is double the value for any of the other materials in the M/**dobdc** series at 0.1 atm. Computational studies suggest that each of the CO_2 molecules forms a 1 : 1 adsorption complex with the Mg^{2+} adsorption site of the MOF framework. The experimentally found values of standard adsorption enthalpy for CO, N_2, and CO_2 on Mg-MOF-74 are −29, −21, and −47 kJ mol^{-1}, respectively. Differences among these values appear to be large enough to facilitate gas separation.[64]

In H_4**dobpdc** (4,4′-dioxido-3,3′-biphenyldicarboxylic acid), the phenolic hydroxyl group and carboxylic acid group have switched positions compared to H_4**dobdc**; we speculate that H_4**dobpdc** was selected for the MOF-74 expansion probably because it was relatively easy to synthesize compared to 3,3′-dioxido-4,4′-biphenyldicarboxylic acid. Two new MOF materials, M_2(**dobpdc**) (M = Zn; Mg) adopting an expanded MOF-74 structure type, were synthesized *via* solvothermal and microwave methods. The expansion leads to 18.4 Å-wide channels lined with open metal coordination sites. Functionalization with mmen (*N,N*′-dimethylethylenediamine) afforded a remarkable CO_2 adsorbent, mmen-Mg_2(**dobpdc**). The large capacity, high selectivity, and fast kinetics of this material for adsorbing CO_2 from dry gas mixtures with N_2 and O_2 make it an attractive adsorbent for applications in which zeolites and inorganic bases are currently used, including the removal of CO_2 from air.[65] However, whether the presence of water in gas mixtures will significantly affect the stability, capacity, selectivity, or regeneration energy of mmen-Mg_2(**dobpdc**) is presently unknown. Although computational simulation confirmed that MOF-74 structure has superior water-resistance compared to isoreticular Zn-MOFs (IRMOF-1 and IRMOF-10),[66] MOF-74's continuous CO_2 capture performance is less than satisfactory under the effect of humidity.[67]

A stepwise expansion of the original phenylene unit of **dot** (**dobdc**) to 2, 3, 4, 5, 6, 7, 9, and 11 phenylene units leads to a series of Mg-MOF-74 isoreticular structures (termed IRMOF-74-I to IRMOF-74-XI) with pore apertures ranging from 14 to 98 Å; 98 Å is the largest pore aperture reported in crystalline materials to date (Fig. 7). All members of this series have non-interpenetrating structures and exhibit robust architectures, as evidenced by their permanent porosity and high thermal stability (up to 300 °C). The large pore apertures were demonstrated to accommodate green fluorescent protein without unfolding. More importantly, they allow the surface modification without significant sacrifice in porosity; IRMOF-74-VII functionalized with oligoethylene glycol shows inclusion of myoglobin, whereas IRMOF-74-VII with hydrophobic hexyl chains shows a negligible amount of inclusion.[14] It is remarkable

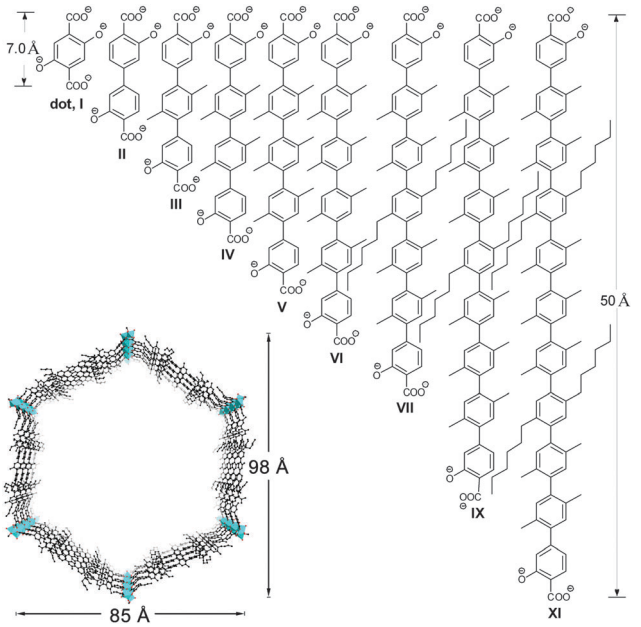

Fig. 7 Chemical structures of organic linkers used in the synthesis of IRMOF-74s.[14] Perspective views of a single one-dimensional channel with 98 Å pore aperture shown for IRMOF-74-XI. Color scheme: Mg (turquoise); O (red); C (black).

that the crystallinity of the IRMOF materials is fully maintained throughout the inclusion process; the diffraction lines in the PXRD patterns of the included samples are in good agreement with those of the starting materials.

Besides forming UiOs, solvothermal reactions of $ZrCl_4$ with **bdc**, **ndc**, **bpdc**, and Cl_2**abdc** (3,3′-dichloro-4,4′-azobenzenedicarboxylate) can produce a whole new series of porous zirconium dicarboxylate solids (MIL-140A to MIL-140D) by carefully adjusting the reaction conditions. These MIL-140 solids are isoreticular structures, containing infinite Zr oxide chains as SBUs *versus* isolated $Zr_6O_4(OH)_4$ oxoclusters in the UiO structures.[68] Although a subtle difference in reaction conditions could lead to different metal clusters, and therefore different MOF structures, again once the metal cluster is controlled as in this case, we can design linkers with different lengths and functionalities to synthesize MOFs with targeted structures through reticular chemistry.

The structures of MIL-53 materials[42,69–71] are made up of chains of corner-sharing $MO_4(OH)_2$ octahedra (M = Cr^{3+}, Al^{3+}, Fe^{3+}, V^{3+}) interconnected by dicarboxylate linkers, featuring three dimensional frameworks containing 1D diamond-shaped channels with nanometre dimensions. An unusual CO_2 adsorption behaviour of the MIL-53 framework has been observed and attributed to a ''breathing'' mechanism of the framework, whereby the structure interchanges between the narrow and the large pore forms (Fig. 8).[72] The structural analysis showed that the breathing effect may be induced by the quadrupole moment of CO_2, and the breathing mechanism can only be induced by molecules with large dipole and quadrupole moments such as H_2O and CO_2. Non-polar molecules such as CH_4 have no such effect.[73] An amine-functionalized

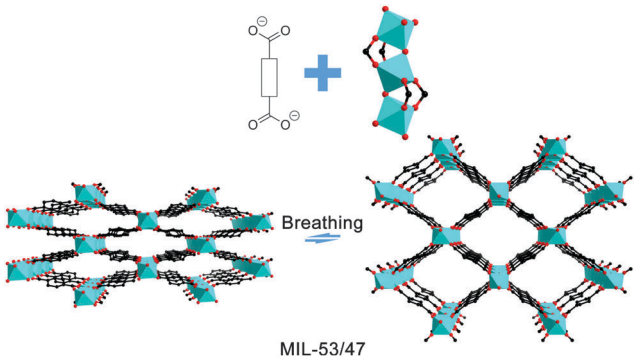

Fig. 8 Illustration of the assembly of MIL-53/47 from ditopic carboxylate linkers and infinite chain clusters; metal ions can be Cr^{3+}, Fe^{3+}, Al^{3+}, and V^{4+} (MIL-47). Breathing effect is illustrated; ditopic carboxylate linkers could be **bdc**, **ndc**, and **bpdc** with/without functionalities. Color scheme: metal (turquoise); O (red); C (black).

MIL-53 (Al) was found to increase its selectivity in CO_2 separations by orders of magnitude while maintaining a very high capacity for CO_2 capture.[74]

2 Tritopic carboxylate linkers

2.1 Tritopic carboxylate linkers with 4-connected paddle-wheel clusters

The linkage of planar tritopic linkers with square SBUs, such as the dicopper paddle-wheel unit, most likely generates two classes of (3,4)-connected nets. They have Reticular Chemistry Structure Resource (RCSR) symbols of **tbo** and **pto** (Fig. 9). One of the first of these MOFs was the iconic HKUST-1,[10] which is built of dicopper paddle-wheel SBU as node and 1,3,5-benzenetricarboxylate (**btc**) as linker. In the framework of HKUST-1, each **btc** linker connects to three dicopper paddle-wheel SBUs to form a T_d octahedron (Scheme 1). Four linkers occupy alternating triangular faces and six SBUs locate at vertices of the T_d-octahedron. Further connection with other units through corner sharing of the octahedron forms a cubic framework with **tbo** topology.

A number of isoreticular MOFs were synthesized by employing elongated tritopic linkers, such as *meso*-MOF-1 with 4,4′,4″-*s*-triazine-1,3,5-triyltri-*p*-aminobenzoate (**tatab**) as linker,[75] PCN-**htb** (PCN = porous coordination polymer) with 4,4′,4″-(1,3,4,6,7,9,9-heptaazaphenalene-2,5,8-triyl)tribenzoate (**htb**) as linker, PCN-6′ with 4,4′,4″-*s*-triazine-2,4,6-triyl-tribenzoate (**tatb**) as linker,[76] MOF-399 with 4,4′,4″-(benzene-1,3,5-triyl-tris(benzene-4,1-diyl))tribenzoate (**bbc**) as linker.[77] Remarkably, the cell volumes of PCN-6′ and MOF-399 are 5.5 and 17.4 times that of HKUST-1, respectively. MOF-399 has the highest void fraction (94%) and lowest density (0.126 g cm^{-3}) of any MOF reported to date.

MOFs with the **pto** topology include MOF-14 (interwoven)[78] and MOF-143[77] with 4,4′,4″-benzene-1,3,5-triyl-benzoate (**btb**) as linker as well as MOF-388 with 4,4′,4″-(triazine-2,4,6-triyl-tris(benzene-4,1-diyl))tribenzoate (**tapb**) as linker.[77] It is worth discussing briefly about what minor difference between similar tritopic linkers leads to distinct framework topologies (**pto** *versus* **tbo**) when they are joined with the same paddle-wheel SBU. Structural analysis shows that in the **pto** net the square SBUs are twisted from the plane of the linker by 55° while in the **tbo** net they are at 90° to the linker. In both nets each carboxylate-group plane is at 90° to the neighbouring square SBU. Thus, in the **tbo** structure the carboxylates are close to coplanar, while in the **pto** structure they are twisted. Indeed, **btb** in MOF-143 is fairly twisted because of the steric hindrance between hydrogen atoms on the central and peripheral benzene rings. Therefore, the **pto** net should be preferred for this linker. In contrast, **tatb** in PCN-6′ is relatively flat and does not show significant twist angles among three carboxylate planes due to the absence of steric hindrance between the central triazine ring and the peripheral benzene rings. Thus, the **tbo** topology is dominating in PCN-6′ (Fig. 10).

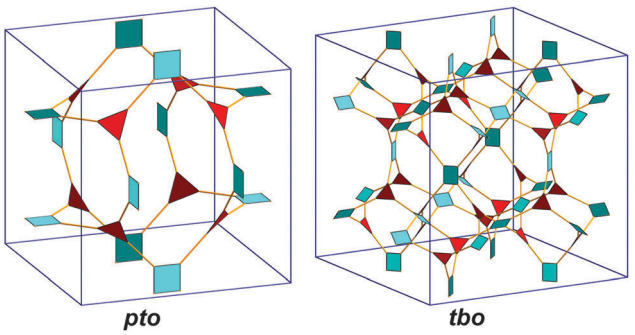

Fig. 9 **pto** and **tbo** nets shown in augmented forms. 4-Connected dicopper paddle-wheel (turquoise), tritopic carboxylate linker (red).

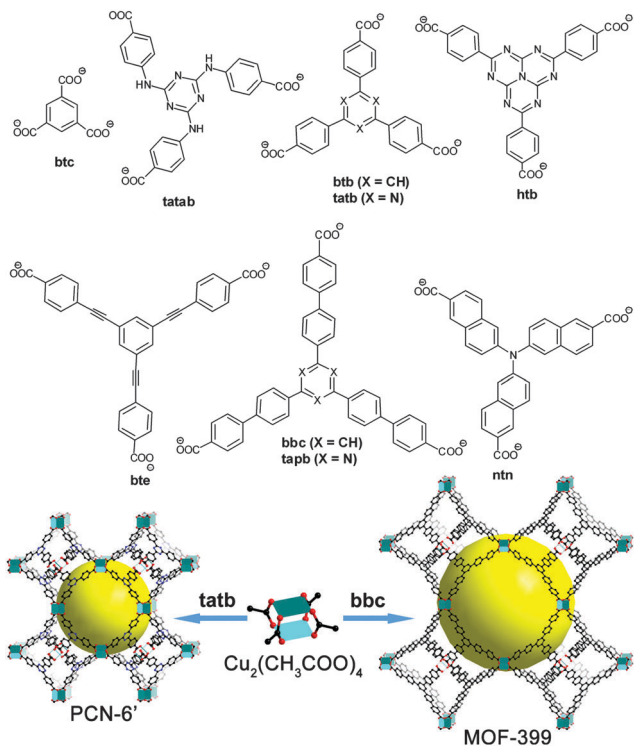

Fig. 10 Some representative tritopic carboxylate linkers and illustration of formation of extended **tbo**-topology networks with dicopper paddle-wheel SBUs. Color scheme: copper (turquoise); O (red); C (black).

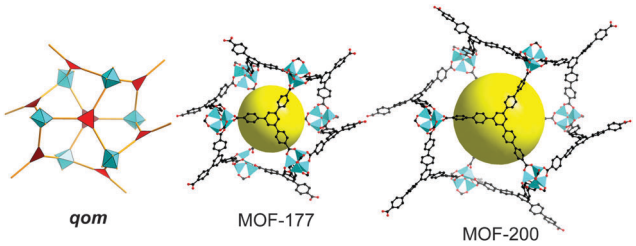

Fig. 11 A **qom** net shown in augmented form and crystal structures of representative MOFs in its net. Color scheme in **qom**: $Zn_4O(CO_2)_6$ octahedral cluster (turquoise); tritopic linker (red); color scheme in MOF-177 and -200: zinc (turquoise); O (red); C (black).

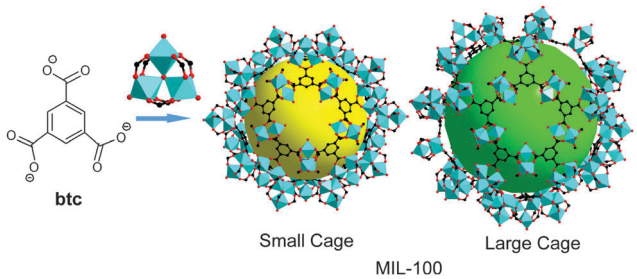

Fig. 12 Illustration of the assembly of MIL-100 from the **btc** linker and the trigonal-prismatic cluster; metal ions can be Cr^{3+}, V^{3+}, Fe^{3+}, and Al^{3+}. Color scheme: chromium (turquoise); O (red); C (black).

2.2 Tritopic carboxylate linkers with 6-connected octahedral clusters

6-Connected octahedral $Zn_4O(CO_2)_6$ clusters in combination with tritopic linkers can produce an isoreticular series of structures featuring **qom** topology (Fig. 11). The first of this series is MOF-177 reported in 2004.[34] The underlying topology of MOF-177 is a (6,3)-connected **qom** net with the centre of the octahedral $Zn_4O(CO_2)_6$ cluster as the site of 6-connection and the centre of the **btb** linker the site of 3-connection. The structure of this net plays an important role in determining pore size by preventing interpenetration. As a result, MOF-177 has extra-large pores capable of binding polycyclic organic guests such as fullerene and a number of dyes. By using extended linkers, two MOFs isoreticular to MOF-177 were reported short after: MOF-180 with 4,4′,4″(benzene-1,3,5-triyl-tris(ethyne-2,1-diyl))tribenzoate (**bte**) as linker and MOF-200 with **bbc** as linker.[79] The cell volumes of MOF-180 and MOF-200 are 1.8 and 2.7 times that of MOF-177, respectively. Contrary to the MOF-5 type IRMOF series, the expanded structures of MOF-177 are non-interpenetrated due to the **qom** topology. Both MOF-180 and -200 have extremely high porosity (89% and 90%, respectively) and ultra-high BET surface areas.

Replacing the central benzene ring with a nitrogen atom gives the linker extra flexibility; assembly of the same octahedral $Zn_4O(CO_2)_6$ cluster and **ntn** linker results in a new porous material SNU-150 with PdF_2-type net topology (**pyr**).[80]

2.3 Tritopic carboxylate linkers with 6-connected trigonal-prismatic clusters

MIL-100(Cr),[81] assembled from the $Cr_3O(CO_2)_6$ cluster and the tritopic linker **btc**, was successfully determined by the combination of simulation and powder X-ray diffraction studies. In its structure, the oxido-centered chromium trimers are interconnected by the tritopic carboxylate linkers along the edges to form the so-called "supertetrahedra (ST)", which is built of four chromium trimmers as the vertices and four organic linkers as the triangular faces. The ST are further connected with each other in a 3D fashion to yield the augmented zeolite Mobil Thirty-Nine (MTN) type of framework. The network of MIL-100 contains two types of mesoporous cages with accessible cage diameters being 25 and 29 Å (Fig. 12). The smaller cages consist of pentagonal windows and the larger cages include both pentagonal and hexagonal windows (apertures of the pentagonal and the hexagonal windows are 4.8 and 8.6 Å). Shortly after the appearance of MIL-100 (Cr), its isostructural series MIL-100 (M) (M = Fe^{3+}, Al^{3+}, and V^{3+}) was prepared by replacing the metals in the inorganic SBUs.[82–84] Such MOFs show superior hydrothermal stability and have found wide applications in adsorption/separation (gas, vapor, and liquid), heterogeneous catalysis, and drug delivery. The extended networks of MIL-100 have not been reported yet but would be anticipated with elongated tritopic linkers.

2.4 Tritopic carboxylate linkers with multiple SBUs

MOFs with two different SBUs are relatively rare and most of them involve tritopic linkers. The high-symmetry **btc** linker demonstrated to be quite versatile in the combination with multiple SBUs in a single MOF.[85] Less symmetrical linkers, however, may drive new modes of network assembly to satisfy the constraints imposed by unique linker geometries. UMCM-150 (UMCM = University of Michigan crystalline material)[86] is the forerunner of such a MOF family with two copper-containing SBUs: a dicopper paddle-wheel and a $Cu_3(CO_2)_6$ SBU with six points of extension. The two SBUs are linked by a C_{2v} symmetry linker, biphenyl-3,4′,5-tricarboxylate (**bhtc**), in which three carboxylate groups are not symmetrically equivalent. Both of the carboxylates at the 3- and 5-positions (isophthalate moiety) of the linker form dicopper paddle-wheel clusters and the carboxylate at the 4′-position (benzoate moiety) forms a $Cu_3(CO_2)_6$ cluster, a novel SBU in MOFs (Fig. 13). Thus, the underlying topology of UMCM-150 is an unusual (3,4,6)-connected net. An isoreticular MOF, named NJU-Bai3,[87] is constructed with the same SBU linked by a longer linker, 5-(4-carboxybenzoylamino)-isophthalate (**caia**). The insertion of the amide group in the linker not only extends the cell length but

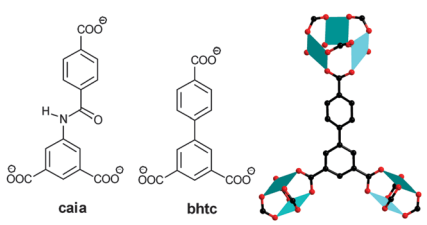

Fig. 13 Tritopic carboxylate linkers **caia** and **bhtc**; illustration of **bhtc** linker in UMCM-150 adjoined with dicopper paddle-wheel and trinuclear copper clusters. Color scheme: copper (turquoise); O (red); C (black).

also disposes densely decorated amide groups on the pore surfaces of the MOF, which significantly enhance CO_2 binding ability and CO_2 selectivity over other gas molecules. Indeed, the CO_2 uptake of NJU-Bai3 can reach 6.21 mmol g^{-1} at 273 K and 1 bar, which is substantially higher than that of UMCM-150 ($\sim$4.68 mmol g^{-1}).

3 Tetratopic carboxylate linkers

Tetratopic carboxylate linkers appear to be very intriguing building units in MOF constructions and have gained an increasing amount of attention in recent years, especially those with tetrahedral geometry. First, the tetrahedral linker has a full T_d symmetry, which is, by far, the highest symmetry in a linker that can be achieved through organic synthesis. High-symmetry building units are always preferred in MOF constructions, as they facilitate the packing process of repetitive units during the assembly of crystalline materials.[88,89] Second, the tetrahedral linker may adopt the symmetry of any T_d subgroup (Fig. 14) and generate diversity in MOF structures. Third, the tetrahedral linker is an inherently three-dimensional, fully extended strut. Once incorporated into a framework, wide channels and/or large pores will be provided to maximize the exposure of the framework struts and eliminate the "dead space". In other words, MOFs with exceptionally large porosities could be constructed with tetrahedral building units and symmetrically compatible SBUs.

Overall, tetrahedral linkers are still relatively less explored in contrast with linear and tritopic ones possibly due to the challenges in organic synthesis. Scheme 2 shows some of the representative tetrahedral carboxylate linkers.

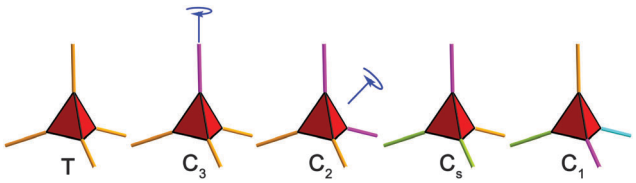

Fig. 14 Symmetry elements of a full T_d symmetry; different colours represent different coordination environments.

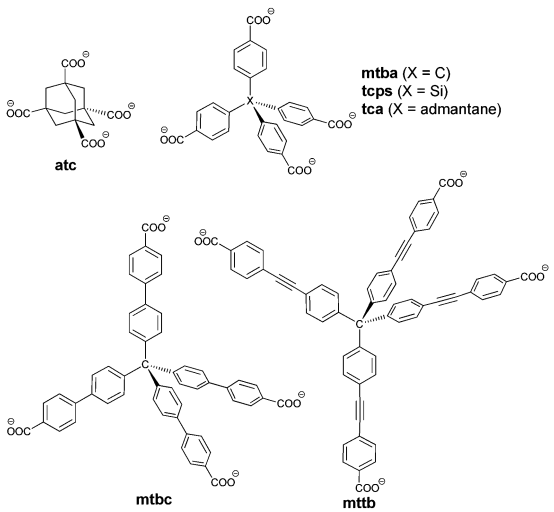

Scheme 2 Some representative tetrahedral carboxylate linkers.

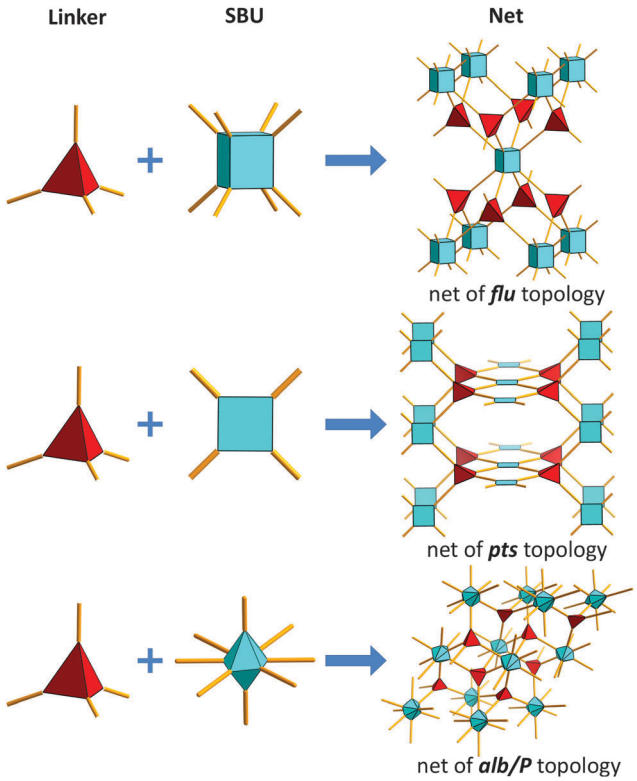

Fig. 15 Graphical representation of the topologies associated with MOFs assembled from tetrahedral linkers.

It should be noted that for a given framework, its porosity, stability and possibility of interpenetration are closely related to its net topology.[90–92] A limited number of net topologies are associated with MOFs assembled from tetrahedral linkers. Among them, the topologies of fluorite (**flu**), platinum sulfide (**pts**) and **alb**/**P** are the most prominent examples of the topologies with potential for high porosity. A graphical representation of these topologies is illustrated in Fig. 15. In particular, the **flu** topology represents a network that combines 4-connected tetrahedral linkers and 8-connected cubical SBUs in a 2 : 1 ratio. It is the default topology where these two nodes are connected by a unique link.[93,94] Similarly, the **pts** topology is the default topology that combines 4-connected tetrahedral linkers and 4-connected square planar SBUs. The **alb**/**P** topology combines 4-connected tetrahedral linkers and 8-connected hexagonal bipyramidal SBUs.

3.1 Tetrahedral carboxylate linkers with 8-connected cubical clusters

The **flu** topology is particularly fascinating for MOF construction due to its large potential cavity and non-interpenetrating nature.[95] Unlike the **dia**, **pts** or **alb**/**P** nets, whose framework may eventually suffer from self-interpenetration when elongated linkers are used, a framework with **flu** topology cannot be translated in any direction without overlapping with itself, as **flu** is not self-dual.[96] In other words, a framework with **flu** topology is not likely to undergo self-interpenetration.

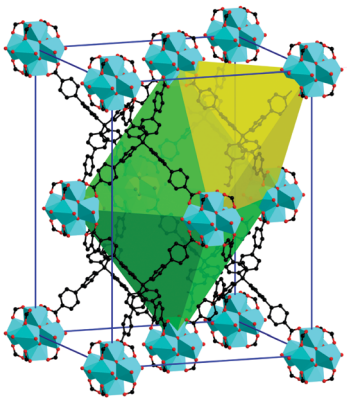

Fig. 16 The structure of PCN-521, a fluorite-topology MOF. Color scheme: Zr (turquoise polyhedra); O (red); C (black). The size of green cavity is 20.5 × 20.5 × 37.4 Å.

In order to construct a framework with fluorite topology, the key is to find an 8-connected metal-containing SBU that can be topologically represented as a cubical node.[95] Combination of a rigid tetrahedral linker (4′,4″,4‴,4⁗-methanetetrayltetrabiphenyl-4-carboxylate, **mtbc**) and the 8-connected Zr_6 cluster yielded a **flu**-topology MOF, PCN-521. A modulated synthesis strategy was adopted in the preparation of this MOF in order to improve its purity and crystallinity.[97] Single crystals of PCN-521 can be obtained by solvothermal reaction of **mtbc** and $ZrCl_4$ in DMF or DEF in the presence of a monocarboxylic acid (typically benzoic acid or trifluoroacetic acid) as a modulating reagent at 120 °C for days. Single crystal X-ray diffraction reveals that it crystallizes in the *I*4/*m* group, which is consistent with its distorted-octahedron shape. As expected, this framework contains the tetrahedral linkers and the 8-connected $[Zr_6(\mu_3\text{-}OH)_8(OH)_8](CO_2)_8$ SBUs in a 2 : 1 ratio to form a framework with the desired topology. The octahedral cavity of the fluorite structure is significantly augmented and it has the size of 20.5 × 20.5 × 37.4 Å (Fig. 16), the largest pore size of any MOF with tetrahedral linkers. The calculated solvent accessible volume of PCN-521 is 78.50%, and its BET surface area is 3411 $m^2\ g^{-1}$, and is the most porous MOF among all the MOFs assembled from tetrahedral linkers to date.[95]

Hafnium is a metal that chemically resembles zirconium in many ways. Due to the lanthanide contraction, zirconium and hafnium have almost identical ionic radii.[98] It is expected that an isotopic MOF can be obtained by replacing the zirconium polyoxo clusters with hafnium polyoxo clusters. PCN-523 was obtained by a similar solvothermal reaction of **mtbc** and $HfCl_4$ in the presence of a modulating reagent. It possesses the 8-connected $[Hf_6(\mu_3\text{-}OH)_8(OH)_8](CO_2)_8$ clusters, and its octahedral cavity has a size of 22.1 × 22.1 × 35.3 Å.

3.2 Tetrahedral carboxylate linkers with 4-connected square planar clusters

Combination of dinuclear paddle-wheel SBU and rigid tetrahedral linker usually results in a framework with **pts** topology. The non-interpenetrated **pts** net usually adopts the tetragonal space group $P4_2/mmc$. MOF-11 (Cu_2(**atc**)·$6H_2O$, **atc** = 1,3,5,7-adamantane tetracarboxylate) was synthesized through hydrothermal reaction of $Cu(NO_3)_2$ with **atc** under basic conditions at 190 °C. It exhibits a permanent porosity with a Langmuir surface area of 560 $m^2\ g^{-1}$ and a pore volume of 0.20 $cm^3\ g^{-1}$.[99] Elongation of tetrahedral linker results in a framework with larger porosity. MOF-36[100] [Zn_2(**mtba**)$(H_2O)_2$·$(DMF)_6(H_2O)_5$, **mtba** = methanetetra(4-benzoate)] consists of **mtba** linker and dizinc paddle-wheel. An isotopic structure with dicopper paddle-wheel SBU was also reported; this framework possesses open channels along all directions and its calculated solvent accessible volume is about 72%. Interestingly, the porosity of this framework is closely related with its activation method. Its experimental BET surface area can be significantly improved from 526 $m^2\ g^{-1}$ (conventional activation) to 1560 $m^2\ g^{-1}$ (freeze-drying activation). Its H_2 uptake was also significantly enhanced to 1.42 wt% from 0.78 wt%.[101]

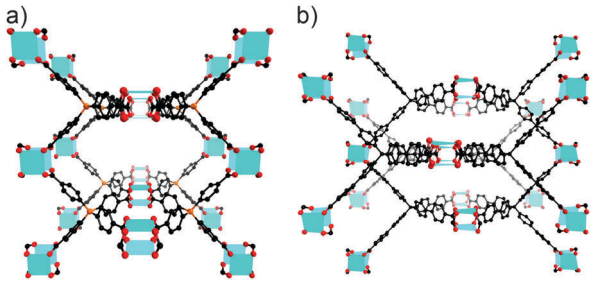

Fig. 17 The crystal structure of (a) PCN-512/IMP-9 with a **pts** topology; (b) Cu_2(**mtbc**)$(H_2O)_2$ with a doubly interpenetrated **pts** topology. Color scheme: metal (turquoise); Si (orange); C (black); O, (red).

A silicon-centered tetrahedral linker **tcps** (4,4′,4″,4‴-tetrakiscarboxyphenylsilane) has also been investigated. PCN-512[102]/IMP-9[103] were synthesized through solvothermal reaction of copper/zinc nitrate with **tcps** in *N*,*N*′-dimethylacetamide (DMA) in the presence of tetrafluoroboric acid (Fig. 17a). The calculated solvent accessible volume of PCN-512 is 72.70% and its BET surface area is 601 $m^2\ g^{-1}$. It appears that the treatment of freeze-drying procedures on this framework did not significantly improve its porosity.[102]

For **pts** topology, further elongation of the tetrahedral linker will eventually result in a self-interpenetrated framework. The combination of **mtbc** linker (in Scheme 2) and dicopper paddle-wheel generates a two-fold interpenetrated network Cu_2(**mtbc**)-$(H_2O)_2$ (Fig. 17b).[101] Due to its two-fold interpenetrating nature, the symmetry of its space group was lowered from $P4_2/mmc$ to $P\bar{4}2_1c$. Self-interpenetration has significantly reduced the size of cavities in this MOF. As a result, this framework has a solvent accessible volume of 73% and a BET surface area of 1020 $m^2\ g^{-1}$ upon freeze-drying activation. Networks with **pts**-topology were also observed for metallo linkers with tetrahedral geometry[104,105] and tetratopic linkers with twisted tetrahedral conformations.[106,107]

3.3 Tetrahedral carboxylate linkers with 8-connected hexagonal bipyramidal clusters

Combining 4-connected tetrahedral linkers and 8-connected hexagonal bipyramidal SBUs produces a net of **alb**/**P** topology. PCN-511,[102] Zn_3(H**tcps**)$_2$, was prepared through solvothermal

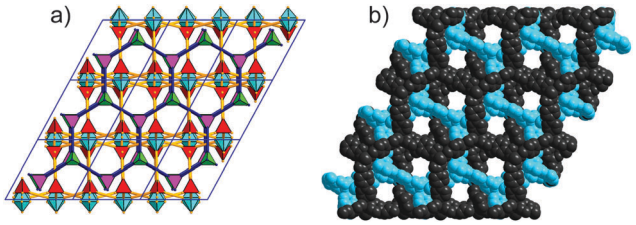

Fig. 18 (a) Graphical representation of the framework of $[Zn_4(\mathbf{mtbc})(H_2\mathbf{mtbc})_2]\cdot(DEF)_{12}(H_2O)_{40}$ that contains two distinctive interpenetrating motifs. (b) A space-filling model of this compound with motif 1 shown in black and motif 2 shown in light blue.

reaction of $Zn(NO_3)_2$ and **tcps** in DEF at 85 °C. In the structure of PCN-511, each 8-connected zinc cluster is connected to eight tetrahedral linkers, generating a 4,8-connected framework with **alb**/**P** topology. It crystallizes in the monoclinic space group *C*2/*c* and it has a solvent accessible volume of 45.60% as well as a BET surface area of 703 $m^2\ g^{-1}$. A same-connectivity MOF, IMP-11,[103] is an ionic framework with dimethylammonium cations trapped in its pores as counterions.

Frameworks with **alb**/**P** topology could also suffer from self-interpenetration. For example, when **mtbc** linker was used, a novel 3D compound containing a two-fold interpenetrated framework was obtained.[108] This MOF crystallizes in the monoclinic space group $P2_1$ and it contains two distinctive interpenetrating motifs with different topological structures (Fig. 18). Motif 1 contains a trizinc SBU that could also be found in PCN-511/IMP-11, with the same **alb**/**P** topology. Motif 2 contains a zinc cation connected by tetrahedral linkers to form a 4,4-connected network with **lon** topology. This framework possesses a solvent accessible volume of 62.40%, and it has a BET surface area of 1284 $m^2\ g^{-1}$ after activation by a freeze-drying procedure.

A few other topologies are also related to MOFs assembled from tetrahedral linkers. For example, the diamond (**dia**) topology is a 4,4-connected network observed when the tetrahedral linkers are combined with SBUs that possess a tetrahedral geometry.[109] Like **pts** and **alb**/**P**, MOFs with **dia** topology could also suffer from self-interpenetration.[110]

3.4 Non-regular tetrahedral carboxylate linkers

Non-regular tetrahedral linkers with flexibility/rigidity intrigue significant interest in MOFs because of their isomerism features.[111] In 2005, temperature-induced supramolecular stereoisomerism with semi-rigid tetracarboxylate linker *N*,*N*,*N*′,*N*′-tetrakis(4-carboxyphenyl)-1,4-phenylenediamine (**tcppda**) was reported. Solvothermal reactions of $Cu(NO_3)_2$ and **tccpda** in dimethyl sulfoxide (DMSO) at 120 or 115 °C resulted in the formation of MOFs bearing **pts** or **nbo** topologies with **tcppda** linker adopting either D_2 or C_{2h} symmetry, respectively (Fig. 19). Nitrogen sorption at 77 K showed that both **pts**- and **nbo**-type MOFs possess type I isotherms with Langmuir surface areas of 627 and 504 $m^2\ g^{-1}$, respectively. The hydrogen storage capacities are 14 mg g^{-1} and 12 mg g^{-1} at 1 bar and 77 K, respectively. The difference in hydrogen storage capacities of the two isomers was

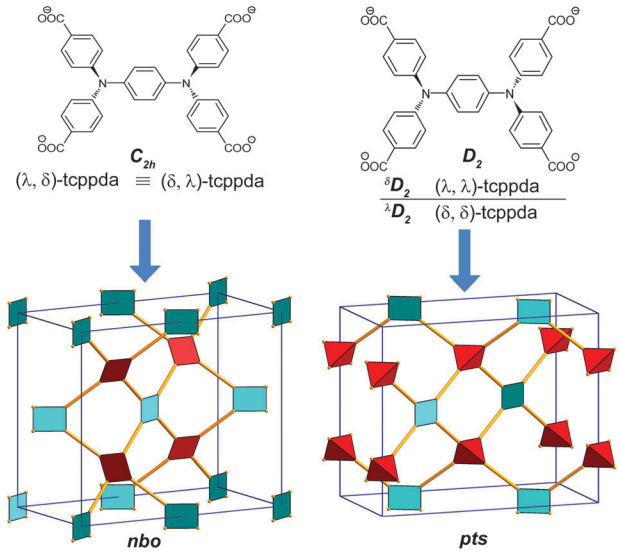

Fig. 19 The construction of MOFs with **pts** and **nbo** net topologies induced by the conformation of D_2-**tcppda** and C_{2h}-**tcppda**, respectively. Color scheme: dicopper paddle-wheel (turquoise); linker (red).

attributed to variation of porosity, consistent with structures and calculated potential solvent-accessible volumes.[112] Further investigation led to five novel MOFs with this linker adopting different geometries, indicating that a semi-rigid linker has significant advantages over a rigid one in the construction of MOFs: such a linker can adopt different geometries, according to the reaction conditions, to meet the coordination requirements of metal ions or metal-containing SBUs. This provides a new strategy in the synthesis of MOFs with various structural topologies.[113] Later, the same group discovered two isomeric phases of the **nbo**-type structure, namely PCN-16 (α phase) and PCN-16′ (β phase), which are symmetry-preserving isomers of each other. Both phases are generated from the assembly of dicopper paddle-wheel SBU and the tetracarboxylate linker, 5,5′-(1,2-ethynediyl)bis(1,3-benzenedicarboxylate) (**ebdc**). The gas sorption studies revealed that the α phase possesses a larger surface area, leading to higher hydrogen and methane storage capacity compared to the β phase.[114]

The extendibility of carboxylate linkers provides a great deal of opportunity to build isoreticular MOFs with predefined topologies. The combination of a dicopper paddle-wheel unit and 3,3′,5,5′-biphenyltetracarboxylate (**bptc**) linker leads to MOF-505,[115] an **nbo**-topology MOF with the carboxylates nearly coplanar to the biphenyl. A series of isoreticular MOF materials were obtained by extending biphenyl to erphenyl and quaterphenyl, including NOTT-100, NOTT-101, and NOTT-102 (NOTT stands for University of Nottingham)[116] with the formula $[Cu_2(\mathbf{L})(H_2O)_2]$ (**L** = tetracarboxylate linkers). The single crystal X-ray study of the NOTTs confirmed that each dicopper paddle-wheel SBU was bridged by four carboxylates to form an **nbo**-topology network. The BET surface areas for desolvated NOTT-100 to NOTT-102 were measured to be 1670, 2247, and 2932 $m^2\ g^{-1}$, respectively. The maximum H_2 uptakes for these three MOFs were estimated to be as high as 4.20 wt%, 6.70 wt% and 7.01 wt%, respectively. In 2009, a systematic expansion of

this **nbo**-type NOTT series was reported by the same group;[117] activation by solvent exchange with acetone coupled with heating cycles under vacuum afforded the desolvated porous materials NOTT-103 to 109. Vacant coordination sites at Cu^{2+} and large pore volume contribute to the high H_2-adsorption capacity. Indeed, NOTT-103 at 77 K and 60 bar shows a very high total H_2-adsorption capacity of 7.78 wt%. The pentaphenyl linker in NOTT-104 led to a doubly interpenetrated network, which has the same network topology as the other systems discussed herein. However, the interpenetration led to reduced porosity, rendering NOTT-104 unsuitable for sorption applications. A pre-synthetic modification strategy was applied to introduce the functionalized groups into the framework NOTT-102, giving NOTT-110 and NOTT-111 by linker curvature (Fig. 20).[118]

PCN-46[119] was synthesized based on an *in situ* formed polyyne-coupled diisophthalate linker by the copper(I)-catalyzed oxidative coupling of terminal acetylenes. The polyyne units in the MOF exhibit high heat of hydrogen adsorption and high pore volume, which is consistent with experimental results and computational simulation.[120] A series of **nbo**-type porous materials isostructural to NOTT-101 with various dialkoxy-substituents were reported by the same group. The moisture stability is increased upon extending the hydrophobic pendant chains, resulting in a superhydrophobic material when $-O^nHex$ is the substituent on the central phenyl ring.[121]

5,5′-(9,10-Anthracenediyl)diisophthalate (**adip**) was synthesized and crystallized with the dicopper paddle-wheel cluster in the *R*-3*c* space group to form a **nbo**-type MOF, namely PCN-14.[122,123] In the linker, the four carboxylate groups and the two phenyl rings of the isophthalate motifs are almost in the same plane, whereas the dihedral angle between the anthracene and the phenyl rings is 70.4°. The Langmuir surface area and pore volume for PCN-14 at 77 K were 2176 $m^2\ g^{-1}$ and 0.87 $cm^3\ g^{-1}$. The built-in anthracene helps to segregate the big cavity into three nanoscopic cages. High-pressure methane adsorption studies showed that PCN-14 exhibited an absolute methane-adsorption capacity of 230 v/v, record high among those reported for methane-storage materials until 2013 when HKUST-1 was found to outperform PCN-14.[124]

NOTT-202, a unique material with partial interpenetration, was assembled from mononuclear $In(CO_2)_4$ SBU and tetracarboxylate linker biphenyl-3,3′,5,5′-tetra-(phenyl-4-carboxylate).[125] The framework structure consisted of two crystallographically independent nets (A and B). The second partial structure net B showed an occupancy of 0.75, thus forming defects throughout the structure. NOTT-300, a MOF constructed from **bptc** (as in MOF-505) and the octahedral chain of $[AlO_4(OH)_2]_\infty$, was reported by the same group. This overall connectivity affords a porous 3D framework structure with 1D channels, and its unique structure was found to facilitate the carbon dioxide and sulfur dioxide capture.[126]

Metal–organic polyhedra (MOPs) are discrete metal–organic molecular assemblies. They are useful as host molecules that can provide tailored internal metrics, functionality, and active metal sites.[127] A MOP can be formed by linking 0°-bridging-angle linker 3,3′-(naphthalene-2,7-diyl)dibenzoate and dinuclear paddle wheel SBU (Fig. 21). This MOP was designated as single molecule trap (SMT) because the metal–metal distance (6.4–8.0 Å) is ideal for holding a CO_2 molecule. In order to build the assembled SMTs into highly porous solids, a linker with two types of carboxylate groups was designed, one to support the SMT and the other for the formation of an extended framework. Accordingly, a tetracarboxylate linker 5,5′-(naphthalene-2,7-diyl)-diisophthalate was designed and synthesized by adding two additional carboxylate groups onto 3,3′-(naphthalene-2,7-diyl)-dibenzoate. Thus, an extended framework PCN-88 with built-in SMTs can be assembled in a one-pot reaction.[128] The high Henry's law selectivities of CO_2 over CH_4 and N_2 (7.3 and 67.9 at 273 K, respectively) suggest potential application of PCN-88 in capturing CO_2 from flue gas or upgrading natural gas.

Another MOP-based MOF structure from tetratopic linkers featuring 90° carbazole-3,6-dicarboxylate moieties was reported recently. In the structure, the octahedral cage contains six dicopper paddle-wheel SBUs as vertices and twelve carbazole moieties as edges, which is extended to three dimensional frameworks by connecting to twelve surrounding octahedral cages. It exhibits very high microporosity with a BET surface

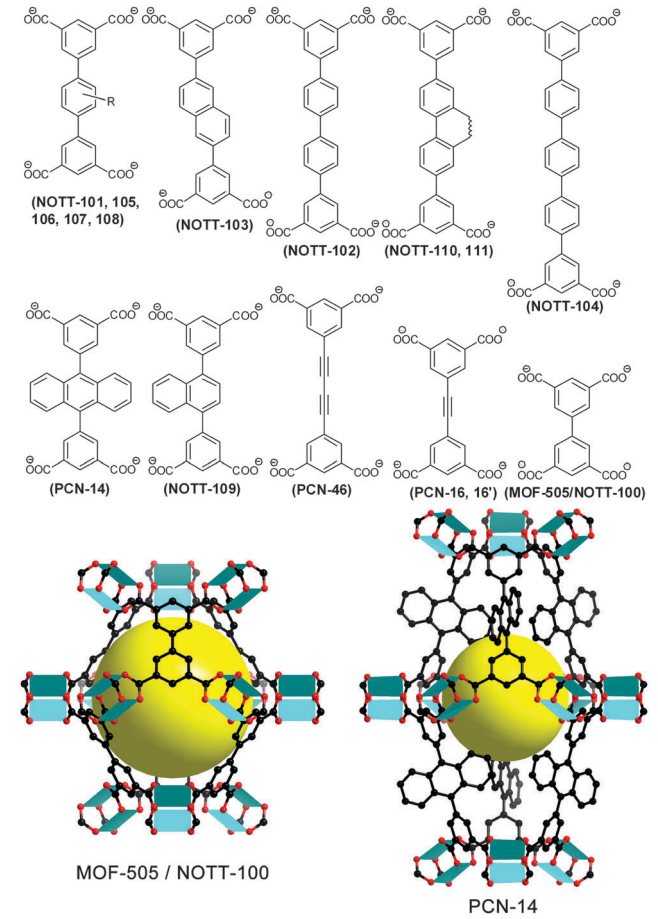

Fig. 20 Some representative tetratopic diisophthalate linkers. In parentheses are the names of MOFs synthesized accordingly; the formation of pore structures in MOF-505/NOTT-100 and PCN-14 with dicopper paddle-wheel is highlighted. Color scheme: Cu (turquoise); Si (orange); C (black); O (red).

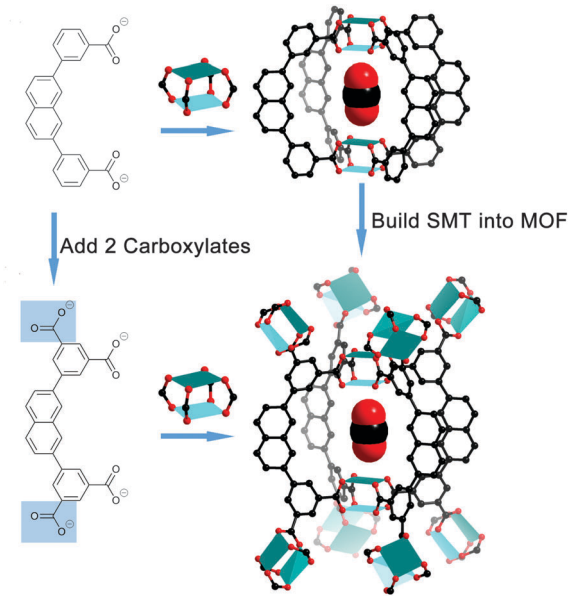

Fig. 21 Linker design for building a pre-designed single molecule trap (SMT) into extended porous solids.

area of 4488 $m^2\ g^{-1}$.[129] At the same time, a highly porous MOF (DUT-49) was synthesized with a one phenylene extended linker 9,9′-([1,1′-biphenyl]-4,4′-diyl)bis(9*H*-carbazole-3,6-dicarboxylate) (**bbcdc**) with a BET surface area of 5476 $m^2\ g^{-1}$ and gravimetric excess methane uptake as high as 291 mg g^{-1} at 80 bar and 298 K.[130]

4 Hexatopic carboxylate linkers

4.1 Hexatopic linkers with 1,3-benzenedicarboxylate units

Linking 24 isophthalate moieties with 12 dinuclear paddle-wheel units forms a cuboctahedron, which can be linked together to form 3D MOFs *via* either coordination bonds or covalent bonds,[132–134] therefore, often referred to as a super-molecular building block (SBB). 5,5′,5″-[1,3,5-Benzenetriyltris(carbonylimino)]tris-1,3-benzenedicarboxylate, a semi-rigid hexatopic linker with C_3 symmetry, was used to construct a MOF with a (3,24)-network topology, where the nanometre-sized SBBs (cuboctahedra) have been incorporated into a cubic close packing (CCP) arrangement, leading to superoctahedral and supertetrahedral cavities.[131] It is critical that, in order to form the aforementioned (3,24)-connected net, the six carboxylate groups in the C_3-symmetric linker must be coplanar (Fig. 22).[135] This (3,24)-connected **rht** topology has been utilized progressively in the practice of isoreticular chemistry, where higher surface areas and larger free pore volumes have been achieved through expansion of the organic linker.

A series of isoreticular (3,24)-connected mesoporous MOFs (PCN-61, -66, -69, and -610) were assembled from dicopper paddle-wheel units and the corresponding hexatopic linkers.[135–137] These MOFs are stabilized by incorporating microwindows, whose size is fixed by the formation of cuboctahedra and supported by the isophthalate moieties throughout the framework. The mesocavities, which are connected by the microwindows, however, are sustained by these nanoscopic linkers and attributed to the porosity improvement with the linker elongation. In addition, the formation of isophthalate-sustained cuboctahedra in the (3,24)-connected network prohibits framework interpenetration, leading to MOFs with close to record-high surface areas. Hydrogen, methane, and carbon dioxide adsorption studies of MOFs in this series also revealed close to record-high gas-adsorption capacities.[136]

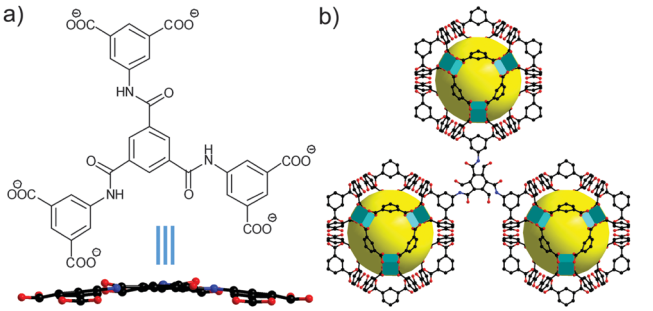

Fig. 22 (a) Linker 5,5′,5″-[1,3,5-benzenetriyltris(carbonylimino)]tris-1,3-benzenedicarboxylate and its conformation in **rht**-MOF; (b) crystal structure of **rht**-MOF composed of nano-sized cuboctahedra covalently linked by C_3 symmetric organic moieties to construct a highly connected (3,24)-network.[131]

By applying supercritical carbon dioxide activation,[138] NU-100 (NU = Northwestern University), synthesized from further elongated linker 5,5′,5″-(((benzene-1,3,5-triyl-tris(ethyne-2,1-diyl))-tris(benzene-4,1-diyl))tris(ethyne-2,1-diyl))triisophthalate (**ttei**), can retain structure integrity after removing guest solvent molecules.[139] It exhibits ultrahigh surface areas and gas storage capacities, and these values are in good agreement with the simulated data. With the help of computational modelling, the surface area limit was pushed even further by using more acetylenes in the organic linkers; solvothermal reaction of 1,3,5-tris[((1,3-carboxylic acid-5-(4-(ethynyl)phenyl))ethynyl)phenyl]-benzene and $Cu(NO_3)_2$ in DMF–EtOH–HCl at 75 °C afforded NU-110E (Fig. 23), featuring the same (3,24)-connected **rht** topology. It displays the highest

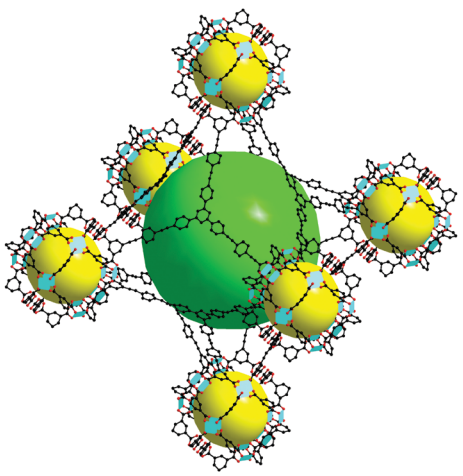

Fig. 23 Crystal structure of NU-110E with **rht** topology.[15]

experimental BET surface areas of any porous materials reported to date (7140 m^2 g^{-1}); the authors also demonstrated computationally that by shifting from phenyl groups to "space efficient" acetylene moieties as linker expansion units, the hypothetical maximum surface area for a MOF material is substantially greater than that previously envisioned [~14 600 m^2 g^{-1} (or greater) *versus* ~10 500 m^2 g^{-1}].[15] This may save experimentalists enormous amounts of time and effort as well as enable the efficient discovery and assessment of promising MOFs in the future.[120]

Hexatopic linkers featuring isophthalate moieties have been widely studied in pursuing MOFs with high surface area and gas storage capacity, such as NOTTs,[140–144] **rht**-MOFs,[145–147] PMOFs,[148,149] and others.[150–155] It is interesting to point out that one of the hexatopic linkers was not observed to take on the (3,24)-connected **rht** net; UTSA-20, assembled from 3,3′,3″,5,5′,5″-benzene-1,3,5-triyl-hexabenzoate (**bhb**) and dicopper paddle-wheel SBU, represents a unique case in hexatopic linkers with C_3 symmetry. The three isophthalate groups of each linker are non-coplanar because the four phenyl rings within **bhb** are tilted with respect to each other owing to the steric hindrance between the central and peripheral phenyl rings. Thus the resulting structure adopts a (3,3,4)-*c* trinodal **zyg** topology.[153] UTSA-20 and other structures[156] based on **bhb** linker demonstrate that coplanar conformation of the six carboxylate groups is crucial to form the (3,24)-connected **rht** net. The open copper sites and optimal pore spaces within UTSA-20 enable the pore spaces to be fully utilized for methane storage, rendering UTSA-20 the material with absolute volumetric methane storage capacity surpassing the Department of Energy methane storage target of 180 cm^3 cm^{-3} at room temperature and 35 bar.[153] The conformation of hexacarboxylate linker determines the resulting structures; if three methyl groups were put on the central phenyl ring of **bhb** linker, the created steric hindrance would drive the isophthalate units to be nearly perpendicular to the central phenyl ring. With this linker (**tmbhb**), two new (3,24)-connected **rht** networks (SDU-1[154] and NPC-5[155]) were obtained; both of them have 3-connected and 4-connected dinuclear paddle-wheel SBUs. Therefore, SBBs sustaining the frameworks are obviously different from aforementioned examples (Scheme 3).

4.2 Hexatopic linkers with 4,4′-azanediyldibenzoate units

Apart from backbone elongation, the distance between carboxylates on the same moieties can also be expanded. As in the case of linker **tta** (H_6**tta** = 4,4′,4″-tris(*N*,*N*-bis(4-carboxylphenyl)-amino)triphenylamine), nine phenyl rings surround three nitrogen atoms, adopting trigonal prismatic conformation in the crystal structure. The 6-connected **nia** net was found in MODF-1 (MODF = metal–organic dendrimer framework). It shows type-I sorption behaviour; the isotherms are reversible and show no hysteresis upon desorption. MODF-1 is the first example of dendritic carboxylate linker used in the construction of MOFs and the only example of hexatopic linker with 4,4′-azanediyldibenzoate subunits (Fig. 24).[157]

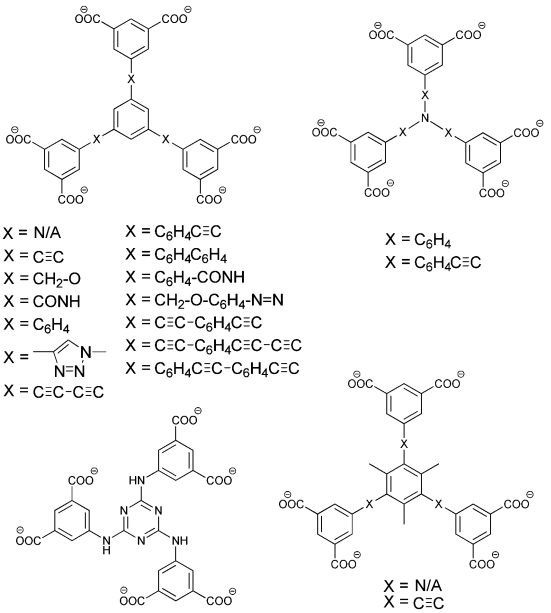

Scheme 3 Some representative hexatopic carboxylate linkers with isophthalate moieties.

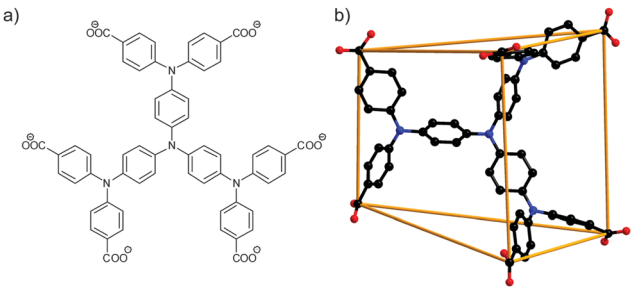

Fig. 24 (a) Linker **tta**; (b) **tta** trigonal prismatic conformation in the crystal structure of MODF-1.

4.3 Hexatopic linkers with 1,1′:3′,1″-terphenyl-4,4″-dicarboxylate units

The distance between carboxylates on the same moieties can be further expanded to 120°-bended three phenylene units. If no obvious steric hindrance embedded, these linkers could still take on planar conformation and form (3,24)-connected **rht** networks sustained by larger cuboctahedra, as in the case of **L1** [H_6**L1** = 1,3,5-tris[(1,3-di(4′-carboxylic acid-phenyl)-phenyl)-5-ethynyl]benzene][158] and **L2** [H_6**L2** = tris-(4-(5′-ethynyl-1,1′:3′,1″-terphenyl-4,4″-dicarboxylic acid)-phenyl)-amine].[146] It is interesting to point out that **L1** takes octahedron conformation when assembled with octahedral $Zn_4O(CO_2)_6$ clusters likely due to the added flexibility. In the case of linkers **tdcpb** and **Me-tdcpb**, conformations in the crystal structures are restricted to non-planars (trigonal prism and octahedron) due to the repulsion between either hydrogens or hydrogens and methyl groups on adjacent phenyl rings; therefore, various networks with topologies other than the (3,24)-connected **rht** net were formed (Fig. 25).[159–162]

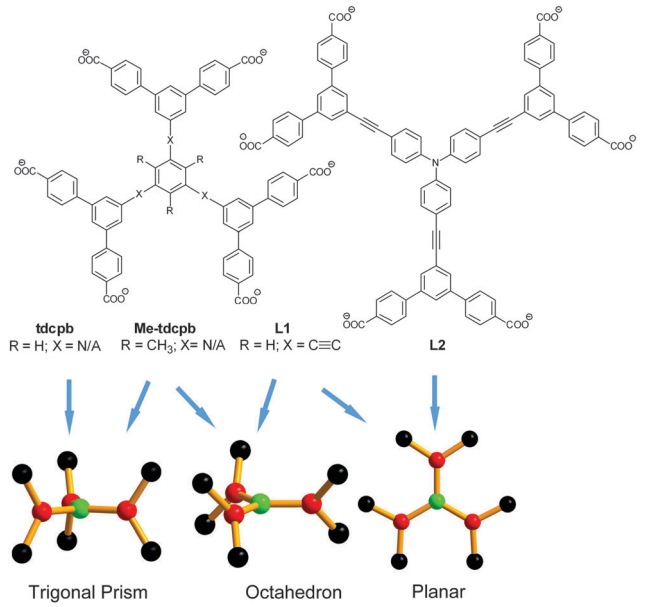

Fig. 25 Some representative hexatopic linkers with 1,1′:3′,1″-terphenyl-4,4″-dicarboxylate moieties and their conformations reported in the literature.

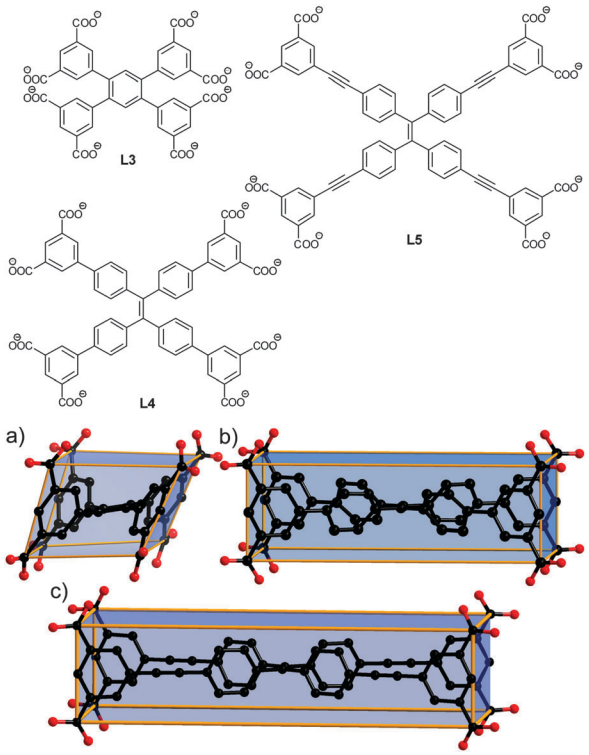

Fig. 26 Some representative octatopic carboxylate linkers and their geometries in crystal structures. (a) **L3**; (b) **L4**; (c) **L5**.

5 Octatopic carboxylate linkers

MOFs with octatopic carboxylate linkers are still rare possibly due to the synthetic challenges in linkers themselves. It has been well known that the frameworks based on linkers with long arms tend to form interpenetrated structures. However, examination of previously reported MOFs constructed from octacarboxylate linkers suggests that polytopic linkers may effectively prevent the interpenetration possibly due to the high connectivity.

UTSA-33a,[163] a microporous MOF, was synthesized by using the octatopic linker **L3** and the zinc metal source. Each metal cluster and organic linker can be regarded as 4- and 8-connected nodes respectively, which are linked together to form a non-interpenetrated 4,8-connected network with **flu** topology. The moderate pore size renders the structure with high selection of acetylene, ethylene and ethane over methane. Using the same linker, another microporous MOF (USTA-34b[164]) with high separation capacity was obtained from assembly with dicopper paddle-wheel. The resulting framework displays **ybh** topology wherein the linker can be considered as a six connected node with two carboxylate groups protonated. Further investigation of the structures of these two MOFs indicates that the steric effect forces the peripheral phenyl rings to deviate from the plane of the central phenyl ring with a dihedral angle of about 50°. As a result **L3** adopts triclinic prism geometry in these frameworks as shown in Fig. 26a.

Assembly of linker **L4** with dizinc paddle-wheel leads to microporous MOF PCN-921 with **scu** topology.[165] Because of the steric effect, the ethylene group and the neighbouring phenyl ring, as well as the vicinal phenyl ring, lie in different planes with the dihedral angles ranging from 40° to 50°. As a result, the peripheral isophthalate moieties are perpendicular to the ethylene group and the linker adopts the standard rectangular prismatic geometry as shown in Fig. 26b. An ethynyl-extended linker **L5** was reported shortly after.[166] The ethynyl group exhibits cylindrical symmetry and is known to promote barrierless torsional motion for vicinal phenyl rings. As a result, the phenyl rings in each arm are lying in the same plane and perpendicular to the central ethylene group (Fig. 26c). Thus this linker adopts the same geometry as **L4** and forms a framework isoreticular to PCN-921. It is worth noting that the minimization of the torsional barrier for the phenyl ring leads to a fluorescent material within a near dark state. This study indicates that, in addition to structure design and control, consideration of the steric effect and torsional barrier during linker design can also be used to impart certain physical properties to frameworks.

Organic linkers with tetrahedral geometry are always on the top list for MOF construction due to the preinstalled 3D geometry. Solvothermal reactions of octadentenate carboxylate linker 5,5′,5″,5‴-silanetetrayltetraisophthalate **L6** and different metal salts afford three new microporous MOFs with interesting structure and properties.[167] An extended tetrahedral octacarboxylate linker **L7** was solvothermally reacted with $Cu(NO_3)_2$ to produce a highly porous MOF, named NOTT-140.[167] The sp^3 hybridization of central atoms dictates these two linkers to adopt tetrahedral geometry with the angles between two arms ranging from 110° to 130°. The appropriate angle allows the central atoms to act as vertices in the cage building; the central

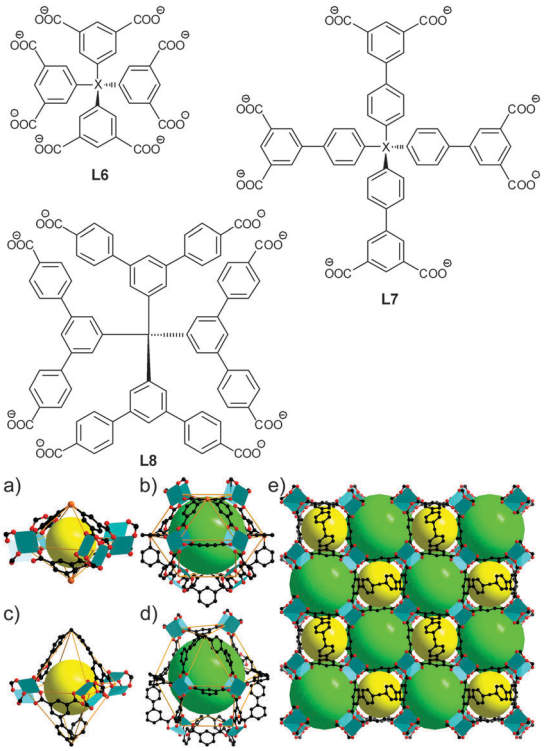

Fig. 27 Some representative octatopic carboxylate linkers with tetrahedral geometry. Views of the structures: octahedral cage (a) and cuboctahedral cage (b) assembled from linker **L6** and dicopper paddle-wheel;[167] octahedral cage (c) and cuboctahedral cage (d) assembled from linker **L7** and dicopper paddle-wheel;[168] the packing of cages along the crystallographic *c*-axis in NOTT-140.[168]

silicon (or carbon for **L7**) atoms are placed at the top and bottom of the octahedron while the four dicopper paddle-wheel units are arranged in a square plane in the middle of the octahedron (Fig. 27a and c). The slightly distorted cuboctahedral cage is composed of eight dicopper paddle-wheels and four silicon atoms (Fig. 27b and d). These two frameworks can be viewed as the alternative packing of octahedral and cuboctahedral cages in the ratio of 1 : 1 with **scu** topology by considering dicopper paddle-wheel as a 4-connected node and the linker as an 8-connected node. Linker **L8** can be seen as a tetrahedral carbon branching out with four 3,5-bis-[(4-carboxy)phenyl]phenyl groups. The angle between two carboxylate groups from the same arm is about 120°. Based on this linker, two MOFs with **sql** and **tph** topologies were obtained when assembled with dicopper paddle-wheel and $Zn_3(\mu_3\text{-OH})$ clusters, respectively.[169] Although displaying geometry similar to **L6** and **L7**, linker **L8** acts as 4- and 6-connected nodes instead of the 8-connected node in frameworks because of the incomplete deprotonation. Further investigation of the structure indicates that the very compactness of the four bulky 3,5-bis[(4-carboxy)phenyl]phenyl groups keeps the linker from approaching each other, and therefore some of the carboxylate groups were isolated as protonated even synthesized in a high temperature (100 °C) and basic environment (addition of NH_4OH). In this case, structure modification to release the

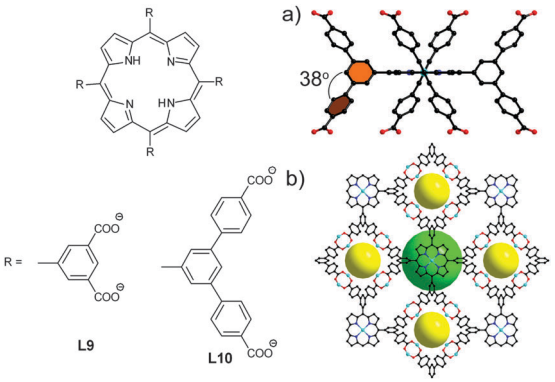

Fig. 28 Octatopic linkers **L9** and **L10**. (a) View of the geometry of the linker **L10** in crystal structure; (b) the 3D packing in UNLPF-1.[170]

steric hindrance will effectively avoid the incomplete coordination of carboxylate groups. This approach was well realized in linkers **L9**, **L10**, and **L11**, wherein the central carbon atom is replaced by spacious aromatic rings and all the carboxylates participate in the framework construction.

With the porphyrin plane as the core branching out four V-shaped arms, **L9** and **L10** are versatile linkers for constructing MOFs.[170–173] The reaction of **L10** and dizinc paddle-wheel leads to the isolation of UNLPF-1.[170] Because of the steric effect, in the crystal structure, the three phenyl rings of 3,5-bis-[(4-carboxy)phenyl]phenyl groups are not coplanar and the dihedral angle is about 38° (Fig. 28). In this case, the 3,5-bis[(4-carboxy)phenyl]phenyl groups are not perpendicular to the porphyrin plane. It can be found that each **L10** linker connects with two cages above and below the porphyrin plane. However, the four arms can only construct channels on the side face of the porphyrin plane because the existence of the dihedral angle makes the two carboxylates point in opposite directions and keep from forming a closed curve required for cage formation. As a result, UNLPF-1 is a highly porous MOF constructed with truncated octahedra and square-shaped channels.

Compared with **L10**, linker **L11** has a biphenyl core connected with four carbazole arms with two carboxylate groups located at the 3 and 6 positions. Reacting the linker with dicopper paddle-wheel can produce a highly microporous MOF, namely PCN-80.[174] Investigation of the structure difference between PCN-80 and UNLPF-1 provides more clues on how the steric effect influences the final structure. It can be found that in PCN-80 the carbazole arms are perpendicular to the central biphenyl ring, while the angle between the carboxylate group and the porphyrin plane is about 130°. With four carbazole arms being parallel to each other, the linker connects with cages not only above and below the biphenyl plane, but also on the four sides of the biphenyl plane as shown in Fig. 29. Therefore, PCN-80 is a cage-based MOF constructed with three kinds of cages in different sizes. Both UNLPF-1 and PCN-80 display the **scu** topology by considering the linker as an 8-connected node and dicopper paddle-wheel as a 4-connected node. Here we should mention that the examples given here

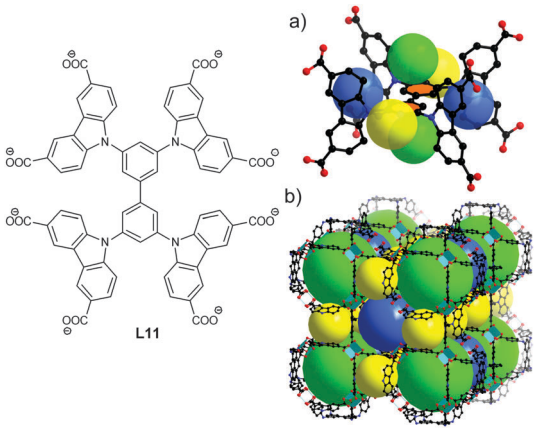

Fig. 29 Octatopic linker **L11**. (a)View of the geometry of the linker **L11** in crystal structure; (b) the 3D packing of PCN-80.[174]

provide a good opportunity for understanding the deconstruction procedure in topological analysis.[85] For MOFs with complicate linkers, the process of deconstruction is less obvious and different procedures have been carried out by different research groups. If two MOFs were deconstructed as the same topology but in fact were fundamentally different, some information may be lost during the deconstruction. For linkers like **L11**, considering each branch point explicitly as a vertex can include valuable information. Based on this point of view, the authors suggest that the PCN-80 be deconstructed as the 3,3,4-*c* 3-nodal **lwg** net considering **L11** as a 3,3-connected node, and UNLPF-1 be deconstructed as the 3,4,4-*c* 3-nodal **fjh** net considering **L11** as a 3,4-connected node. The importance of this principal topological knowledge was nicely illustrated in these examples, and more importantly, we can evaluate potential structure on the basis of this concept for linker design.

A series of isoreticular frameworks were synthesized by chiral 1,1′-binaphthyl-derived octacarboxylate linkers **L12** and **L13** bearing different R groups (Scheme 4). MOF assembled from **L12** and dicopper paddle-wheel crystallizes in the asymmetric space group of *P*4 with **scu** topology. The porosity trend is consistent with the decreasing bulkiness of benzyloxyl, ethoxyl and hydroxyl groups at the binaphthyl rings of the linkers, which indicates that the MOF porosity could be

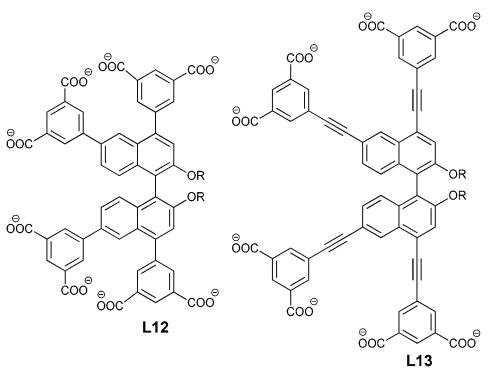

Scheme 4 Representative octatopic carboxylate linkers with chirality.

controlled by introduction of different side chains during linker design. Elongating **L12** to **L13**, the obtained structures remain in the same space group as well as topology. Again this is an example of construction of isoreticular frameworks by introduction of ethynyl groups in linker to minimize torsional motion of vicinal phenyl rings.[175,176]

6 Mixed linkers

6.1 Ditopic–ditopic linear linkers

Multivariate MOFs (MTV-MOFs) are assembled from linkers with different functional groups whose orientation, number, relative position, and ratio along the backbone (metal-oxide and phenylene units) are controlled by virtue of the unchanged length of the linker and its unaltered connectivity.[177] In MTV-MOF-5, although the backbone (zinc oxide and phenylene units) of the frameworks was regularly ordered, the distribution of functional groups was randomly disordered in three different ways based on interactions between linkers (Fig. 30). First, linkers with no preferences (or attractions) are randomly dispersed throughout the crystal structure. Second, linkers with preferential interactions with each other lead to cluster formation. Finally, linkers with preferential interactions with different linkers form alternating arrangement. Different interactions between linkers can lead to different apportionment scenarios, which were demonstrated by using solid-state nuclear magnetic resonance measurements combined with Monte Carlo and molecular dynamics simulations.[178] Interestingly, MTV-MOFs showed enhanced selectivity for CO_2 capture and H_2 uptake compared to mixtures of single-linker derived materials.

Random mixed-linker coordination copolymers could achieve enhanced properties compared to either homopolymer. The suppressing effect on interpenetration was demonstrated in a biphenyl-based IRMOF series by using a mixed-linker strategy.[179] The presence of 9,10-bis(triisopropylsilyloxy)phenanthrene-2,7-dicarboxylate (**tpdc**) in the reaction of 3,3′,5,5′-tetramethyl-4,4′-biphenyldicarboxylate (**Me_4bpdc**) with $Zn(NO_3)_2$ in DEF solution leads to a non-interpenetrated mixed-linker MOF, in which the less bulky **Me_4bpdc** linker increased the proportion of accessible adsorption sites, resulting in a higher surface area (up to $\sim$3000 m^2 g^{-1}) than that of the non-interpenetrated Zn_4O(**tpdc**)$_3$ and interpenetrated Zn_4O(**Me_4bpdc**)$_3$ frameworks. Later, the same group demonstrated a new mixed-linker strategy

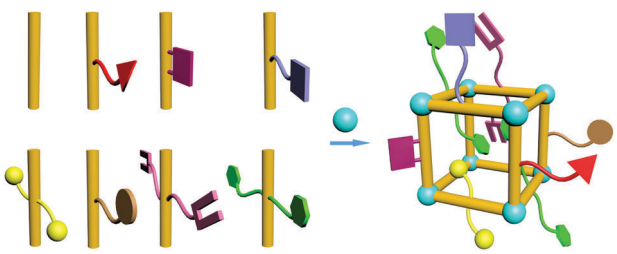

Fig. 30 Illustration of MTV-MOF-5 structure with eight different functionalities.[177]

by using two linear linkers with different lengths. In UMCM-8 (Zn_4O(**bdc**)$_{1.5}$(**ndc**)$_{1.5}$) and UMCM-9 (Zn_4O(**ndc**)$_{1.5}$(**bpdc**)$_{1.5}$), the two linkers are commercially available. By enforcing different spacings between network nodes, the interpenetration of the frameworks was suppressed, resulting in exceptional surface areas which cannot be obtained in single-linker derived MOFs.[180]

6.2 Tritopic carboxylate–ditopic carboxylate linkers

Two linkers that are coordinatively identical but distinct in shape could form new MOF structures. **bdc** as the organic linker yields MOF-5, while **btb** affords MOF-177 under essentially same synthetic conditions. Combining these two linkers in the presence of zinc nitrate leads to a completely new MOF, UMCM-1, with both linkers involved in assembly.[181] A systematic study (ditopic linker plus tritopic linker plus $ZnO_4(CO_2)_6$ octahedral cluster) demonstrated that both the geometric factor (length ratio between two linkers) and the statistical factor (mole fraction of two linkers) played critical and interactive roles in determining MOF structures that were formed.[182] Slight changes in these two factors could result in significantly different MOF structures (UMCM-1, 2, 3, and 4) or failure of coassembly (Fig. 31). By using a mixed-linker strategy, several MOFs with ultrahigh porosity were reported in 2010.[79] Among them, MOF-210, coassembled from the ditopic linker **bpdc** and the tritopic linker **bte** as well as the $ZnO_4(CO_2)_6$ octahedral cluster, reached the then-record-high surface area (BET over 6000 $m^2\ g^{-1}$). Another example of this mixed-linker strategy is DUT-6, a non-interpenetrated mesoporous MOF obtained from the reaction of **btb**, **ndc**, and $Zn(NO_3)_2$ in a ratio of 3 : 2 : 14.[183]

6.3 Carboxylate–pyridine linkers

Pillared-layer MOFs are one of the well-studied mixed-linker structures (Fig. 32). Their flexibility, interpenetration, and framework elasticity make them unique from other MOF structures.

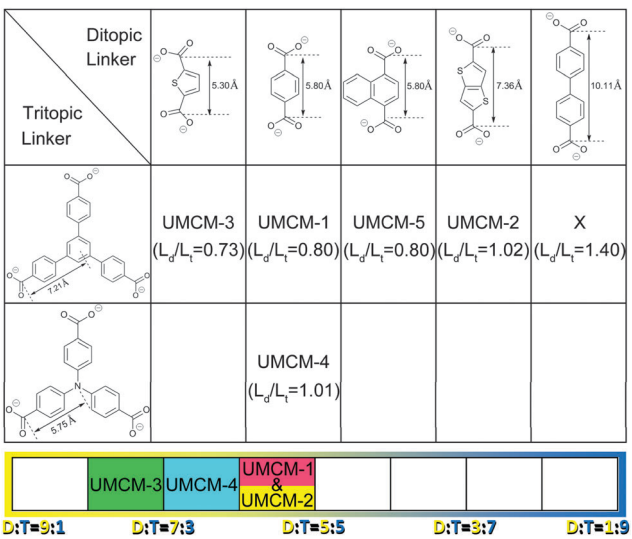

Fig. 31 The combinations and ratios of tritopic and ditopic linkers used for the preparation of UMCM-1, 2, 3, and 4.

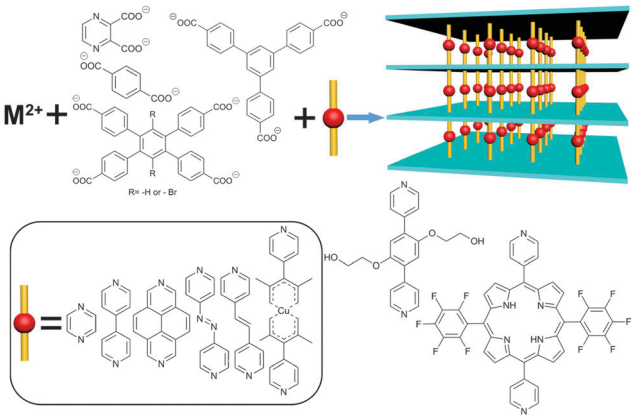

Fig. 32 Synthetic scheme for MOFs with polycarboxylate and dipyridyl linkers.

The pyridyl derivatives were usually used as pillar linkers to link 2D sheets into pillared-layer structures.[184,185] In this system, the 2D sheets functioned as scaffolds for dipyridyl linkers, allowing diverse functionalities to be incorporated into MOFs. Simple modification of the dipyridyl linker can change the channel size and functionality as well as adjust the degree of flexibility and hydrophobicity of the framework while maintaining its pillared-layer structure. For example, the rotatable pillar bearing ethylene glycol side chain acts as a molecular gate with locking–unlocking interactions in response to guest inclusion.[186] In addition, the slight difference in the pillar linkers (–N═N– *versus* –CH═CH–) could lead to distinct selectivity of H_2O and methanol over others owing to guest-responsive expanding and shrinking aperture of the channels.[187] The $-SO_3^{2-}$ group on the surface induces a polarized environment and strong acid–base interaction with acidic guests like CO_2.[188] The same group also demonstrated that the crystal size of a two-fold-interpenetration pillared-layer framework regulates the structural flexibility.[189] Crystal downsizing to the mesoscale induced metastable open dried phase by restraining the structural mobility and stabilizing the unusual open dried phase.

Control over catenation in a pillared paddlewheel metal–organic framework was achieved *via* solvent-assisted linker exchange of a previously reported non-interpenetrated material.[190–192] Furthermore, non-interpenetrated ZnPO-MOF constructed by using a bulky porphyrin linker showed a high degree of porosity, accessible by substances for catalytic reactions.[193] The porphyrin moiety in the framework as an analogue of a homogeneous catalyst functioned as a well-defined, single site catalyst allowing shape-, size-, chemo-, or enantioselective catalytic reactions. Redox active linkers within a pillared-layer MOF allowed doping the framework with alkali metal ions through the framework reduction process, leading to remarkably enhanced H_2 sorption.[194,195]

Four porous isostructural mixed-metal–organic frameworks (M′MOFs) have been synthesized and structurally characterized. The pores within these MMOFs are systematically tuned by the interplay of both the metallolinkers and organic linkers.[196] The chiral spaces in MMOFs were used for both chiral

and achiral separation of small molecules. A chiral porous zeolite-like MOF was constructed with mixed linkers of dipyridylfunctionalized chiral Ti(salan) and **bpdc**.[197] The framework shows an efficient and recyclable heterogeneous catalytic activity for enantioselective sulfoxidation (up to 82% ee). A confinement of substances in cavity results in a marked enhancement of enantioselectivity over the homogeneous catalyst. An exceptionally porous MOF material (bio-MOF-100) was built of a Zn-adeninate octahedral building unit (ZABU) as a vertex interconnected with linear biphenyldicarboxylate **bpdc**.[198] It exhibits a high surface area (4300 $m^2\ g^{-1}$), one of the lowest crystal densities (0.302 g cm^{-3}) and one of the largest pore volumes reported to date in MOFs (4.3 $cm^3\ g^{-1}$); another MOF is NU-110E with a pore volume of 4.4 $cm^3\ g^{-1}$.[15]

Apart from acting as pillar linkers, dipyridyl derivatives have also been reported to participate in the framework construction. Reaction of **btb**, 4,4′-bipy and $Zn(ClO_4)_2$ in DMF affords single crystals of FJI-1 with extended Pt_3O_4 topology, in which each **btb** links to three Zn(II) paddle-wheel SBUs and each SBU links to four **btb** linkers. The axial sites of each paddle-wheel are occupied by two nitrogen atoms from two different 4,4′-bipy linkers. FJI-1 is highly porous and the N_2 sorption measurements reveal that its Langmuir surface area is 4624 $m^2\ g^{-1}$. High-pressure hydrogen sorption studies show excess and total H_2 uptake as high as 6.52 wt% at 36 bar, 77 K and 9.08 wt% at 62 bar, 77 K, respectively.[199]

6.4 Linkers coordinatively identical but distinct in shape

If the driving force for crystal growth with the majority linker is sufficient, the minority linker coordinatively identical but distinct in shape will be randomly copolymerized into the final MOF products. The new material with MOF-5 structure derived from the majority ditopic carboxylate linker **bdc** and the minority tritopic carboxylate **btb** linker shows a significant number of dangling carboxylates in the cavities as defect sites. These uncoordinated carboxylates have high affinity toward Pd^{2+}. Catalytic activity for C–H phenylation of naphthalene has been studied in the Pd^{2+} functionalized MOF as a heterogeneous catalyst.[200] Another MOF-5 type material having structural heterogeneity without losing the overall crystalline order was obtained by using a mixture of two ditopic carboxylate linkers, **bdc** and 4-(dodecyloxy)benzoate (**dba**).[201] In the new crystal, the micropores, mesopores, and macropores were juxtaposed and/or completely enclosed by the thick microporous crystalline MOF-5, depending on the ratios of **bdc** to **dba**.

A metal–ligand-fragment coassembly strategy to introduce not only functional groups but also functionalized cavities into microporous MOFs was reported in 2012 (Fig. 33).[202] To demonstrate this strategy, a **nbo**-type topological MOF (NOTT-101)[116] with terphenyltetracarboxylate (**tptc**) and dicopper paddle-wheel SBU was chosen as a model structure; the primitive linker (**tptc**) and its linker fragment (R-isoph) were coassembled to generate a series of isostructural MOFs with pendant functional groups (R). Therefore, the interior of the MOFs can be tuned by a wide variety of functional groups on the ligand fragments randomly incorporated into the MOFs.

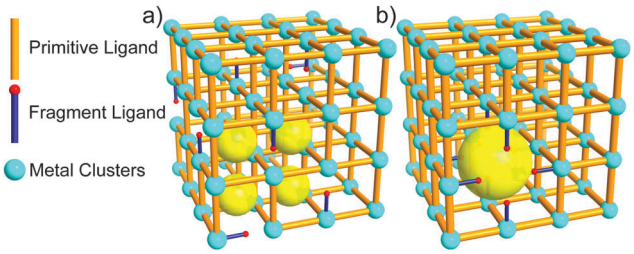

Fig. 33 Schematic illustration of a metal–ligand-fragment coassembly strategy: introduction of functionalized micropores (a) and mesopores (b).

Most importantly, most of the ligand fragments in this report are readily available or can be easily prepared; it provides a platform to obtain functionalized MOF materials while minimizing the time and resources required in the linker preparation.

7 Desymmetrized linkers

Linkers with higher symmetry naturally facilitate crystallization in high-symmetry space groups. The resulting MOF structures are both aesthetically pleasing and easy to be perceived. More importantly, extension of high-symmetry linkers has been successfully implemented to achieve record-high porosity. On the other hand, linkers with reduced symmetry offer a largely unexploited direction to the MOF synthesis by increasing the topological complexity and driving a new mode of framework assembly.[86,203] The desymmetrized linkers can be obtained by asymmetrically adding/removing chemical entities into/from high symmetric linkers,[86,203–206] or rearranging the carboxylates.[207]

Assembled from tritopic carboxylate linkers with three carboxylates distributed in an unsymmetrical fashion, a series of MOF materials named UMCM-150 to 154 were reported,[86,203] demonstrating reduced-symmetry linkers for the synthesis of non-interpenetrated MOFs with new network topologies (Scheme 5). Even the linkers have the same number of carboxylates and C_{2v} symmetry; UMCM-151 does not have the same net as UMCM-150. UMCM-151 possesses two kinds of paddle-wheel SBUs to link the carboxylates in different chemical environments. UMCM-152 and UMCM-153 are polymorphic frameworks both containing dicopper paddle-wheel SBU and the same linker. The SBU of UMCM-152 links the *p*-benzoate moieties in *cis* position while that of UMCM-153 links them in *trans* position. The SBU of UMCM-154 is an uncommon three-bladed zinc paddle-wheel with two carboxylates coordinated at axial positions.[203]

Recently, a ligand-truncation strategy, in which a high-symmetry triisophthalate linker was truncated into a diisophthalate linker, was reported (Scheme 6).[204] The assembly of the truncated linker with dicopper paddle-wheel resulted in a framework with a unique 4-*c* 4-nodal net. A series of isostructural MOFs have been synthesized by using linkers with different functional groups on the middle phenyl ring. All the MOFs showed excellent CO_2 adsorption capacity as well as high H_2 uptake. In this case, it seems like the adsorption

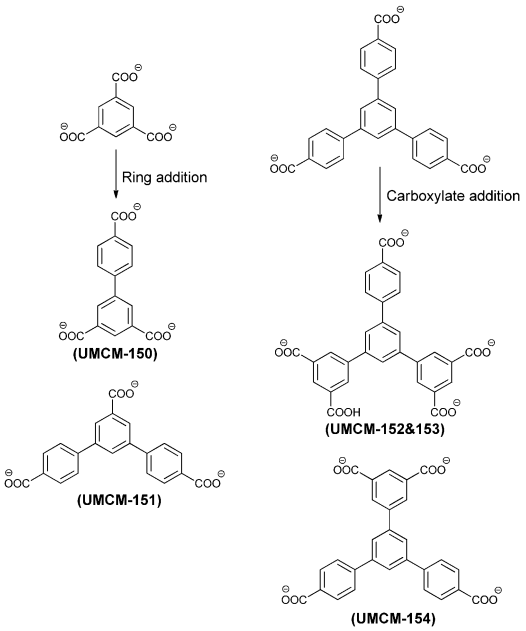

Scheme 5 Linker design through ring and carboxylate addition. In parentheses are the names of MOFs synthesized accordingly.[86,203]

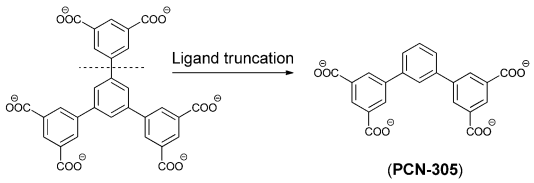

Scheme 6 Ligand-truncation strategy. In parentheses is the name of MOF synthesized accordingly.[204]

performance is more related to the MOF structure itself instead of the functional group.[204]

More recently, a new MOF was constructed from 5,5′-(9-oxo-9,10-dihydroacridine-2,7-diyl)-diisophthalate (**oaddi**), which can be viewed as truncated from the hexatopic linker 4′,4″,4‴-nitrilotribiphenyl-3,5-dicarboxylate (**nbpd**) (Scheme 7).[205] It is interesting to point out that **oaddi** was generated *in situ* from 5,5′-(acridine-2,7-diyl)diisophthalate (**addi**). Although somewhat distorted, all the three polyhedral building units were surprisingly observed in the new MOF as in the original **rht** MOF (NOTT-115) built from **nbpd**. Further removal of two carboxylates of the tetratopic linker **addi** resulted an C_{2v} ditopic linker 3,3′-(acridine-2,7-diyl)dibenzoate (**addb**), which was *in situ* oxidized to **oaddb** (3,3′-(9-oxo-9,10-dihydroacridine-2,7-diyl)dibenzoate) in the solvothermal condition and formed a lantern-shaped MOP containing dicopper paddle-wheel SBU.[205]

Pyridyl dicarboxylate linkers could also be categorized as desymmetrized linkers. Two dicopper-paddle-wheel MOFs with novel topologies have been constructed based on 5-(pyridin-4-yl)isophthalate and 5-(pyridin-3-yl)isophthalate, respectively. The results suggest that a combination of dicarboxylate and pyridyl groups in a T-shaped linker may yield nanotubular MOFs with borderline transition-metal ions.[208]

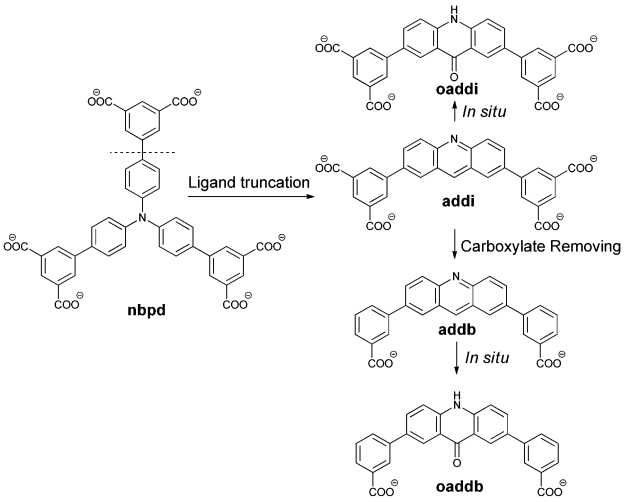

Scheme 7 Ligand-truncation strategy. Illustration of linker design and *in situ* transformation.[205]

8 Metallo-linkers

Introduction of secondary metal centres into MOF voids has attracted extensive attention due to the potential applications of these added metal centres as catalytic active sites to promote a wide range of organic reactions.[209,210] Several strategies have been developed in this area: (a) construct MOFs with linkers designed to have secondary functional groups and sequentially introduce metal centres *via* post-synthetic modifications,[211] (b) prepare MOFs from pre-formed metal complexes,[212–214] (c) introduce metal complexes through post-synthetic linker exchange[57–59,215] (Fig. 34). In this section, metallo-linkers are categorized based upon different electron donor groups attached on the organic linkers; herein the donor groups refer to secondary functional groups other than the primary binding sites (*e.g.* carboxylates or azolates).

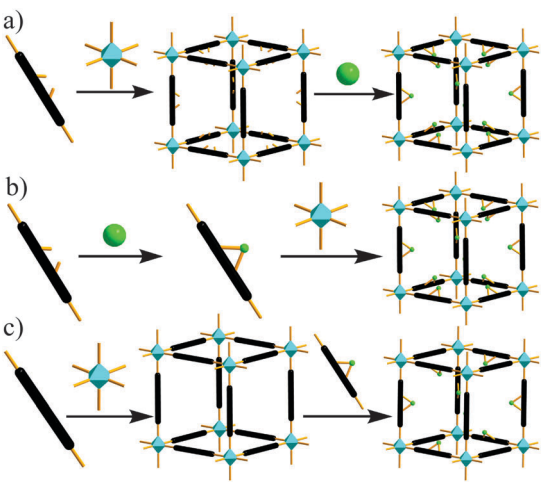

Fig. 34 Graphical representation of strategies to introduce secondary metal centres into MOFs through (a) post-synthetic modification; (b) pre-formed metal complexes; (c) linker exchange.

8.1 Metallo-linkers with oxygen and sulfur donors

A catalytically active homochiral MOF by utilizing orthogonal functionality within the backbone of BINOL-derived linker was a successful demonstration of the post-synthetic modification strategy: in an axially chiral linker (*R*)-6,6′-dichloro-2,2′-dihydroxy-1,1′-binaphthyl-4,4′-bipyridine, the primary functionality bipyridyl was used to construct a homochiral porous network through the linkage of 1D zigzag $[Cd(\mu\text{-}Cl)_2]_n$ SBU, while the orthogonal chiral 2,2′-dihydroxyl secondary functionality was used to incorporate $Ti(O^iPr)_4$ to form a chiral catalytic centre. The resulting MOF complex is capable of catalyzing the diethylzinc addition to aldehydes with high enantiomeric excess up to 93% and size selectivity for aldehydes (Fig. 35).[216] The authors claimed that only one-third of the dihydroxyl groups have been metalated (purple spheres in Fig. 35a), and the other two-thirds are shaded and protected by strong hydrogen-bonding and π···π stacking interactions (red spheres in Fig. 35a). Indeed, a follow-up study suggested that the catalytic activity was dependent on the accessibility and enantioselectivity was highly dependent on the MOF topology.[217,218]

Later, the same group reported a series of isoreticular non-interpenetrated chiral MOFs assembled from corresponding BINOL-based tetratopic carboxylate linkers (Fig. 36) and dicopper paddle-wheel SBUs.[219] These 4,4-connected **pts**-topology MOFs contain pore sizes ranging from 0.8 nm to 2.1 nm along the *c*-axis. A series of Lewis-acid catalysts were generated upon post-synthetic modification with $Ti(O^iPr)_4$, and the enantioselectivity of these catalysts was found to be largely correlated to the sizes of these open channels.

Direct synthesis of MOFs from thiolated linkers usually forms metalation of these thiol groups during the construction of the frameworks.[220] The first iron–sulfur-cluster-containing MOF UiO-66-[FeFe](**dcbdt**)$(CO)_6$ (**dcbdt** = 1,4-dicarboxylbenzene-2,3-dithiolate) was synthesized upon post-synthetic linker exchange.[221] The successful replacement of the **bdc** linkers with the iron–sulfur-cluster-containing linkers was confirmed by a variety of spectroscopic studies, and the exchange degree was estimated to be ~14%. When incorporated with photosensitizer ($[Ru(bpy)_3]^{2+}$) and sacrificial electron donor (ascorbate), UiO-66-[FeFe](**dcbdt**)$(CO)_6$ was found to be an active proton reduction catalyst under irradiation. Surprisingly, the

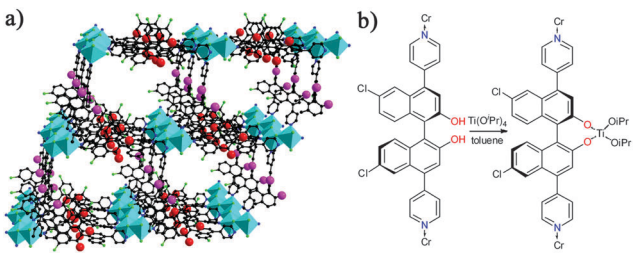

Fig. 35 (a) Crystal structure of the 3D framework constructed from the BINOL functionalized linker with large channels (red and purple spheres represent hydroxyl groups inside the channels). (b) Schematic representation of the metalation on the hydroxyl groups by $Ti(O^iPr)_4$.

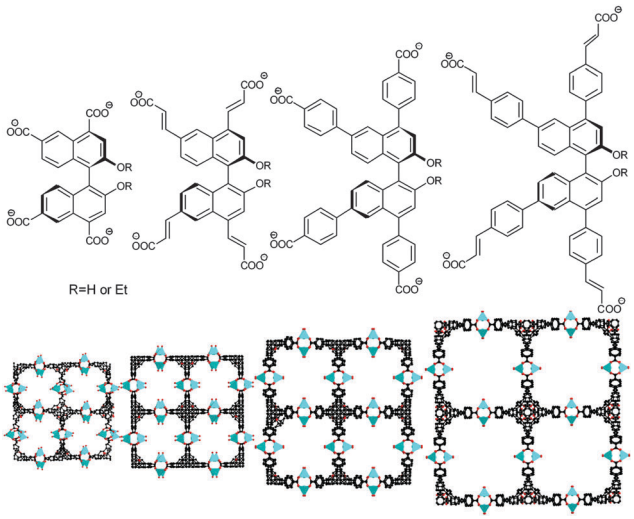

Fig. 36 BINOL-containing tetracarboxylate linkers; packing diagrams of MOFs constructed from these linkers as viewed along the *c* axis.[219]

UiO-66-[FeFe](**dcbdt**)$(CO)_6$ shows superior catalytic performance compared to its parent complex ([FeFe](bdt)$(CO)_6$). It is suggested and evidenced that the increased catalytic activity was mainly due to the enhanced stability of the iron–sulfur clusters by its heterogeneous nature and the protection from the UiO-66 framework.

8.2 Metallo-linkers with nitrogen and phosphine donors

Direct solvothermal reactions of linkers with the 2,2′-bipyridyl (bpy) components usually result in metal-chelated bipyridyl sites. A series of MOFs have been constructed from ditopic linkers containing metallo-bpy complexes, and their luminescent properties,[222,223] photocatalysis for water oxidation,[55,214] as well as hydrogen evolution[224] have been studied.

Direct solvothermal assembly of **bpydc** (2,2′-bipyridine-5,5′-dicarboxylate) to afford MOFs with uncoordinated bipyridyl sites was reported in 2010.[211] The hard–soft acid–base theory of coordination chemistry was wisely applied here. Al^{3+}, which shall be classified as a hard and oxophilic metal, prefers to interact with the hard carboxylate donor during the solvothermal reaction and build the MOF backbone with no metal coordination on the soft bpy sites. PXRD patterns of the obtained MOF-253 indicate that it is isoreticular to MIL-53 and isostructural to Al(OH)(**bpdc**) (DUT-5).[225]

By soaking MOF-253 in acetonitrile solutions of $PdCl_2$ or $Cu(BF_4)_2$, three metalated MOFs, MOF-253·0.08$PdCl_2$, MOF-253·0.83$PdCl_2$, and MOF-253·0.97$Cu(BF_4)_2$, were obtained and confirmed by elemental analyses. The adsorption selectivity of CO_2 over N_2 was significantly enhanced for $Cu(BF_4)_2$-metalated material, and selectivity factor (the mass of CO2 taken up at 0.15 bar divided by the mass of N2 taken up at 0.75 bar at 298 K) was calculated to be 12 for MOF-253·0.97$Cu(BF_4)_2$, which is four times greater than that of MOF-253 (Fig. 37).[211]

Assembled from a 1,10-phenanthroline-based linker, MOF-1040 highlights the incorporation of 30-member pseudo-rotaxanate rings.[226] Some of the copper(I) centres were found to

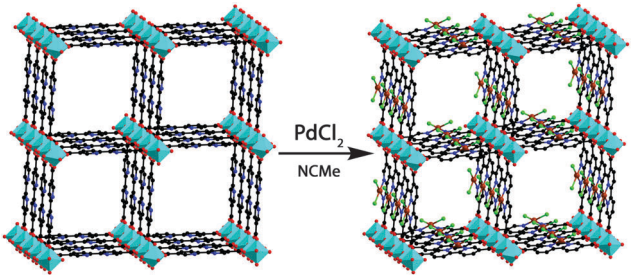

Fig. 37 Graphical representation of the crystal structure of MOF-253 and the incorporation of the $PdCl_2$ moiety upon post-synthetic modification (the structure of MOF-253·$PdCl_2$ was simulated based upon DUT-5).

be readily oxidized or removed upon post-synthetic modification without disrupting the crystallinity of the frameworks. The fact that at least some of the copper ions can be oxidized to their dicationic states indicates the presence of electronic switches which are presumably accompanied by geometrical changes involving shrinking and flattening in the coordination sphere of the copper ions in question.

In 1994, a porphyrin MOF with large channels by the linkage of 4,4′,4″,4‴-tetracyanotetraphenylmethane *via* copper(I) centers was synthesized which provides an example of deliberate construction of a diamond-related network.[227] Reported here, however, is the synthesis of an extended family of MOFs that directly incorporate a variety of metalloporphyrins (specifically Al^{3+}, Zn^{2+}, Pd^{2+}, Mn^{3+}, and Fe^{3+} complexes) featuring large channels and readily accessible active sites. As an illustrative example, one of the manganese-containing MOFs is shown to be catalytically competent for the oxidation of alkenes and alkanes.[228] The ability to synthesize MOFs from a variety of metalloporphyrin struts opens up possibilities for the design of a wide range of porphyrinic MOF materials suitable for catalysis, chemical separations, and energy transfer.[223,229,230] 5,10,15,20-Tetrakis(4-carboxyphenyl)porphyrin (**tcpp**) perhaps is the most used metalloporphyrin linker in MOF synthesis.[20,231–233] Proper rotation between the porphyrin plane and phenyl rings together with symmetry diversity of Zr clusters resulted in 12, 8, 6-connection modes of Zr clusters. Due to the stability of the Zr cluster and multifunctionality of porphyrin, these stable Zr-MOFs were applied as biomimetic catalysts,[20,232] CO_2 fixators,[233] and pH sensors.[231]

By using phosphine-containing carboxylate linkers [*i.e.* **ptbc** (4,4′,4″-phosphanetriyltribenzoate)], a series of unique MOF materials (PCMs, PCM = phosphine coordination material) were reported.[234,235] The uncoordinated phosphine sites were later doped with Au(I), and adsorption selectivity for 1-hexane over *n*-hexane was observed. More recently, the same group reported a new PCM with tetracarboxylate-organophosphine-based linker **pbptbc** (4,4′,4″,4‴-(1,2-phenylenebis(phosphanetriyl))-tetrabenzoate).[213] $CODMCl_2$ (COD = 1,5-cyclooctadiene, M = Pd/Pt) was used to form a planar P_2MCl_2 species in order to lock the flexible **pbptbc** into a rigid building block (Fig. 38). The **pbptbc** linker can be viewed as a tetratopic planar node which contains a diphosphine functional group in the center. The MOF material (M-PCM-18) was obtained by mixing corresponding P_2MCl_2 linker with zinc salt in an ethanol–DMF solvent mixture at low temperature (45 °C).

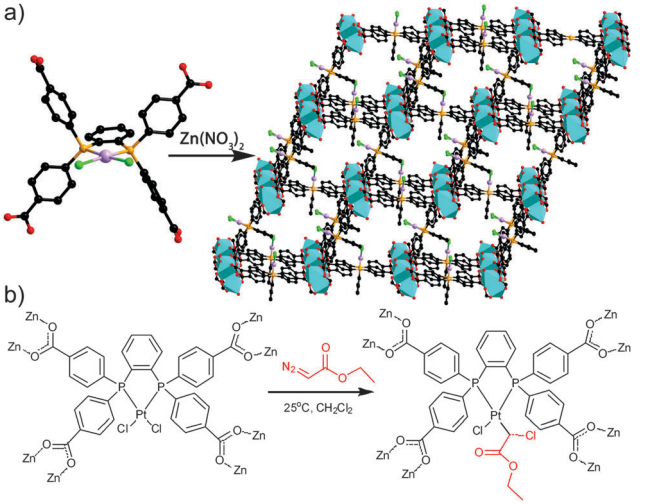

Fig. 38 (a) Graphical representation of synthesis of P_2MCl_2-based MOF (Pt-PCM-18). Color scheme: Zn (turquoise polyhedra); Pt (purple); P (orange); Cl (green); O (red); C (black). (b) Illustration of Pt-PCM-18 activation with diazoacetate under mild conditions.

M-PCM-18 (M = Pd/Pt) is a 3D network with a puckered square grid topology. It has been proved by the solid state NMR studies that the Pt–Cl bond inside the material can be activated in a high yield upon treatment with ethyl 2-diazoacetate in methylene chloride solution for three days (Fig. 38). Therefore, as stated by the authors, this material could potentially be used as a catalyst for hydroformylation reactions.[213]

8.3 Metallo-linkers with carbon donors

Although it seems unusual and difficult to use carbon atoms as secondary electron donor groups, there are actually several reports on NHC-based (N-heterocyclic carbene) and arene-based organic linkers to bind secondary metals before or after forming MOFs.[212,236–239]

In one scenario, a ditopic bended NHC-carboxylate linker was used to react with both Cu_2O and Ce^{3+}. An intriguing 3D structure was obtained underlying the coordination of two Ce^{3+} centers bridged and chelated by eight carboxylate groups. More importantly, copper(I)–Cl groups have been observed at every other NHC site. The authors explained the formation of such a material based upon the hard–soft acid–base theory, where the harder Ce^{3+} binds to the hard carboxylate site, and the softer copper(I) bind to the NHC site. The fact that only half of the NHC sites were metalated in this system results in a neutral MOF material with increased stability compared to the fully metalated species, which would be positively charged.[235]

Two NHC-containing IRMOFs with a ditopic linker (4,7-bis(4-carboxylphenyl)-1,3-dimethyl-benzimidazolium-tetrafluoroborate) were reported. This NHC-carboxylate linker was first directly reacted with Zn^{2+} to afford a MOF material (IRMOF-76), which is isoreticular to MOF-5; however, introduction of Pd^{2+} species through post-synthetic modification was

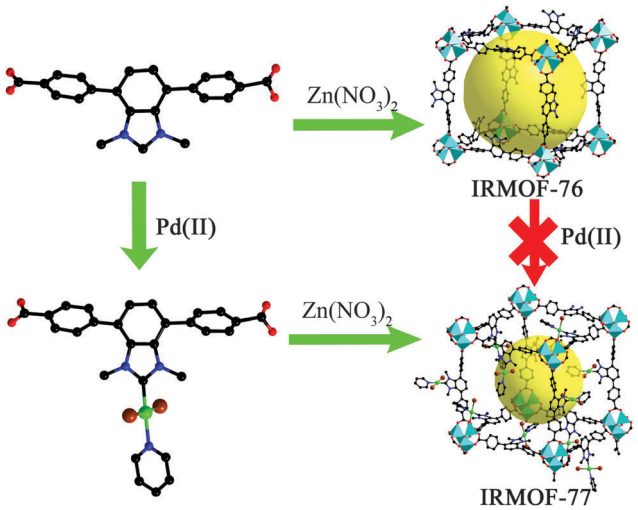

Fig. 39 Graphical representation of the synthesis of IRMOF-76 and IRMOF-77. Color scheme: Zn (turquoise polyhedra); Pd (green); I (brown); Cl (green); N (blue); O (red); C (black).

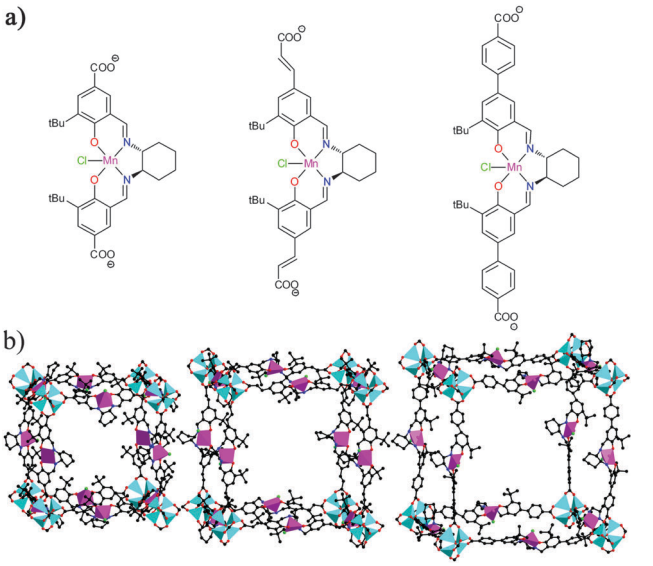

Fig. 40 (a) Salen–Mn-based linkers; (b) stick/polyhedra models showing different sized cages constructed from the linkers (interpenetrations were omitted for clarity).[246] Color scheme: Zn (turquoise polyhedra); Mn (pink polyhedra); Cl (green); O (red); N (blue); C (black).

not successful in this case. On the other hand, the Pd-preinstalled linker, NHC–Pd(II)-carboxylate, was successfully applied to construct MOF material (IRMOF-77), which is also isoreticular to MOF-5 (Fig. 39).[212]

Post-synthetic modification of IRMOF-1 where the phenyl rings were metalated by $Cr(CO)_6$ formed a piano stool Cr(0) arene complex.[238] A similar work was reported to modify UiO-66 with $Cr(CO)_6$.[239] The successful metalation was supported by FTIR, UV-vis, XANES (X-ray absorption near-edge structure) and EXAFS (extended X-ray absorption fine structure).

8.4 Metallo-linkers with mixed donor groups

The ppy-based (ppy = phenylpyridine) linker shall be considered as a linker with mixed donor groups since the metal (iridium) binds to both the nitrogen and carbon atoms.[55,214]

Another very well studied mixed donor linker is Schiff base compounds, in which the functional sites consist of both nitrogen and oxygen donor groups.[240] The activity and stability of (salen)Mn(III) as epoxidation catalysts were found to be largely increased upon supramolecular complexation.[241] Later, the same group prepared mixed-linker MOFs where dizinc paddle-wheel SBUs were connected by the linear **bpdc**/**btbc** linkers to form 2D sheets, and those sheets were further connected by the pillar linker salen–py–Mn complex [(*R*,*R*)-(2)-1,2-cyclohexanediamino-*N*,*N*′-bis(3-*tert*-butyl-5-(4-pyridyl)salicylic-dene)-Mn(III)Cl].[242,243] The immobilized salen complexes showed great advantages in catalysing olefin epoxidation, including increased stability, easier separation, and substrate size selectivity. Another interesting example of 3D networks with Schiff base type metalloligands as linkers was reported featuring an infinite SBU.[244] A series of metallo-complexes were used to react with Zn^{2+} to afford the salen-based MOFs, in which the Zn^{2+} ions possess two different (tetrahedral and octahedral) coordination environments, the four coordinated Zn^{2+} interacting with two hydroxide anions and two carboxylate oxygen atoms, whereas the 8-coordinated Zn^{2+} interacting with two hydroxide anions and four carboxylate oxygen atoms. The edge shared tetrahedra further share corners with the neighbouring octahedra to form infinite SBUs, which is rare in the literature.[245]

By reacting different metallo-linkers with zinc salts, a series of Mn–salen complex-based MOF materials isoreticular to MOF-5 (Fig. 40) were obtained.[246] It was demonstrated that the dimensions of channels can be tuned by controlling the interpenetration achieved by applying different templating solvents. A study on alkene epoxidation reactions with these MOF complexes as enantioselective catalysts shows that (1) these isoreticular chiral MOFs were proved to be highly active enantioselective alkene epoxidation catalysts; (2) the rates of epoxidation reactions were found to be strongly correlated with the MOF open channel sizes, which further demonstrated that the reaction rates are dependent on the diffusion of reactant and product molecules; (3) the catalytic activity of the MOFs with large open channels (where presumably the reaction rates are not limited by the diffusion) is limited by the reactivity of the catalytic molecular species.

9 N-Heterocyclic linkers

It is well known that the strength of nitrogen–transition metal bonds is greater than that of oxygen–transition metal bonds in solution.[247] Organic linkers containing nitrogen donor(s), such as pyridine and azole derivatives, have been extensively studied aiming to achieve stable MOFs *via* nitrogen–metal coordination.

9.1 Ditopic N-heterocyclic linkers

Recently in the MOF field, dipyridyl linkers have been largely used as pillars to knit 2D layers into 3D frameworks.

For example, a 3D pillared-layer coordination polymer with a specifically designed dipyridyl pillar linker (2,5-bis-(2-hydroxyethoxy)-1,4-bis(4-pyridyl)benzene) exhibits a locking–unlocking system which accounts for gate-opening type sorption profiles.[186] Bipyridyl linkers with different lengths, such as 4,4′-dipyridylacetylene (**dpa**) and pyrazine, have been utilized to demonstrate a crystal engineering/reticular chemistry approach to pore size control; the resulting cubic-topology porous materials show exceptional selectivity, recyclability and moisture stability in the context of several industrially relevant CO_2 separation applications.[248] Ditopic azoles can also be utilized as pillars for constructing MOFs in the same fashion. For example Hanson and co-workers successfully utilized a series of imidazolate derivatives (*e.g.*, 1,4-bis(imidazolyl)-benzene and 1,5-bis(imidazol-1-ylmethyl)naphthalene) as pillars to connect sheets composed of Co(II) and phosphites to 3D frameworks, which were thermally stable at 425 °C (Scheme 8).[249]

Pyridyl linkers show quite straightforward characteristics with respect to the coordination numbers and directions. The chemistry of coordination polymers of pyridyl linkers has recently been reviewed.[250,251] Compared to carboxylate linkers with bridging coordination modes, however, their relatively weak donor-ability has been addressed as a disadvantage when it comes to the construction of MOFs. As such, azole-based linkers caught MOF researchers' eye because of their strong binding ability to metals. Azoles are a class of five-membered aromatic N-heterocycles that include imidazole (Him), pyrazole (Hpz), 1,2,4-triazole (Htz), 1,2,3-triazole (Hta), and tetrazole (Httz). Deprotonation of azoles to yield corresponding azolates is mostly achieved by amines, which can be obtained from the decomposition of amide solvents used in solvothermal reactions.[252]

As one of the well-known classes of MOFs, metal–imidazolate frameworks, which are commonly known as zeolitic imidazolate frameworks (ZIFs), have been extensively studied in the last decade. The bridging angle between imidazolate and two bound metals (M–Im–M) is similar to that of Si–O–Si found in zeolites (145°); a large number of ZIFs have been synthesized with tetrahedral metal ions (*e.g.*, Fe^{2+}, Co^{2+}, Cu^{2+}, Zn^{2+}) leading to topologically isomorphic structures to zeolites.[252]

A library of ZIFs were reported in 2006. Among them, ZIF-8 ($Zn(\mathbf{MeIm})_2$) and ZIF-11 ($Zn(\mathbf{bIm})_2$), where **MeIm** and **PhIm** stand for 2-methylimidazolate and benzimidazolate respectively, have shown permanent porosity and exceptional thermal stability up to 500 °C. On top of that, ZIF-8 shows remarkable chemical stability in refluxing organic solvents and aqueous alkaline solutions.[253] Compared to carboxylates, azolates have been less chosen for the linkers until recently, possibly because the bridging length of azolates seems to be short. As ZIFs were highlighted, however, many metal imidazolate frameworks have been reported with new topologies that have been undiscovered in zeolites.

ZIF-95 ($Zn(\mathbf{cbIm})_2$; **cbIm** = 5-chlorobenzimidazolate) and ZIF-100 ($Zn_{20}(\mathbf{cbIm})_{39}(OH)$) not only have structural novelty and permanent porosity (Langmuir surface areas: 1240 $m^2\ g^{-1}$ and 780 $m^2\ g^{-1}$, respectively) but also show selective CO_2 adsorption–desorption properties, and their thermal stability is up to 500 °C.[254] Although crystallization is not fully investigated yet, structural diversity resulting from linker functionalization opens a new direction to synthesize rationally tailored imidazolate-based porous materials for desired applications.

The chemical stability of ZIFs in both aqueous and organic media makes them capable of performing organic reactions at crystal level while maintaining the original topology of the ZIF structures. Accordingly, ZIF-90, which has an aldehyde moiety at the 2-position, was successfully transformed into ZIF-91 and 92 by reduction of aldehyde with $NaBH_4$ and reaction with ethanolamine in refluxing methanol, respectively (Fig. 41), which demonstrated that crystals can be used as molecules to conduct organic reactions due to their chemical stability.[255]

The chemical and thermal stability of ZIFs also make them interesting candidates for many other applications, such as CO_2 capture.[256,257] The judiciously designed imidazolate linkers can be used to adjust the resulting pore size while maintaining the underlying topology, making ZIFs highly attractive for many studies, including selective separation from industrially relevant gas mixtures.[254,258,259]

A 3D coordination polymer with interesting selectivity for some aromatic molecules was reported.[260] This framework, $[Ag_2(\mathbf{Me_4bpz})]$ ($H_2\mathbf{Me_4bpz}$ = 3,3,5,5-tetramethyl-4,4-bipyrazole),

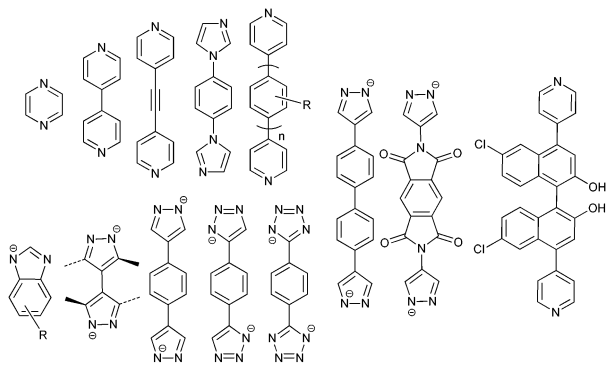

Scheme 8 Some representative ditopic N-heterocyclic linkers.

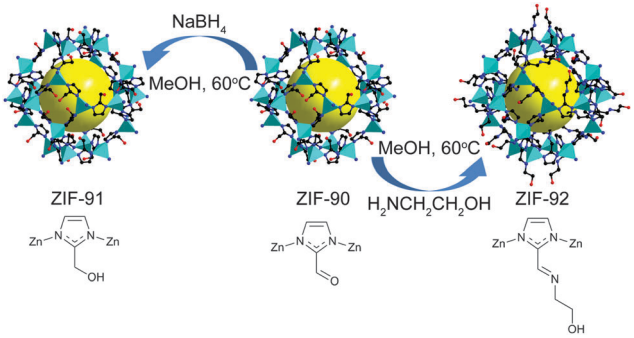

Fig. 41 Illustration of ZIF-90 transformed to ZIF-91 by reduction with $NaBH_4$ and to ZIF-92 by reaction with ethanolamine. Color scheme: Zn (turquoise polyhedra); O (red); N (blue); C (black).

showed not only reversible sorption properties but also guest responsive flexibility towards benzene and toluene in a single-crystal to single-crystal manner. It is worth noting that the framework flexibility may not only come from the low-connectivity topology, but also arise from rotatability of **Me$_4$bpz** around the central C–C single bond (dihedral angle $\varphi \approx 50$–90°).[260] In a continued study with the same linker, framework flexibilities were demonstrated by adsorption measurements and single-crystal diffraction analyses. The guest-accessible Ag(I)/Cu(I) unsaturated metal centers have been demonstrated to facilitate the accommodation of unsaturated hydrocarbons such as benzene, toluene, mesitylene, and acetylene *via* weak metal$\cdots\pi$ interactions.[261]

As bridging ligands, carboxylates are of immense interest in the construction of MOFs. To find a suitable substitute for linear dicarboxylates, ditetrazolate,[262] dipyrazolate,[263,264] and di(1*H*-1,2,3-triazolate)[265] were selected because their acid forms have pK_a values close to those of carboxylic acids. Likely due to the bridging coordination, MOFs constructed with these linkers show high thermal and chemical stability. The high basicity of pyrazolate relative to tetrazolate imparts increased strength to the metal–nitrogen bonds, which in turn confers higher thermal and chemical stability to the framework. Pyrazolate-bridged MOFs have been shown to exhibit a high chemical stability even in boiling water, organic solvents, and acidic media.[263] Such materials are of immense importance for their ability to tolerate adventitious water that may be present in the storage tank or the hydrogen fuel. The coordination behaviours of homofunctional linkers (dicarboxylates) and heterofunctional linkers (one carboxylate and one tetrazolate) with rare-earth metals have been studied. Interestingly, both carboxylate and tetrazolate moieties lead to *in situ* generation of hexanuclear molecular building blocks, and the construction of a series of robust 12-connected **fcu**-MOFs suggests that carboxylate and tetrazolate may have comparable coordination strength toward lanthanides.[266]

9.2 Polytopic N-heterocyclic linkers

The similarity between carboxylate and pyrazolate in terms of coordination has led to numerous pyrazolate-based MOFs as well. Although the small bridging angle and the short link might have made the utilization of pyrazolate-based linkers somewhat limited, this could be resolved by adopting polytopicity while maintaining strong coordination ability (Scheme 9).

Four pyrazolate-bridged MOFs M$_3$(**btp**)$_2$·Xsolvent (M = Ni, Cu, Zn, and Co; H$_3$**btp** = 1,3,5-tris(1*H*-pyrazol-4-yl)benzene) were reported.[267] Upon activation, microporosities were realized with BET surface areas of 1650, 1860, 930, and 1027 m^2 g^{-1}, respectively. Among these, Zn$_3$(**btp**)$_2$ shows high thermal stability up to *ca.* 500 °C, and Ni$_3$(**btp**)$_2$ shows chemical stability in boiling aqueous solutions at different pH values (range of 2−14) for two weeks. This chemical stability in such extreme conditions allows it to be an interesting candidate for many applications.

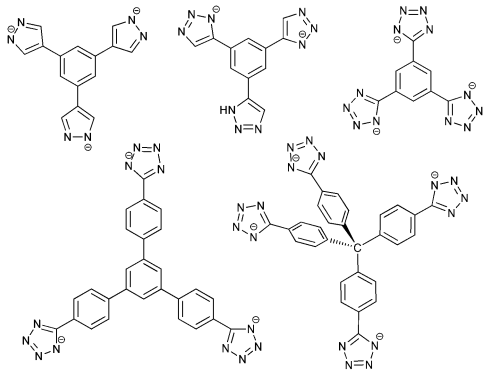

Scheme 9 Some representative polytopic N-heterocyclic linkers.

Likely due to the easy mode of synthesis (*i.e.*, [2+3] cycloaddition between azides and organonitriles), tetrazolate-based frameworks have been extensively studied.[268] Compared to other azolates, low basicity (pK_a = 4.9 in dimethylsulfoxide)[221] and weak coordination to metals result in relatively low thermal/chemical stability of MOFs constructed with tetrazoles. Nevertheless, it is worth discovering new metal–tetrazolate frameworks and studying the differences and/or similarities with their structural analogues of linkers.

Tritopic tetrazolate linker **btt** (**btt** = 1,3,5-benzenetristetrazolate) has been well studied in combination with several metals.[269–271] This series of MOFs showed coordination *via* the two middle nitrogens, which is similar to that of pyrazolates. Mn-**btt**, a 3,8-connected microporous anionic porous material, showed permanent porosity and excellent H_2 uptake of 6.9 wt% at 77 K and 90 bar. The high uptake was attributed to the rigid framework and unsaturated metal centers, which are believed to have better affinity towards H_2. As a matter of fact, neutron diffraction study did show direct H_2 binding to unsaturated manganese centers.[87]

With the combination of DFT calculation and experimental data, a further study on the effect of metal and anion substitution on the M-**btt** system suggests that the impact of constitution within the isostructural MOFs does play a decisive role in controlling the H_2 affinity. For instance, two predominant binding sites were examined by loading-dependent powder neutron diffraction data (Fig. 42); site I showed the highest affinity towards H_2, whereas a bowl-shaped cavity on the chloride anion of the metal cluster was another populated site. Other than those experimentally prepared M-**btt** platforms, DFT calculations also provided potential synthetic targets such as Zn-**btt**, which was calculated to have enhanced heat of adsorption for H_2.[272]

The reaction between tetrahedral linker **ttpm** (H$_4$**ttpm** = tetrakis(4-tetrazolylphenyl)methane) and $CuCl_2$ resulted in a 4,8-connected **flu**-topology MOF material based on chloride-centered tetranuclear SBU. This anionic MOF could undergo transformation from anionic to neutral MOF upon activation *via* solvent exchange, giving rise to Cu$_4$(**ttpm**)$_2$·0.7$CuCl_2$ with a high BET surface area of 2506 m^2 g^{-1} and substantial hydrogen uptake (2.8 wt% at 77 K and 1.2 bar). The elimination of Cl^-

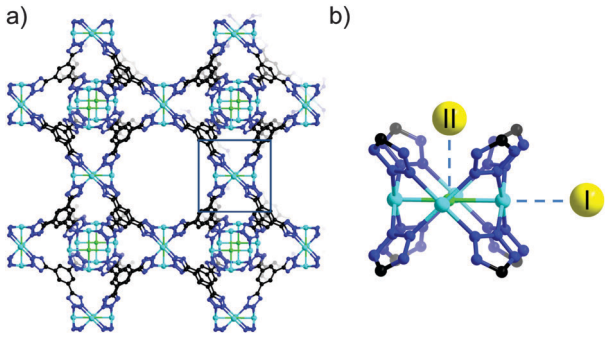

Fig. 42 (a) A portion of the structure of the M-**btt** (M = Mn, Fe, Cu) type. Color scheme: M (turquoise); O (red); N (blue); Cl (green); C (black). (b) An expanded view of the region enclosed by the outline in the left figure showing the two predominant D_2 binding sites as observed in powder neutron diffraction experiments.[272]

from square-planar $[Cu_4Cl]^{7+}$ was confirmed by shortened Cu–N bonds and *trans* Cu···Cu distances, and this likely provides strong binding sites for guest molecules.[273]

10 Conclusions

During the early age of MOF research, discovery of new MOF structures has largely been serendipitous. As an important tool for understanding phenomena at molecular level, computational simulation is being increasingly used in guiding MOF synthesis through linker design.[274–276] Further breakthrough in MOF research could very much rely on active collaboration between synthetic chemists and computational chemists. For example, computational modelling results clearly show that the strategy of using more acetylenes in the organic linkers has the potential of creating ordered structures with surface areas substantially higher than those previously envisioned for MOF materials. Following this strategy, NU-110E[15] was synthesized and found to be closely matching the simulated structure with a record-high surface area.

Reticular chemistry has led to substantial development in the MOF area with numerous structures identified; now it has to come down to real applications. Integration of application-oriented linker design into MOF synthesis could sustain its continuous prosperity. In addition to exploring new MOF structures and their applications, one can always review the thousands of published MOF structures; most of them have not been studied or thoroughly studied in the application aspect. It does not necessarily have to be gas-related applications[277–280] where work on MOFs first began with; a wide range of potential applications deserve intensive probing such as host–guest chemistry,[35] catalysis,[209,210,281] biomedical imaging,[282] drug delivery,[283] sensing,[284,285] proton conductivity,[286] hydrocarbon separation,[287,288] and membrane fabrication.[289,290]

A major obstacle from raw to ready lies in the execution and optimisation of the process. The ever increasing knowledge of underlying metal coordination environments, orientation of organic linkers, and possible combinations (topologies) between these two elements helps us understand and direct the synthetic efforts specifically. Besides conventional hydrothermal and solvothermal synthesis, a variety of new preparative approaches could be used to help fulfil our design, such as microwave-assisted synthesis, electrochemical synthesis, mechanochemical synthesis, and sonochemical synthesis.[291]

The MOF field has been a hot research spot and actively explored for the last two decades. Their unconventional porosity and tunable chemical environment continuously fascinate researchers around the world. Although MOF synthesis through linker design sometimes is still elusive from an experimental point of view, an increasing number of MOFs with predesigned channels or cavities have been achieved. We believe that successful implementation in this direction lies in extensive collaboration of scientists with different scientific backgrounds.

Author contributions

W. Lu and H.-C. Zhou conceived and coordinated the writing of the manuscript; W. Lu and J. Tian led the writing of ditopic and tritopic linkers sections; M. Zhang and Z.-Y. Gu led the writing of the tetratopic linker section; J. Park (Jinhee) and J. Park (Jihye) led the writing of mixed and N-heterocyclic linkers sections; T.-F. Liu and Q. Zhang led the writing of octatopic and metallo linkers sections; W. Lu and Z. Wei led the writing of hexatopic and desymmetrized linkers sections; W. Lu, T. Gentle, M. Bosch, and H.-C. Zhou compiled and revised the manuscript; all the authors discussed and commented on the manuscript.

Acknowledgements

This work was supported by the U.S. Department of Energy, the U.S. Office of Naval Research, and the Welch Foundation.

Notes and references

1 J. R. Long and O. M. Yaghi, *Chem. Soc. Rev.*, 2009, **38**, 1213–1214.
2 H.-C. Zhou, J. R. Long and O. M. Yaghi, *Chem. Rev.*, 2012, **112**, 673–674.
3 N. R. C. S. R. Batten, X.-M. Chen, J. Garcia-Martinez, S. Kitagawa, L. Öhrström, M. O'Keeffe, M. P. Suh and J. Reedijk, *Pure Appl. Chem.*, 2013, **85**, 1715–1924.
4 B. F. Hoskins and R. Robson, *J. Am. Chem. Soc.*, 1990, **112**, 1546–1554.
5 S. Kitagawa, M. Munakata and T. Tanimura, *Inorg. Chem.*, 1992, **31**, 1714–1717.
6 O. M. Yaghi, G. Li and H. Li, *Nature*, 1995, **378**, 703–706.
7 H. Furukawa, K. E. Cordova, M. O'Keeffe and O. M. Yaghi, *Science*, 2013, **341**, 1230444.
8 M. Eddaoudi, D. B. Moler, H. Li, B. Chen, T. M. Reineke, M. O'Keeffe and O. M. Yaghi, *Acc. Chem. Res.*, 2001, **34**, 319–330.
9 H. Li, M. Eddaoudi, M. O'Keeffe and O. M. Yaghi, *Nature*, 1999, **402**, 276–279.

10 S. S.-Y. Chui, S. M.-F. Lo, J. P. H. Charmant, A. G. Orpen and I. D. Williams, *Science*, 1999, **283**, 1148–1150.
11 G. Férey, C. Mellot-Draznieks, C. Serre, F. Millange, J. Dutour, S. Surblé and I. Margiolaki, *Science*, 2005, **309**, 2040–2042.
12 N. L. Rosi, J. Kim, M. Eddaoudi, B. Chen, M. O'Keeffe and O. M. Yaghi, *J. Am. Chem. Soc.*, 2005, **127**, 1504–1518.
13 S. R. Caskey, A. G. Wong-Foy and A. J. Matzger, *J. Am. Chem. Soc.*, 2008, **130**, 10870–10871.
14 H. Deng, S. Grunder, K. E. Cordova, C. Valente, H. Furukawa, M. Hmadeh, F. Gándara, A. C. Whalley, Z. Liu, S. Asahina, H. Kazumori, M. O'Keeffe, O. Terasaki, J. F. Stoddart and O. M. Yaghi, *Science*, 2012, **336**, 1018–1023.
15 O. K. Farha, I. Eryazici, N. C. Jeong, B. G. Hauser, C. E. Wilmer, A. A. Sarjeant, R. Q. Snurr, S. T. Nguyen, A. Ö. Yazaydın and J. T. Hupp, *J. Am. Chem. Soc.*, 2012, **134**, 15016–15021.
16 Metal–Organic Frameworks Editorial [Special Issue], H.-C. Zhou, J. R. Long, O. M. Yaghi, ed., *Chem. Rev.* 2012, **112**(2).
17 J. R. Long and O. M. Yaghi, *Chem. Soc. Rev.*, 2009, **38**, 1213–1214.
18 M. O'Keeffe, *Chem. Soc. Rev.*, 2009, **38**, 1215–1217.
19 O. M. Yaghi, M. O'Keeffe, N. W. Ockwig, H. K. Chae, M. Eddaoudi and J. Kim, *Nature*, 2003, **423**, 705–714.
20 D. Feng, Z.-Y. Gu, J.-R. Li, H.-L. Jiang, Z. Wei and H.-C. Zhou, *Angew. Chem., Int. Ed.*, 2012, **51**, 10307–10310.
21 G. K. H. Shimizu, R. Vaidhyanathan and J. M. Taylor, *Chem. Soc. Rev.*, 2009, **38**, 1430–1449.
22 K. J. Gagnon, H. P. Perry and A. Clearfield, *Chem. Rev.*, 2011, **112**, 1034–1054.
23 H. Li, M. Eddaoudi, T. L. Groy and O. M. Yaghi, *J. Am. Chem. Soc.*, 1998, **120**, 8571–8572.
24 H. Furukawa, J. Kim, N. W. Ockwig, M. O'Keeffe and O. M. Yaghi, *J. Am. Chem. Soc.*, 2008, **130**, 11650–11661.
25 K. Tanaka, S. Oda and M. Shiro, *Chem. Commun.*, 2008, 820–822.
26 M. Eddaoudi, J. Kim, M. O'Keeffe and O. M. Yaghi, *J. Am. Chem. Soc.*, 2001, **124**, 376–377.
27 M. Eddaoudi, J. Kim, D. Vodak, A. Sudik, J. Wachter, M. O'Keeffe and O. M. Yaghi, *Proc. Natl. Acad. Sci. U. S. A.*, 2002, **99**, 4900–4904.
28 M. O'Keeffe, M. Eddaoudi, H. Li, T. Reineke and O. M. Yaghi, *J. Solid State Chem.*, 2000, **152**, 3–20.
29 S. S. Kaye, A. Dailly, O. M. Yaghi and J. R. Long, *J. Am. Chem. Soc.*, 2007, **129**, 14176–14177.
30 N. W. Ockwig, O. Delgado-Friedrichs, M. O'Keeffe and O. M. Yaghi, *Acc. Chem. Res.*, 2005, **38**, 176–182.
31 M. Eddaoudi, J. Kim, N. Rosi, D. Vodak, J. Wachter, M. O'Keeffe and O. M. Yaghi, *Science*, 2002, **295**, 469–472.
32 A. G. Wong-Foy, A. J. Matzger and O. M. Yaghi, *J. Am. Chem. Soc.*, 2006, **128**, 3494–3495.
33 D. Britt, D. Tranchemontagne and O. M. Yaghi, *Proc. Natl. Acad. Sci. U. S. A.*, 2008, **105**, 11623–11627.
34 H. K. Chae, D. Y. Siberio-Perez, J. Kim, Y. Go, M. Eddaoudi, A. J. Matzger, M. O'Keeffe and O. M. Yaghi, *Nature*, 2004, **427**, 523–527.
35 Q. Li, W. Zhang, O. Š. Miljanić, C.-H. Sue, Y.-L. Zhao, L. Liu, C. B. Knobler, J. F. Stoddart and O. M. Yaghi, *Science*, 2009, **325**, 855–859.
36 L. Bellarosa, J. M. Castillo, T. Vlugt, S. Calero and N. López, *Chem.–Eur. J.*, 2012, **18**, 12260–12266.
37 L. Bellarosa, S. Calero and N. Lopez, *Phys. Chem. Chem. Phys.*, 2012, **14**, 7240–7245.
38 S. Surble, C. Serre, C. Mellot-Draznieks, F. Millange and G. Ferey, *Chem. Commun.*, 2006, 284–286.
39 P. Horcajada, F. Salles, S. Wuttke, T. Devic, D. Heurtaux, G. Maurin, A. Vimont, M. Daturi, O. David, E. Magnier, N. Stock, Y. Filinchuk, D. Popov, C. Riekel, G. Férey and C. Serre, *J. Am. Chem. Soc.*, 2011, **133**, 17839–17847.
40 J. J. Low, A. I. Benin, P. Jakubczak, J. F. Abrahamian, S. A. Faheem and R. R. Willis, *J. Am. Chem. Soc.*, 2009, **131**, 15834–15842.
41 F. Millange, C. Serre and G. Ferey, *Chem. Commun.*, 2002, 822–823.
42 C. Serre, F. Millange, C. Thouvenot, M. Noguès, G. Marsolier, D. Louër and G. Férey, *J. Am. Chem. Soc.*, 2002, **124**, 13519–13526.
43 G. Ferey, *Chem. Soc. Rev.*, 2008, **37**, 191–214.
44 F. Carson, J. Su, A. E. Platero-Prats, W. Wan, Y. Yun, L. Samain and X. Zou, *Cryst. Growth Des.*, 2013, **13**, 5036–5044.
45 S. Bauer, C. Serre, T. Devic, P. Horcajada, J. R. M. Marrot, G. R. Férey and N. Stock, *Inorg. Chem.*, 2008, **47**, 7568–7576.
46 P. Serra-Crespo, E. V. Ramos-Fernandez, J. Gascon and F. Kapteijn, *Chem. Mater.*, 2011, **23**, 2565–2572.
47 K. M. L. Taylor-Pashow, J. D. Rocca, Z. Xie, S. Tran and W. Lin, *J. Am. Chem. Soc.*, 2009, **131**, 14261–14263.
48 M. Lammert, S. Bernt, F. Vermoortele, D. E. De Vos and N. Stock, *Inorg. Chem.*, 2013, **52**, 8521–8528.
49 A. Sonnauer, F. Hoffmann, M. Fröba, L. Kienle, V. Duppel, M. Thommes, C. Serre, G. Férey and N. Stock, *Angew. Chem.*, 2009, **121**, 3849–3852.
50 S. Biswas, S. Couck, M. Grzywa, J. F. M. Denayer, D. Volkmer and P. Van Der Voort, *Eur. J. Inorg. Chem.*, 2012, 2481–2486.
51 W. B. Blumenthal, *The chemical behavior of zirconium*, D. Van Nostrand Company, Princeton, NJ, 1958.
52 J. H. Cavka, S. Jakobsen, U. Olsbye, N. Guillou, C. Lamberti, S. Bordiga and K. P. Lillerud, *J. Am. Chem. Soc.*, 2008, **130**, 13850–13851.
53 K.-K. Yee, N. Reimer, J. Liu, S.-Y. Cheng, S.-M. Yiu, J. Weber, N. Stock and Z. Xu, *J. Am. Chem. Soc.*, 2013, **135**, 7795–7798.
54 H.-L. Jiang, D. Feng, T.-F. Liu, J.-R. Li and H.-C. Zhou, *J. Am. Chem. Soc.*, 2012, **134**, 14690–14693.
55 C. Wang, J.-L. Wang and W. Lin, *J. Am. Chem. Soc.*, 2012, **134**, 19895–19908.
56 A. Schaate, P. Roy, T. Preuße, S. J. Lohmeier, A. Godt and P. Behrens, *Chem.–Eur. J.*, 2011, **17**, 9320–9325.
57 M. Kim, J. F. Cahill, Y. Su, K. A. Prather and S. M. Cohen, *Chem. Sci.*, 2012, **3**, 126–130.
58 M. Kim and S. M. Cohen, *CrystEngComm*, 2012, **14**, 4096–4104.

59 M. Kim, J. F. Cahill, H. Fei, K. A. Prather and S. M. Cohen, *J. Am. Chem. Soc.*, 2012, **134**, 18082–18088.
60 J. B. DeCoste, G. W. Peterson, H. Jasuja, T. G. Glover, Y.-g. Huang and K. S. Walton, *J. Mater. Chem. A*, 2013, **1**, 5642–5650.
61 V. Bon, V. Senkovskyy, I. Senkovska and S. Kaskel, *Chem. Commun.*, 2012, **48**, 8407–8409.
62 M. Dan-Hardi, C. Serre, T. O. Frot, L. Rozes, G. Maurin, C. M. Sanchez and G. R. Férey, *J. Am. Chem. Soc.*, 2009, **131**, 10857–10859.
63 Y. Fu, D. Sun, Y. Chen, R. Huang, Z. Ding, X. Fu and Z. Li, *Angew. Chem., Int. Ed.*, 2012, **51**, 3364–3367.
64 L. Valenzano, B. Civalleri, S. Chavan, G. T. Palomino, C. O. Areán and S. Bordiga, *J. Phys. Chem. C*, 2010, **114**, 11185–11191.
65 T. M. McDonald, W. R. Lee, J. A. Mason, B. M. Wiers, C. S. Hong and J. R. Long, *J. Am. Chem. Soc.*, 2012, **134**, 7056–7065.
66 S. S. Han, S.-H. Choi and A. C. T. van Duin, *Chem. Commun.*, 2010, **46**, 5713–5715.
67 A. C. Kizzie, A. G. Wong-Foy and A. J. Matzger, *Langmuir*, 2011, **27**, 6368–6373.
68 V. Guillerm, F. Ragon, M. Dan-Hardi, T. Devic, M. Vishnuvarthan, B. Campo, A. Vimont, G. Clet, Q. Yang, G. Maurin, G. Férey, A. Vittadini, S. Gross and C. Serre, *Angew. Chem., Int. Ed.*, 2012, **51**, 9267–9271.
69 T. Loiseau, C. Serre, C. Huguenard, G. Fink, F. Taulelle, M. Henry, T. Bataille and G. Férey, *Chem.–Eur. J.*, 2004, **10**, 1373–1382.
70 K. Barthelet, J. Marrot, D. Riou and G. Férey, *Angew. Chem., Int. Ed.*, 2002, **41**, 281–284.
71 P. Horcajada, C. Serre, G. Maurin, N. A. Ramsahye, F. Balas, M. a. Vallet-Regí, M. Sebban, F. Taulelle and G. r. Férey, *J. Am. Chem. Soc.*, 2008, **130**, 6774–6780.
72 N. A. Ramsahye, G. Maurin, S. Bourrelly, P. L. Llewellyn, T. Loiseau, C. Serre and G. Ferey, *Chem. Commun.*, 2007, 3261–3263.
73 S. Bourrelly, C. Serre, A. Vimont, N. A. Ramsahye, G. Maurin, M. Daturi, Y. Filinchuk, G. Férey and P. L. Llewellyn, in *Stud. Surf. Sci. Catal.*, ed. Z. G. J. C. Ruren Xu and Y. Wenfu, Elsevier, 2007, vol. 170, pp. 1008–1014.
74 S. Couck, J. F. M. Denayer, G. V. Baron, T. Rémy, J. Gascon and F. Kapteijn, *J. Am. Chem. Soc.*, 2009, **131**, 6326–6327.
75 X.-S. Wang, S. Ma, D. Sun, S. Parkin and H.-C. Zhou, *J. Am. Chem. Soc.*, 2006, **128**, 16474–16475.
76 S. Ma, D. Sun, M. Ambrogio, J. A. Fillinger, S. Parkin and H.-C. Zhou, *J. Am. Chem. Soc.*, 2007, **129**, 1858–1859.
77 H. Furukawa, Y. B. Go, N. Ko, Y. K. Park, F. J. Uribe-Romo, J. Kim, M. O'Keeffe and O. M. Yaghi, *Inorg. Chem.*, 2011, **50**, 9147–9152.
78 B. Chen, M. Eddaoudi, S. T. Hyde, M. O'Keeffe and O. M. Yaghi, *Science*, 2001, **291**, 1021–1023.
79 H. Furukawa, N. Ko, Y. B. Go, N. Aratani, S. B. Choi, E. Choi, A. Ö. Yazaydin, R. Q. Snurr, M. O'Keeffe, J. Kim and O. M. Yaghi, *Science*, 2010, **329**, 424–428.
80 M.-H. Choi, H. J. Park, D. H. Hong and M. P. Suh, *Chem.–Eur. J.*, 2013, **19**, 17432–17438.
81 G. Férey, C. Serre, C. Mellot-Draznieks, F. Millange, S. Surblé, J. Dutour and I. Margiolaki, *Angew. Chem., Int. Ed.*, 2004, **43**, 6296–6301.
82 P. Horcajada, S. Surble, C. Serre, D.-Y. Hong, Y.-K. Seo, J.-S. Chang, J.-M. Greneche, I. Margiolaki and G. Ferey, *Chem. Commun.*, 2007, 2820–2822.
83 C. Volkringer, D. Popov, T. Loiseau, G. R. Férey, M. Burghammer, C. Riekel, M. Haouas and F. Taulelle, *Chem. Mater.*, 2009, **21**, 5695–5697.
84 A. Lieb, H. Leclerc, T. Devic, C. Serre, I. Margiolaki, F. Mahjoubi, J. S. Lee, A. Vimont, M. Daturi and J.-S. Chang, *Microporous Mesoporous Mater.*, 2012, **157**, 18–23.
85 M. Li, D. Li, M. O'Keeffe and O. M. Yaghi, *Chem. Rev.*, 2014, **114**, 1343–1370.
86 A. G. Wong-Foy, O. Lebel and A. J. Matzger, *J. Am. Chem. Soc.*, 2007, **129**, 15740–15741.
87 J. Duan, Z. Yang, J. Bai, B. Zheng, Y. Li and S. Li, *Chem. Commun.*, 2012, **48**, 3058–3060.
88 D. Zhao, D. J. Timmons, D. Yuan and H.-C. Zhou, *Acc. Chem. Res.*, 2010, **44**, 123–133.
89 F. A. Almeida Paz, J. Klinowski, S. M. F. Vilela, J. P. C. Tome, J. A. S. Cavaleiro and J. Rocha, *Chem. Soc. Rev.*, 2012, **41**, 1088–1110.
90 M. O'Keeffe and O. M. Yaghi, *Chem. Rev.*, 2011, **112**, 675–702.
91 L. Carlucci, G. Ciani and D. M. Proserpio, *Coord. Chem. Rev.*, 2003, **246**, 247–289.
92 V. A. Blatov, L. Carlucci, G. Ciani and D. M. Proserpio, *CrystEngComm*, 2004, **6**, 378–395.
93 O. Delgado-Friedrichs, M. O'Keeffe and O. M. Yaghi, *Phys. Chem. Chem. Phys.*, 2007, **9**, 1035–1043.
94 O. Delgado-Friedrichs, M. O'Keeffe and O. M. Yaghi, *Acta Crystallogr., Sect. A: Found. Crystallogr.*, 2006, **62**, 350–355.
95 M. Zhang, Y.-P. Chen, M. Bosch, T. Gentle, K. Wang, D. Feng, Z. U. Wang and H.-C. Zhou, *Angew. Chem., Int. Ed.*, 2014, **53**, 815–818.
96 O. Delgado Friedrichs, M. O'Keeffe and O. M. Yaghi, *Solid State Sci.*, 2003, **5**, 73–78.
97 A. Schaate, P. Roy, A. Godt, J. Lippke, F. Waltz, M. Wiebcke and P. Behrens, *Chem.–Eur. J.*, 2011, **17**, 6643–6651.
98 P. Pyykko, *Chem. Rev.*, 1988, **88**, 563–594.
99 B. Chen, M. Eddaoudi, T. M. Reineke, J. W. Kampf, M. O'Keeffe and O. M. Yaghi, *J. Am. Chem. Soc.*, 2000, **122**, 11559–11560.
100 J. Kim, B. Chen, T. M. Reineke, H. Li, M. Eddaoudi, D. B. Moler, M. O'Keeffe and O. M. Yaghi, *J. Am. Chem. Soc.*, 2001, **123**, 8239–8247.
101 L. Ma, A. Jin, Z. Xie and W. Lin, *Angew. Chem., Int. Ed.*, 2009, **48**, 9905–9908.
102 M. Zhang, Y.-P. Chen and H.-C. Zhou, *CrystEngComm*, 2013, **15**, 9544–9552.
103 R. P. Davies, R. Less, P. D. Lickiss, K. Robertson and A. J. P. White, *Cryst. Growth Des.*, 2010, **10**, 4571–4581.
104 M. J. Murphy, D. M. D'Alessandro and C. J. Kepert, *Dalton Trans.*, 2013, **42**, 13308–13310.
105 A.-H. Yuan, R.-Q. Lu, H. Zhou, Y.-Y. Chen and Y.-Z. Li, *CrystEngComm*, 2010, **12**, 1382–1384.

106 M. Xue, G. Zhu, Y. Li, X. Zhao, Z. Jin, E. Kang and S. Qiu, *Cryst. Growth Des.*, 2008, **8**, 2478–2483.
107 Q.-F. Zhang, J.-H. Luo and A.-H. Yuan, *Z. Anorg. Allg. Chem.*, 2013, **639**, 1804–1807.
108 L. Wen, P. Cheng and W. Lin, *Chem. Sci.*, 2012, **3**, 2288–2292.
109 L. Wen, P. Cheng and W. Lin, *Chem. Commun.*, 2012, **48**, 2846–2848.
110 J. M. Taylor, A. H. Mahmoudkhani and G. K. H. Shimizu, *Angew. Chem., Int. Ed.*, 2007, **46**, 795–798.
111 T. A. Makal, A. A. Yakovenko and H.-C. Zhou, *J. Phys. Chem. Lett.*, 2011, **2**, 1682–1689.
112 D. Sun, Y. Ke, T. M. Mattox, B. A. Ooro and H.-C. Zhou, *Chem. Commun.*, 2005, 5447–5449.
113 D. Sun, D. J. Collins, Y. Ke, J.-L. Zuo and H.-C. Zhou, *Chem.–Eur. J.*, 2006, **12**, 3768–3776.
114 D. Sun, S. Ma, J. M. Simmons, J.-R. Li, D. Yuan and H.-C. Zhou, *Chem. Commun.*, 2010, **46**, 1329–1331.
115 B. Chen, N. W. Ockwig, A. R. Millward, D. S. Contreras and O. M. Yaghi, *Angew. Chem.*, 2005, **117**, 4823–4827.
116 X. Lin, J. Jia, X. Zhao, K. M. Thomas, A. J. Blake, G. S. Walker, N. R. Champness, P. Hubberstey and M. Schröder, *Angew. Chem., Int. Ed.*, 2006, **45**, 7358–7364.
117 X. Lin, I. Telepeni, A. J. Blake, A. Dailly, C. M. Brown, J. M. Simmons, M. Zoppi, G. S. Walker, K. M. Thomas, T. J. Mays, P. Hubberstey, N. R. Champness and M. Schröder, *J. Am. Chem. Soc.*, 2009, **131**, 2159–2171.
118 S. Yang, X. Lin, A. Dailly, A. J. Blake, P. Hubberstey, N. R. Champness and M. Schröder, *Chem.–Eur. J.*, 2009, **15**, 4829–4835.
119 D. Zhao, D. Yuan, A. Yakovenko and H.-C. Zhou, *Chem. Commun.*, 2010, **46**, 4196–4198.
120 O. K. Farha, C. E. Wilmer, I. Eryazici, B. G. Hauser, P. A. Parilla, K. O'Neill, A. A. Sarjeant, S. T. Nguyen, R. Q. Snurr and J. T. Hupp, *J. Am. Chem. Soc.*, 2012, **134**, 9860–9863.
121 T. A. Makal, X. Wang and H.-C. Zhou, *Cryst. Growth Des.*, 2013, **13**, 4760–4768.
122 S. Ma, D. Sun, J. M. Simmons, C. D. Collier, D. Yuan and H.-C. Zhou, *J. Am. Chem. Soc.*, 2007, **130**, 1012–1016.
123 S. Ma, J. M. Simmons, D. Sun, D. Yuan and H.-C. Zhou, *Inorg. Chem.*, 2009, **48**, 5263–5268.
124 Y. Peng, V. Krungleviciute, I. Eryazici, J. T. Hupp, O. K. Farha and T. Yildirim, *J. Am. Chem. Soc.*, 2013, **135**, 11887–11894.
125 S. Yang, X. Lin, W. Lewis, M. Suyetin, E. Bichoutskaia, J. E. Parker, C. C. Tang, D. R. Allan, P. J. Rizkallah, P. Hubberstey, N. R. Champness, K. Mark Thomas, A. J. Blake and M. Schröder, *Nat. Mater.*, 2012, **11**, 710–716.
126 S. Yang, J. Sun, A. J. Ramirez-Cuesta, S. K. Callear, I. F. DavidWilliam, D. P. Anderson, R. Newby, A. J. Blake, J. E. Parker, C. C. Tang and M. Schröder, *Nat. Chem.*, 2012, **4**, 887–894.
127 D. J. Tranchemontagne, Z. Ni, M. O'Keeffe and O. M. Yaghi, *Angew. Chem., Int. Ed.*, 2008, **47**, 5136–5147.
128 J.-R. Li, J. Yu, W. Lu, L.-B. Sun, J. Sculley, P. B. Balbuena and H.-C. Zhou, *Nat. Commun.*, 2013, **4**, 1538.
129 W. Lu, D. Yuan, T. A. Makal, Z. Wei, J.-R. Li and H.-C. Zhou, *Dalton Trans.*, 2013, **42**, 1708–1714.
130 U. Stoeck, S. Krause, V. Bon, I. Senkovska and S. Kaskel, *Chem. Commun.*, 2012, **48**, 10841–10843.
131 Y. Zou, M. Park, S. Hong and M. S. Lah, *Chem. Commun.*, 2008, 2340–2342.
132 G. J. McManus, Z. Wang and M. J. Zaworotko, *Cryst. Growth Des.*, 2003, **4**, 11–13.
133 J. J. Perry IV, V. C. Kravtsov, G. J. McManus and M. J. Zaworotko, *J. Am. Chem. Soc.*, 2007, **129**, 10076–10077.
134 A. J. Cairns, J. A. Perman, L. Wojtas, V. C. Kravtsov, M. H. Alkordi, M. Eddaoudi and M. J. Zaworotko, *J. Am. Chem. Soc.*, 2008, **130**, 1560–1561.
135 D. Zhao, D. Yuan, D. Sun and H.-C. Zhou, *J. Am. Chem. Soc.*, 2009, **131**, 9186–9188.
136 D. Yuan, D. Zhao, D. Sun and H.-C. Zhou, *Angew. Chem., Int. Ed.*, 2010, **49**, 5357–5361.
137 D. Yuan, D. Zhao and H.-C. Zhou, *Inorg. Chem.*, 2011, **50**, 10528–10530.
138 A. P. Nelson, O. K. Farha, K. L. Mulfort and J. T. Hupp, *J. Am. Chem. Soc.*, 2008, **131**, 458–460.
139 O. K. Farha, A. Özgür Yazaydın, I. Eryazici, C. D. Malliakas, B. G. Hauser, M. G. Kanatzidis, S. T. Nguyen, R. Q. Snurr and J. T. Hupp, *Nat. Chem.*, 2010, **2**, 944–948.
140 Y. Yan, X. Lin, S. Yang, A. J. Blake, A. Dailly, N. R. Champness, P. Hubberstey and M. Schroder, *Chem. Commun.*, 2009, 1025–1027.
141 Y. Yan, I. Telepeni, S. Yang, X. Lin, W. Kockelmann, A. Dailly, A. J. Blake, W. Lewis, G. S. Walker, D. R. Allan, S. A. Barnett, N. R. Champness and M. Schröder, *J. Am. Chem. Soc.*, 2010, **132**, 4092–4094.
142 Y. Yan, A. J. Blake, W. Lewis, S. A. Barnett, A. Dailly, N. R. Champness and M. Schröder, *Chem.–Eur. J.*, 2011, **17**, 11162–11170.
143 Y. Yan, S. Yang, A. J. Blake, W. Lewis, E. Poirier, S. A. Barnett, N. R. Champness and M. Schroder, *Chem. Commun.*, 2011, **47**, 9995–9997.
144 Y. Yan, M. Suyetin, E. Bichoutskaia, A. J. Blake, D. R. Allan, S. A. Barnett and M. Schroder, *Chem. Sci.*, 2013, **4**, 1731–1736.
145 F. Nouar, J. F. Eubank, T. Bousquet, L. Wojtas, M. J. Zaworotko and M. Eddaoudi, *J. Am. Chem. Soc.*, 2008, **130**, 1833–1835.
146 J. F. Eubank, F. Nouar, R. Luebke, A. J. Cairns, L. Wojtas, M. Alkordi, T. Bousquet, M. R. Hight, J. Eckert, J. P. Embs, P. A. Georgiev and M. Eddaoudi, *Angew. Chem., Int. Ed.*, 2012, **51**, 10099–10103.
147 R. Luebke, J. F. Eubank, A. J. Cairns, Y. Belmabkhout, L. Wojtas and M. Eddaoudi, *Chem. Commun.*, 2012, **48**, 1455–1457.
148 S. Hong, M. Oh, M. Park, J. W. Yoon, J.-S. Chang and M. S. Lah, *Chem. Commun.*, 2009, 5397–5399.
149 X. Song, S. Jeong, D. Kim and M. S. Lah, *CrystEngComm*, 2012, **14**, 5753–5756.
150 B. Li, Z. Zhang, Y. Li, K. Yao, Y. Zhu, Z. Deng, F. Yang, X. Zhou, G. Li, H. Wu, N. Nijem, Y. J. Chabal, Z. Lai,

Y. Han, Z. Shi, S. Feng and J. Li, *Angew. Chem., Int. Ed.*, 2012, **51**, 1412–1415.
151 B. Zheng, J. Bai, J. Duan, L. Wojtas and M. J. Zaworotko, *J. Am. Chem. Soc.*, 2010, **133**, 748–751.
152 C. E. Wilmer, O. K. Farha, T. Yildirim, I. Eryazici, V. Krungleviciute, A. A. Sarjeant, R. Q. Snurr and J. T. Hupp, *Energy Environ. Sci.*, 2013, **6**, 1158–1163.
153 Z. Guo, H. Wu, G. Srinivas, Y. Zhou, S. Xiang, Z. Chen, Y. Yang, W. Zhou, M. O'Keeffe and B. Chen, *Angew. Chem., Int. Ed.*, 2011, **50**, 3178–3181.
154 X. Zhao, X. Wang, S. Wang, J. Dou, P. Cui, Z. Chen, D. Sun, X. Wang and D. Sun, *Cryst. Growth Des.*, 2012, **12**, 2736–2739.
155 L. Li, S. Tang, X. Lv, M. Jiang, C. Wang and X. Zhao, *New J. Chem.*, 2013, **37**, 3662–3670.
156 Z. Chen, S. Xiang, T. Liao, Y. Yang, Y.-S. Chen, Y. Zhou, D. Zhao and B. Chen, *Cryst. Growth Des.*, 2010, **10**, 2775–2779.
157 H. K. Chae, M. Eddaoudi, J. Kim, S. I. Hauck, J. F. Hartwig, M. O'Keeffe and O. M. Yaghi, *J. Am. Chem. Soc.*, 2001, **123**, 11482–11483.
158 I. Eryazici, O. K. Farha, B. G. Hauser, A. Ö. Yazaydın, A. A. Sarjeant, S. T. Nguyen and J. T. Hupp, *Cryst. Growth Des.*, 2012, **12**, 1075–1080.
159 Y. He, H. Furukawa, C. Wu, M. O'Keeffe, R. Krishna and B. Chen, *Chem. Commun.*, 2013, **49**, 6773–6775.
160 J. Jia, F. Sun, Q. Fang, X. Liang, K. Cai, Z. Bian, H. Zhao, L. Gao and G. Zhu, *Chem. Commun.*, 2011, **47**, 9167–9169.
161 J. Jia, F. Sun, T. Borjigin, H. Ren, T. Zhang, Z. Bian, L. Gao and G. Zhu, *Chem. Commun.*, 2012, **48**, 6010–6012.
162 J. Jia, F. Sun, H. Ma, L. Wang, K. Cai, Z. Bian, L. Gao and G. Zhu, *J. Mater. Chem. A*, 2013, **1**, 10112–10115.
163 Y. He, Z. Zhang, S. Xiang, F. R. Fronczek, R. Krishna and B. Chen, *Chem.–Eur. J.*, 2012, **18**, 613–619.
164 Y. He, Z. Zhang, S. Xiang, H. Wu, F. R. Fronczek, W. Zhou, R. Krishna, M. O'Keeffe and B. Chen, *Chem.–Eur. J.*, 2012, **18**, 1901–1904.
165 Z. Wei, W. Lu, H.-L. Jiang and H.-C. Zhou, *Inorg. Chem.*, 2013, **52**, 1164–1166.
166 N. B. Shustova, A. F. Cozzolino and M. Dincă, *J. Am. Chem. Soc.*, 2012, **134**, 19596–19599.
167 Y.-S. Xue, F.-Y. Jin, L. Zhou, M.-P. Liu, Y. Xu, H.-B. Du, M. Fang and X.-Z. You, *Cryst. Growth Des.*, 2012, **12**, 6158–6164.
168 C. Tan, S. Yang, N. R. Champness, X. Lin, A. J. Blake, W. Lewis and M. Schroder, *Chem. Commun.*, 2011, **47**, 4487–4489.
169 D. Liu, H. Wu, S. Wang, Z. Xie, J. Li and W. Lin, *Chem. Sci.*, 2012, **3**, 3032–3037.
170 J. A. Johnson, Q. Lin, L.-C. Wu, N. Obaidi, Z. L. Olson, T. C. Reeson, Y.-S. Chen and J. Zhang, *Chem. Commun.*, 2013, **49**, 2828–2830.
171 X.-S. Wang, M. Chrzanowski, C. Kim, W.-Y. Gao, L. Wojtas, Y.-S. Chen, X. Peter Zhang and S. Ma, *Chem. Commun.*, 2012, **48**, 7173–7175.
172 X.-L. Yang, M.-H. Xie, C. Zou, Y. He, B. Chen, M. O'Keeffe and C.-D. Wu, *J. Am. Chem. Soc.*, 2012, **134**, 10638–10645.
173 X.-S. Wang, M. Chrzanowski, W.-Y. Gao, L. Wojtas, Y.-S. Chen, M. J. Zaworotko and S. Ma, *Chem. Sci.*, 2012, **3**, 2823–2827.
174 W. Lu, D. Yuan, T. A. Makal, J.-R. Li and H.-C. Zhou, *Angew. Chem., Int. Ed.*, 2012, **51**, 1580–1584.
175 L. Ma, D. J. Mihalcik and W. Lin, *J. Am. Chem. Soc.*, 2009, **131**, 4610–4612.
176 D. J. Mihalcik, T. Zhang, L. Ma and W. Lin, *Inorg. Chem.*, 2012, **51**, 2503–2508.
177 H. Deng, C. J. Doonan, H. Furukawa, R. B. Ferreira, J. Towne, C. B. Knobler, B. Wang and O. M. Yaghi, *Science*, 2010, **327**, 846–850.
178 X. Kong, H. Deng, F. Yan, J. Kim, J. A. Swisher, B. Smit, O. M. Yaghi and J. A. Reimer, *Science*, 2013, **341**, 882–885.
179 T.-H. Park, K. Koh, A. G. Wong-Foy and A. J. Matzger, *Cryst. Growth Des.*, 2011, **11**, 2059–2063.
180 K. Koh, J. D. Van Oosterhout, S. Roy, A. G. Wong-Foy and A. J. Matzger, *Chem. Sci.*, 2012, **3**, 2429–2432.
181 K. Koh, A. G. Wong-Foy and A. J. Matzger, *Angew. Chem., Int. Ed.*, 2008, **47**, 677–680.
182 K. Koh, A. G. Wong-Foy and A. J. Matzger, *J. Am. Chem. Soc.*, 2010, **132**, 15005–15010.
183 N. Klein, I. Senkovska, K. Gedrich, U. Stoeck, A. Henschel, U. Mueller and S. Kaskel, *Angew. Chem., Int. Ed.*, 2009, **48**, 9954–9957.
184 R. Kitaura, S. Kitagawa, Y. Kubota, T. C. Kobayashi, K. Kindo, Y. Mita, A. Matsuo, M. Kobayashi, H.-C. Chang, T. C. Ozawa, M. Suzuki, M. Sakata and M. Takata, *Science*, 2002, **298**, 2358–2361.
185 R. Kitaura, K. Fujimoto, S.-i. Noro, M. Kondo and S. Kitagawa, *Angew. Chem.*, 2002, **114**, 141–143.
186 J. Seo, R. Matsuda, H. Sakamoto, C. Bonneau and S. Kitagawa, *J. Am. Chem. Soc.*, 2009, **131**, 12792–12800.
187 T. K. Maji, K. Uemura, H.-C. Chang, R. Matsuda and S. Kitagawa, *Angew. Chem., Int. Ed.*, 2004, **43**, 3269–3272.
188 S. Horike, S. Bureekaew and S. Kitagawa, *Chem. Commun.*, 2008, 471–473.
189 Y. Sakata, S. Furukawa, M. Kondo, K. Hirai, N. Horike, Y. Takashima, H. Uehara, N. Louvain, M. Meilikhov, T. Tsuruoka, S. Isoda, W. Kosaka, O. Sakata and S. Kitagawa, *Science*, 2013, **339**, 193–196.
190 O. K. Farha, C. D. Malliakas, M. G. Kanatzidis and J. T. Hupp, *J. Am. Chem. Soc.*, 2009, **132**, 950–952.
191 W. Bury, D. Fairen-Jimenez, M. B. Lalonde, R. Q. Snurr, O. K. Farha and J. T. Hupp, *Chem. Mater.*, 2013, **25**, 739–744.
192 O. Karagiaridi, W. Bury, E. Tylianakis, A. A. Sarjeant, J. T. Hupp and O. K. Farha, *Chem. Mater.*, 2013, **25**, 3499–3503.
193 A. M. Shultz, O. K. Farha, J. T. Hupp and S. T. Nguyen, *J. Am. Chem. Soc.*, 2009, **131**, 4204–4205.
194 K. L. Mulfort and J. T. Hupp, *J. Am. Chem. Soc.*, 2007, **129**, 9604–9605.
195 K. L. Mulfort, O. K. Farha, C. L. Stern, A. A. Sarjeant and J. T. Hupp, *J. Am. Chem. Soc.*, 2009, **131**, 3866–3868.
196 M. C. Das, Q. Guo, Y. He, J. Kim, C.-G. Zhao, K. Hong, S. Xiang, Z. Zhang, K. M. Thomas, R. Krishna and B. Chen, *J. Am. Chem. Soc.*, 2012, **134**, 8703–8710.

197 W. Xuan, C. Ye, M. Zhang, Z. Chen and Y. Cui, *Chem. Sci.*, 2013, **4**, 3154–3159.
198 J. An, O. K. Farha, J. T. Hupp, E. Pohl, J. I. Yeh and N. L. Rosi, *Nat. Commun.*, 2012, **3**, 604.
199 D. Han, F.-L. Jiang, M.-Y. Wu, L. Chen, Q.-H. Chen and M.-C. Hong, *Chem. Commun.*, 2011, **47**, 9861–9863.
200 T.-H. Park, A. J. Hickman, K. Koh, S. Martin, A. G. Wong-Foy, M. S. Sanford and A. J. Matzger, *J. Am. Chem. Soc.*, 2011, **133**, 20138–20141.
201 K. M. Choi, H. J. Jeon, J. K. Kang and O. M. Yaghi, *J. Am. Chem. Soc.*, 2011, **133**, 11920–11923.
202 J. Park, Z. U. Wang, L.-B. Sun, Y.-P. Chen and H.-C. Zhou, *J. Am. Chem. Soc.*, 2012, **134**, 20110–20116.
203 J. K. Schnobrich, O. Lebel, K. A. Cychosz, A. Dailly, A. G. Wong-Foy and A. J. Matzger, *J. Am. Chem. Soc.*, 2010, **132**, 13941–13948.
204 Y. Liu, J.-R. Li, W. M. Verdegaal, T.-F. Liu and H.-C. Zhou, *Chem.–Eur. J.*, 2013, **19**, 5637–5643.
205 Y. Xie, H. Yang, Z. U. Wang, Y. Liu, H.-C. Zhou and J.-R. Li, *Chem. Commun.*, 2014, **50**, 563–565.
206 Z. Guo, G. Li, L. Zhou, S. Su, Y. Lei, S. Dang and H. Zhang, *Inorg. Chem.*, 2009, **48**, 8069–8071.
207 L. Feng, Z. Chen, T. Liao, P. Li, Y. Jia, X. Liu, Y. Yang and Y. Zhou, *Cryst. Growth Des.*, 2009, **9**, 1505–1510.
208 S. Xiang, J. Huang, L. Li, J. Zhang, L. Jiang, X. Kuang and C.-Y. Su, *Inorg. Chem.*, 2011, **50**, 1743–1748.
209 J. Lee, O. K. Farha, J. Roberts, K. A. Scheidt, S. T. Nguyen and J. T. Hupp, *Chem. Soc. Rev.*, 2009, **38**, 1450–1459.
210 L. Ma, C. Abney and W. Lin, *Chem. Soc. Rev.*, 2009, **38**, 1248–1256.
211 E. D. Bloch, D. Britt, C. Lee, C. J. Doonan, F. J. Uribe-Romo, H. Furukawa, J. R. Long and O. M. Yaghi, *J. Am. Chem. Soc.*, 2010, **132**, 14382–14384.
212 K. Oisaki, Q. Li, H. Furukawa, A. U. Czaja and O. M. Yaghi, *J. Am. Chem. Soc.*, 2010, **132**, 9262–9264.
213 A. M. Bohnsack, I. A. Ibarra, V. I. Bakhmutov, V. M. Lynch and S. M. Humphrey, *J. Am. Chem. Soc.*, 2013, **135**, 16038–16041.
214 C. Wang, Z. Xie, K. E. deKrafft and W. Lin, *J. Am. Chem. Soc.*, 2011, **133**, 13445–13454.
215 S. Pullen, H. Fei, A. Orthaber, S. M. Cohen and S. Ott, *J. Am. Chem. Soc.*, 2013, **135**, 16997–17003.
216 C.-D. Wu, A. Hu, L. Zhang and W. Lin, *J. Am. Chem. Soc.*, 2005, **127**, 8940–8941.
217 C.-D. Wu and W. Lin, *Angew. Chem., Int. Ed.*, 2007, **46**, 1075–1078.
218 L. Ma, C.-D. Wu, M. M. Wanderley and W. Lin, *Angew. Chem., Int. Ed.*, 2010, **49**, 8244–8248.
219 L. Ma, J. M. Falkowski, C. Abney and W. Lin, *Nat. Chem.*, 2010, **2**, 838–846.
220 L. Sun, T. Miyakai, S. Seki and M. Dincă, *J. Am. Chem. Soc.*, 2013, **135**, 8185–8188.
221 F. G. Bordwell, *Acc. Chem. Res.*, 1988, **21**, 456–463.
222 C. Wang and W. Lin, *J. Am. Chem. Soc.*, 2011, **133**, 4232–4235.
223 C. A. Kent, D. Liu, T. J. Meyer and W. Lin, *J. Am. Chem. Soc.*, 2012, **134**, 3991–3994.
224 C. Wang, K. E. deKrafft and W. Lin, *J. Am. Chem. Soc.*, 2012, **134**, 7211–7214.
225 I. Senkovska, F. Hoffmann, M. Fröba, J. Getzschmann, W. Böhlmann and S. Kaskel, *Microporous Mesoporous Mater.*, 2009, **122**, 93–98.
226 A. Coskun, M. Hmadeh, G. Barin, F. Gándara, Q. Li, E. Choi, N. L. Strutt, D. B. Cordes, A. M. Z. Slawin, J. F. Stoddart, J.-P. Sauvage and O. M. Yaghi, *Angew. Chem., Int. Ed.*, 2012, **51**, 2160–2163.
227 B. F. Abrahams, B. F. Hoskins, D. M. Michail and R. Robson, *Nature*, 1994, **369**, 727–729.
228 O. K. Farha, A. M. Shultz, A. A. Sarjeant, S. T. Nguyen and J. T. Hupp, *J. Am. Chem. Soc.*, 2011, **133**, 5652–5655.
229 E.-Y. Choi, P. M. Barron, R. W. Novotny, H.-T. Son, C. Hu and W. Choe, *Inorg. Chem.*, 2008, **48**, 426–428.
230 C. Y. Lee, O. K. Farha, B. J. Hong, A. A. Sarjeant, S. T. Nguyen and J. T. Hupp, *J. Am. Chem. Soc.*, 2011, **133**, 15858–15861.
231 H.-L. Jiang, D. Feng, K. Wang, Z.-Y. Gu, Z. Wei, Y.-P. Chen and H.-C. Zhou, *J. Am. Chem. Soc.*, 2013, **135**, 13934–13938.
232 D. Feng, H.-L. Jiang, Y.-P. Chen, Z.-Y. Gu, Z. Wei and H.-C. Zhou, *Inorg. Chem.*, 2013, **52**, 12661–12667.
233 D. Feng, W.-C. Chung, Z. Wei, Z.-Y. Gu, H.-L. Jiang, Y.-P. Chen, D. J. Darensbourg and H.-C. Zhou, *J. Am. Chem. Soc.*, 2013, **135**, 17105–17110.
234 S. M. Humphrey, P. K. Allan, S. E. Oungoulian, M. S. Ironside and E. R. Wise, *Dalton Trans.*, 2009, 2298–2305.
235 A. J. Nunez, L. N. Shear, N. Dahal, I. A. Ibarra, J. Yoon, Y. K. Hwang, J.-S. Chang and S. M. Humphrey, *Chem. Commun.*, 2011, **47**, 11855–11857.
236 J. Chun, I. G. Jung, H. J. Kim, M. Park, M. S. Lah and S. U. Son, *Inorg. Chem.*, 2009, **48**, 6353–6355.
237 J. Chun, H. S. Lee, I. G. Jung, S. W. Lee, H. J. Kim and S. U. Son, *Organometallics*, 2010, **29**, 1518–1521.
238 S. S. Kaye and J. R. Long, *J. Am. Chem. Soc.*, 2007, **130**, 806–807.
239 S. Chavan, J. G. Vitillo, M. J. Uddin, F. Bonino, C. Lamberti, E. Groppo, K.-P. Lillerud and S. Bordiga, *Chem. Mater.*, 2010, **22**, 4602–4611.
240 B. Chen, X. Zhao, A. Putkham, K. Hong, E. B. Lobkovsky, E. J. Hurtado, A. J. Fletcher and K. M. Thomas, *J. Am. Chem. Soc.*, 2008, **130**, 6411–6423.
241 G. A. Morris, S. T. Nguyen and J. T. Hupp, *J. Mol. Catal. A: Chem.*, 2001, **174**, 15–20.
242 S.-H. Cho, B. Ma, S. T. Nguyen, J. T. Hupp and T. E. Albrecht-Schmitt, *Chem. Commun.*, 2006, 2563–2565.
243 A. M. Shultz, O. K. Farha, D. Adhikari, A. A. Sarjeant, J. T. Hupp and S. T. Nguyen, *Inorg. Chem.*, 2011, **50**, 3174–3176.
244 R. Kitaura, G. Onoyama, H. Sakamoto, R. Matsuda, S.-i. Noro and S. Kitagawa, *Angew. Chem., Int. Ed.*, 2004, **43**, 2684–2687.
245 N. L. Rosi, M. Eddaoudi, J. Kim, M. O'Keeffe and O. M. Yaghi, *Angew. Chem., Int. Ed.*, 2002, **41**, 284–287.
246 F. Song, C. Wang, J. M. Falkowski, L. Ma and W. Lin, *J. Am. Chem. Soc.*, 2010, **132**, 15390–15398.

247 R. D. Hancock and A. E. Martell, *Chem. Rev.*, 1989, **89**, 1875–1914.
248 P. Nugent, Y. Belmabkhout, S. D. Burd, A. J. Cairns, R. Luebke, K. Forrest, T. Pham, S. Ma, B. Space, L. Wojtas, M. Eddaoudi and M. J. Zaworotko, *Nature*, 2013, **495**, 80–84.
249 J. Fan, G. T. Yee, G. Wang and B. E. Hanson, *Inorg. Chem.*, 2005, **45**, 599–608.
250 S. A. Barnett and N. R. Champness, *Coord. Chem. Rev.*, 2003, **246**, 145–168.
251 H. W. Roesky and M. Andruh, *Coord. Chem. Rev.*, 2003, **236**, 91–119.
252 A. Phan, C. J. Doonan, F. J. Uribe-Romo, C. B. Knobler, M. O'Keeffe and O. M. Yaghi, *Acc. Chem. Res.*, 2009, **43**, 58–67.
253 K. S. Park, Z. Ni, A. P. Côté, J. Y. Choi, R. Huang, F. J. Uribe-Romo, H. K. Chae, M. O'Keeffe and O. M. Yaghi, *Proc. Natl. Acad. Sci. U. S. A.*, 2006, **103**, 10186–10191.
254 B. Wang, A. P. Cote, H. Furukawa, M. O'Keeffe and O. M. Yaghi, *Nature*, 2008, **453**, 207–211.
255 W. Morris, C. J. Doonan, H. Furukawa, R. Banerjee and O. M. Yaghi, *J. Am. Chem. Soc.*, 2008, **130**, 12626–12627.
256 R. Banerjee, A. Phan, B. Wang, C. Knobler, H. Furukawa, M. O'Keeffe and O. M. Yaghi, *Science*, 2008, **319**, 939–943.
257 W. Morris, N. He, K. G. Ray, P. Klonowski, H. Furukawa, I. N. Daniels, Y. A. Houndonougbo, M. Asta, O. M. Yaghi and B. B. Laird, *J. Phys. Chem. C*, 2012, **116**, 24084–24090.
258 R. Banerjee, H. Furukawa, D. Britt, C. Knobler, M. O'Keeffe and O. M. Yaghi, *J. Am. Chem. Soc.*, 2009, **131**, 3875–3877.
259 H. Hayashi, A. P. Cote, H. Furukawa, M. O'Keeffe and O. M. Yaghi, *Nat. Mater.*, 2007, **6**, 501–506.
260 J.-P. Zhang, S. Horike and S. Kitagawa, *Angew. Chem., Int. Ed.*, 2007, **46**, 889–892.
261 J.-P. Zhang and S. Kitagawa, *J. Am. Chem. Soc.*, 2008, **130**, 907–917.
262 M. Dincaă, A. F. Yu and J. R. Long, *J. Am. Chem. Soc.*, 2006, **128**, 8904–8913.
263 H. J. Choi, M. Dinca, A. Dailly and J. R. Long, *Energy Environ. Sci.*, 2010, **3**, 117–123.
264 N. Masciocchi, S. Galli, V. Colombo, A. Maspero, G. Palmisano, B. Seyyedi, C. Lamberti and S. Bordiga, *J. Am. Chem. Soc.*, 2010, **132**, 7902–7904.
265 A. Demessence and J. R. Long, *Chem.–Eur. J.*, 2010, **16**, 5902–5908.
266 D.-X. Xue, A. J. Cairns, Y. Belmabkhout, L. Wojtas, Y. Liu, M. H. Alkordi and M. Eddaoudi, *J. Am. Chem. Soc.*, 2013, **135**, 7660–7667.
267 V. Colombo, S. Galli, H. J. Choi, G. D. Han, A. Maspero, G. Palmisano, N. Masciocchi and J. R. Long, *Chem. Sci.*, 2011, **2**, 1311–1319.
268 J.-P. Zhang, Y.-B. Zhang, J.-B. Lin and X.-M. Chen, *Chem. Rev.*, 2011, **112**, 1001–1033.
269 M. Dincă, A. Dailly, Y. Liu, C. M. Brown, D. A. Neumann and J. R. Long, *J. Am. Chem. Soc.*, 2006, **128**, 16876–16883.
270 M. Dincă, W. S. Han, Y. Liu, A. Dailly, C. M. Brown and J. R. Long, *Angew. Chem., Int. Ed.*, 2007, **46**, 1419–1422.
271 K. Sumida, S. Horike, S. S. Kaye, Z. R. Herm, W. L. Queen, C. M. Brown, F. Grandjean, G. J. Long, A. Dailly and J. R. Long, *Chem. Sci.*, 2010, **1**, 184–191.
272 K. Sumida, D. Stück, L. Mino, J.-D. Chai, E. D. Bloch, O. Zavorotynska, L. J. Murray, M. Dincă, S. Chavan, S. Bordiga, M. Head-Gordon and J. R. Long, *J. Am. Chem. Soc.*, 2012, **135**, 1083–1091.
273 M. Dincă, A. Dailly and J. R. Long, *Chem.–Eur. J.*, 2008, **14**, 10280–10285.
274 R. B. Getman, Y.-S. Bae, C. E. Wilmer and R. Q. Snurr, *Chem. Rev.*, 2011, **112**, 703–723.
275 C. E. Wilmer, M. Leaf, C. Y. Lee, O. K. Farha, B. G. Hauser, J. T. Hupp and R. Q. Snurr, *Nat. Chem.*, 2012, **4**, 83–89.
276 R. L. Martin, L.-C. Lin, K. Jariwala, B. Smit and M. Haranczyk, *J. Phys. Chem. C*, 2013, **117**, 12159–12167.
277 M. P. Suh, H. J. Park, T. K. Prasad and D.-W. Lim, *Chem. Rev.*, 2011, **112**, 782–835.
278 L. J. Murray, M. Dinca and J. R. Long, *Chem. Soc. Rev.*, 2009, **38**, 1294–1314.
279 K. Sumida, D. L. Rogow, J. A. Mason, T. M. McDonald, E. D. Bloch, Z. R. Herm, T.-H. Bae and J. R. Long, *Chem. Rev.*, 2011, **112**, 724–781.
280 T. A. Makal, J.-R. Li, W. Lu and H.-C. Zhou, *Chem. Soc. Rev.*, 2012, **41**, 7761–7779.
281 M. Yoon, R. Srirambalaji and K. Kim, *Chem. Rev.*, 2011, **112**, 1196–1231.
282 J. Della Rocca, D. Liu and W. Lin, *Acc. Chem. Res.*, 2011, **44**, 957–968.
283 P. Horcajada, R. Gref, T. Baati, P. K. Allan, G. Maurin, P. Couvreur, G. Férey, R. E. Morris and C. Serre, *Chem. Rev.*, 2011, **112**, 1232–1268.
284 L. E. Kreno, K. Leong, O. K. Farha, M. Allendorf, R. P. Van Duyne and J. T. Hupp, *Chem. Rev.*, 2011, **112**, 1105–1125.
285 M. D. Allendorf, C. A. Bauer, R. K. Bhakta and R. J. T. Houk, *Chem. Soc. Rev.*, 2009, **38**, 1330–1352.
286 M. Yoon, K. Suh, S. Natarajan and K. Kim, *Angew. Chem., Int. Ed.*, 2013, **52**, 2688–2700.
287 Y. He, R. Krishna and B. Chen, *Energy Environ. Sci.*, 2012, **5**, 9107–9120.
288 H. Wu, Q. Gong, D. H. Olson and J. Li, *Chem. Rev.*, 2012, **112**, 836–868.
289 A. Bétard and R. A. Fischer, *Chem. Rev.*, 2011, **112**, 1055–1083.
290 D. Zacher, O. Shekhah, C. Woll and R. A. Fischer, *Chem. Soc. Rev.*, 2009, **38**, 1418–1429.
291 N. Stock and S. Biswas, *Chem. Rev.*, 2011, **112**, 933–969.